CHARACTERIZATION OF GROUND-PENETRATING RADAR ECHO PATTERN OF WATER TABLE

By

SHENG LIANG

UNIVERSITY OF FLORIDA LIBRARIES

A DISSERTATION PRESENTED TO THE GRADUATE SCHOOL
OF THE UNIVERSITY OF FLORIDA IN PARTIAL FULFILLMENT
OF THE REQUIREMENTS FOR THE DEGREE OF
DOCTOR OF PHILOSOPHY

UNIVERSITY OF FLORIDA

1990

Copyright 1990

by

Sheng Liang

ACKNOWLEDGMENTS

I wish to express my appreciation to the Ministry of Education, Republic of China, for financial support from September 1986 to August 1988, and to the chairman of my supervisory committee, Dr. S.F. Shih, for partial financial aid from October 27, 1989, to May 4, 1990. I also would like to thank the members of my supervisory committee: Dr. F.S. Zazueta for his help on Chapter 4, Dr. D.L. Myhre for the use of his lab, Professor J.J. Gaffney for the use of his lab and for his assistance in finding the GPR transect sites, and Dr. B.E. Ruth for some valuable comments.

Thanks are also given to M.O. Crews, Ralph Hoffman, Curtis Weldon, O. Lanni, Jack Jordan, K.S. Cheng, and Hsing Chein Cheng for their help with various aspects of this research.

I owe appreciation to my wife, Lin Chun, for the thousand hours of labor and the extra support in the experiment performance and dissertation preparation and to my children, KerSue, Hong, and Zer, for their patience during my studies.

TABLE OF CONTENTS

	Page
ACKNOWLEDGMENTS	iii
LIST OF TABLES	viii
LIST OF FIGURES	xi
KEY TO SYMBOLS	xiv
ABSTRACT	xviii
CHAPTER 1 INTRODUCTION	1
1.1 The Advantages of GPR in Water-Table Determination	1
1.2 The Disadvantages of the Graphic Image Produced from the Graphic Recorder for Water-Table Determination	2
1.3 Prospects for Improvement of GPR in Water-Table Determination	4
1.4 Objectives of Research	5
CHAPTER 2 LITERATURE REVIEW	7
2.1 GPR Echoes from the Layered Interfaces	7
2.2 The GPR Echo from a Subsurface Cavity	8
2.3 The GPR Echo from a Saline Boundary	9
2.4 The GPR as a Monitoring Tool	10
2.5 The Effective Radar Range	11
CHAPTER 3 THE ORIGIN AND THE STATE-OF-THE-ART OF GPR.	13
3.1 Tracing Four Patents Chronologically	13
3.2 The Echo Signal of GPR and the Image	14

3.3 The Bow-Tie Antenna and the Borehole Probe 14

3.4 Multiple Receivers 14

3.5 The Underground Pipe Detector 15

3.6 The Elevated Antenna Method 15

3.7 Methods for Locating the Targets 15

3.8 Migration of the Personal Computer 16

CHAPTER 4 THE FUNDAMENTAL PRINCIPLES OF THE READOUTS OF GPR 21

4.1 Governing Equations for Electromagnetic Sine Waves in a Homogeneous Isotropic Conductive Medium 21

4.1.1 Maxwell's Equation 21

4.1.2 In a Conductive Medium 22

4.1.3 Sine Wave 23

4.2 Solutions and Properties of the Uniform Plane Wave Propagated in Direction Z 25

4.3 Reflected Readouts for an Interface Formed by Electromagnetic Wave Directly Incident to Boundaries Between Medium 1 and Medium 2 26

4.4 The Reflected Readouts for Various Subsurface Interfaces 32

4.4.1 Conductors and Dielectrics 32

4.4.2 Case 1 33

4.4.3 Case 2 34

4.4.4 Case 3 35

4.4.5 Case 4 35

CHAPTER 5 DATA ACQUISITION APPROACH FOR GPR 40

5.1 The Personal Computer-Based Data Acquisition Approach 40

5.2 DAS-50 and Real-Time Programming 40

5.3 Fourier Transformation and Effective Echo Frequencies 42

5.4 Double Mass Analysis and Actual Sample Size 46

CHAPTER 6 COMPONENTS OF THE DIGITAL ECHO SIGNAL 58

6.1 The Separation Technique Used in This Research 59

6.2 The Portion of Transmitter Loss TL 60

6.3 The Portion of Surface Reflection SR 62

6.4 The Portion of Subsurface Interface SI 63

6.5 Probing with the 120 Mhz Antenna 63

6.6 The Elevated Antenna Method 64

CHAPTER 7 CHARACTERISTICS OF ECHO SIGNALS FROM THE WATER TABLE 90

7.1 The Characteristics of the Full Spectrograms and Their Corresponding Time-Domain Series . 90

7.2 Location of Zero Surface Position in Echo Signal of a 4-M Transect Line 90

7.2.1 The E_{SR} Values for 39 GPR Transect Sites 90

7.2.2 The Ground Condition and Echo Signal of SR 91

7.3 The SI Portion from Water-Table Profile 92

7.3.1 The Typical Pattern and the Tail Peak 92

7.3.2 The Water Content of a Medium 92

7.4 Computation of Water-Table Depth 93

7.4.1 Time Scaling in the Time-Domain Series 93

7.4.2 Computation of Water-Table Depth..... 94

7.5 The Pattern and Decay of Echo Signals from the Water-Table Interface 95

7.5.1 Reflection Coefficients from Water-Table Interface..... 95

7.5.2 Pattern and Dacay 96

CHAPTER 8 MAPPING THE WATER TABLE 108

8.1 Procedure for Mapping the Water Table 108

8.2 Sampling by DAS-50 108

8.3 Removal of Transmitter Loss TL 109

8.4 Removal of Surface Reflection SR and Replacement of Ground Elevation 109

8.5 Computation of Water Table 111

8.6 Mapping the Water Table 112

CHAPTER 9 CONCLUSIONS AND SUGGESTIONS 116

9.1 Conclusions 116

9.2 Suggestions 118

APPENDIX A DATA ACQUISITION PROGRAM FOR USING DAS-50 120

APPENDIX B AN EXAMPLE OF THE SAMPLED DATA FILE BY DAS-50 128

APPENDIX C THE TIME-DOMAIN PLOTS OF A WATER-TABLE TRANSECT OF 4 M BY USING 300 MHz ANTENNA 137

APPENDIX D THE PHASE CHANGE ϕ_c OF THE 39 MEASURING SITES FROM A 4-M GPR TRANSECT LINE 145

APPENDIX E WATER CONTENTS OF SOIL PROFILES AND LOCATION OF TAIL PEAK FOR GPR PROBING SITES 147

APPENDIX F REFLECTION COEFFICIENTS FROM VARIOUS REGIONS ALONG GROUND TRUTH SOIL PROFILES.. 149

APPENDIX G THE CALIBRATION RELATIONSHIP BETWEEN WATER-TABLE DEPTH FROM GROUND SURFACE AND THE DISTANCE FROM THE WATER BODY 151

APPENCIX H THE MISCELLANEOUS..... 153

REFERENCES 156

BIOGRAPHICAL SKETCH 167

LIST OF TABLES

Page

Table 5.1. Important specifications of DAS-50 49

Table 5.2. The theoretical sample sizes (N_T) for various combinations of machine factors and sampling parameters using the DAS-50 card 50

Table 5.3. The R^2 and N_A values for various GPR perfor mance conditions using a 300 MHz antenna 51

Table 5.4. The R^2 and N_A values for various GPR performance conditions using a 120 MHz antenna 52

Table 6.1. The characteristics of a digital echo signal obtained from a good reflector in a frequency-domain analysis 65

Table 6.2. The characteristics of TL portion in time-domain plot 66

Table 6.3. The characteristics of TL portion in frequency domain for condition A (dry soil) .. 67

Table 6.4. The characteristics of TL portion in frequency domain for condition B (wet soil) .. 68

Table 6.5. The characteristics of TL portion in frequency domain for condition C (dry soil + water bag) 69

Table 6.5. The characteristics of TL portion in frequency domain for condition D (wet soil + water table) 70

Table 6.7. The characteristics of TL portion in frequency domain for condition E (water-table depth = 79 cm) 71

Table 6.8. The characteristics of TL portion in frequency domain for condition F (water-table depth = 96 cm) 72

Table 6.9. The characteristics of SR portion in frequency domain for condition A (dry soil) .. 73

Table 6.10. The characteristics of SR portion in frequency domain for condition B (wet soil) .. 74

Table 6.11. The characteristics of SR portion in frequency domain for condition C (dry soil + water bag) 75

Table 6.12. The characteristics of SR portion in frequency domain for condition D (wet soil + water table) 76

Table 6.13. The characteristics of SR portion in frequency domain for condition E (water-table site with 3 cm grass ground cover) 77

Table 6.14. The characteristics of SR portion in frequency domain for condition F (water-table site with 6 cm grass ground cover) 78

Table 6.15. The characteristics of portion SR in time-domain plot 79

Table 6.16. Weight of ΣR_p^2 of each component 80

Table 6.17. The characteristics of frequency domain for condition D by using 120 MHz antenna 81

Table 7.1. Actual sample size N_A, and end point location E_{TL}, and the important peaks for a 4-M GPR transect line.. 97

Table 7.2. End point location E_{SR} and the important peaks after TL is removed for a 4-M GPR transect line 98

Table 7.3. B_{WT}, T_{WT}, and water-table depth evaluated for a 4-M GPR transect line 99

Table 7.4. Reflection coefficient R_r calculated from sites with various soil conditions 100

Table D.1. The phase change ϕ_c of the measuring sites from a 4-M GPR transect line..... 146

Table E.1. Water contents of soil profiles and location of tail peak for GPR probing sites 148

Table F.1. Reflection coefficients from various regions along ground truth soil profiles 150

Table H.1. The operation condition of GPR in this research 154

LIST OF FIGURES

Page

Figure 1.1 An example of the graphic representation 6

Figure 2.1 Variation of maximum depth (D_e) of penetration as a function of attenuation (A) for different frequencies and of a relative dielectric constant for different earth materials..... 12

Figure 3.1 Block diagram of GPR 18

Figure 3.2 The layout of the dual antenna measurement method 19

Figure 3.3 Solving V and D for a soil layer 20

Figure 4.1 Relationship between time-varying and phasor quantities 36

Figure 4.2 Propagation of the electromagnetic wave 37

Figure 4.3 Reflection and transmission at a boundary between two conductive media 38

Figure 4.4 Boundary conditions for solving A_i and B_i in a homogenous medium 39

Figure 5.1 The personal computer-based data acquisition approach 53

Figure 5.2 The frequency spectrum shows the information sources of echo signals of experimental site.. 54

Figure 5.3 The meaning of phase change ϕ_c 55

Figure 5.4 Double mass analysis on two consecutive traces $(\Sigma x_t)_1$ and $(\Sigma x_t)_2$ for a 300 MHz antenna 56

Figure 5.5 Schematic relationship of N_T, N_A, N_P, and the scanning signals 57

Figure 6.1 Digital echo-signal plots obtained from a strong reflector 82

Figure 6.2 Time-domain plot of six different soil conditions 83

Figure 6.3 Frequency-domain spectrograms before and after the removal of TL..... 84

Figure 6.4 Various sites measured with 300 MHz antenna 85

Figure 6.5 Spectrogram for searching E_{SR} 86

Figure 6.6 Measurements of conditions B and D with the 120 MHz antenna 87

Figure 6.7 Time-domain plot and spectrograms of condition F (natural water site with 6 cm grass) for elevated positions of 300 MHz antenna 88

Figure 6.8 Decay pattern of the envelope curve from elevated position of 300 MHz antenna 89

Figure 7.1 Topographic variation versus [ϕ_c] in 39 sites of the 4-M GPR transect line 101

Figure 7.2 Relationship between the tail peak and average volumetric water content in the region above the reflected interface 102

Figure 7.3 The smoothed curve and the corresponding reflection coefficients of SI portion for site 0 M + 0 Cm 103

Figure 7.4 The smoothed curve and the corresponding reflection coefficients of SI portion for site 2 M + 10 Cm 104

Figure 7.5 The smoothed curve and the corresponding reflection coefficients of SI portion for site 3 M + 0 Cm 105

Figure 7.6 The smoothed curve and the corresponding reflection coefficients of SI portion for site 3 M + 80 Cm 106

Figure 7.7 The relationship between B_{WT} and ground truth water-table depth D_{WT} 107

Figure 8.1 Flow chart for mapping water table from a digital echo signal 113

Figure 8.2 Sketch of water-table depth in digital echo signal 114

Figure 8.3 Mappping the water table 115

Figure C.1 Time-domain plots of echo signal from sites 0 M + 0 Cm ~ 0 + 50 Cm 138

Figure C.2 Time-domain plots of echo signal from sites 0 M + 60 Cm ~ 1 M + 10 Cm 139

Figure C.3 Time-domain plots of echo signal from sites 1 M + 20 Cm ~ 1 M + 70 Cm 140

Figure C.4 Time-domain plots of echo signal from sites 1 M + 80 Cm ~ 2 M + 30 Cm 141

Figure C.5 Time-domain plots of echo signal from sites 2 M + 40 Cm ~ 2 M + 90 Cm 142

Figure C.6 Time-domain plots of echo signal from sites 3 M + 0 Cm ~ 3 M + 50 Cm 143

Figure C.7 Time-domain plots of echo signal from sites 3 M + 60 Cm ~ 3 M + 80 Cm 144

Figure G.1 The calibrated curve of water table vs distance from water in a 4-M transect line... 152

Figure H.1 The control experimental site for the artificial interfaces 155

KEY TO SYMBOLS

Symbol	Definition
$\nabla \times$	Curl
$\nabla \cdot$	Divergence
α	Attenuation coefficient of a medium
β	Phase coefficient
ϵ	Permittivity (dielectric constant)
ϵ_r	Relative dielectric constant
ϵ_x	Relative dielectric constant of a medium x
ϕ	Angle
v	Volumetric water content of soil
f	Wavelength of electromagnetic wave
μ	Permeability of a medium
ρ	Charge density
σ	Conductivity of a medium
ϕ_p	Phase
ϕ_x	Phase at location x
ϕ_c	Phase change
ω	Angular frequency

p	Angular frequency at p_{th} harmonic
A	Attenuation of a medium
A_i	Constants
a	Constant
A_o	Mean of X_t
A_n	Final constant of A
A_p	Constant of Pth harmonics
B_p	Constant of pth
$\mathbf{B}$	Magnetic strength vector in medium
B_i	Constants
b	Constant
$\mathbf{D}$	Electric strength vector in medium
D, $D_{x,r}$	Depth
D_e	Maximum exploring depth of GPR
$\mathbf{E}$	Electric strength vector
E_i	Incident electric strength
E_r	Reflected electric strength
E_t	Transmitted electric strength
E_s	Electric strength at initial condition
E_l	Electric strength at distance l
E_o	Electric strength of initial resource
$E(t)$	Electric strength is a function of time
$E(r,t)$	Phasor expression of electric strength

E_z	Electric strength along z direction
f	Period of electromagnetic waves
G	Antenna at ground
H	Magnetic strength vector
(H)	Antenna elevated at 11 inches
(2H)	Antenna elevated at 22 inches
H_i	Incident magnetic strength
H_r	Reflected magnetic strength
H_t	Transmitted magnetic strength
H_s	Magnetic strength at initial condition
H_l	Magnetic strength at distance l
H_y	Magnetic strength along Y direction
J	Conductive strength vector in a medium
j	Value in imaginary axis
K	Propagation coefficient
L	Thickness of a medium
n	Relative reflection ratio
N_T	Theoretical sample size
N_A	Actual sample size
N_p	Programmed sample size
p	u_2/u_1
q	Amplitude of the relative reflection ratio in a interface made up from two media
R^2	Percentage of interpretation

$\bar{X}_t$	Mean of X_t
X_t	Time-domain series
R_p	Amplitude of p_{th} harmonic
R_p^2	Spectrum ordinate
Σy_1	Mass value of trace 1
Σy_2	Mass value of trace 2
R	Reflection coefficient
R_e	Value in real axis
$t_{x,r}$	The travelling time of the reflected signal in dual method
t	Time
V	Propagation velocity of electromagnetic waves
V_x	Propagation velocity in the x material
$V_{x,r}$	Average velocity of the reflected signal in dual method
x	Distance between antenna in dual method
z	Distance along z direction

Abstract of Dissertation Presented to the Graduate School of the University of Florida in Partial Fulfillment of the Requirements for the Degree of Doctor of Philosophy

CHARACTERIZATION OF GROUND-PENETRATING RADAR ECHO PATTERN OF WATER TABLE

By

SHENG LIANG

August 1990

Chairperson: S.F. Shih
Major Department: Agricultural Engineering

Ground Penetrating Radar (GPR) digital echo signals obtained from a data-acquisition board were used to distinguish the water table. The theoretical explanation for the water-table detection in terms of the dielectric constants is given. The echo signals from a 4-M GPR transect of a natural site, an artificial water-table site, and a strong reflector (steel plate) were studied.

A new procedure is described in which the echo signals are separated into three components--transmitter loss (TL), surface reflection (SR), and subsurface interfaces (SI). The criteria for defining these components include characteristics from the convertible relationship between time-domain series and frequency-domain spectrograms.

The users of GPR are interested only in the SI portion because it consists of all the information from the subsurface

interfaces. This research is the first to discover that the SI portion of a water table forms a single tail peak pattern in the spectrogram and that the phase change of this tail peak appears at approximately 180°. The exclusion of the TL and SR portions depends on recognizing this unique typical pattern. This research is also significant as it proposes that a digital data file can be developed to record the ground surface readings and to extract and store the SI portion for further analyses. The frequency of the tail peak indicates the water content and thus verifies the theory that the travelling velocity of the GPR electromagnetic wave decreases in a medium with higher water content.

The important information in the SI portion for this research is the part corresponding to the water-table interface WT. The water-table signals, starting from the beginning point B_{WT}, vary with the reflection coefficients of the water-table profile. The reflection coefficient of water-table interfaces ranges from -0.05 to -0.12. The maximum reflection coefficient in the SI portion ranges from -0.10 to -0.21. Therefore, the maximum readout does not necessarily occur at a water-table interface.

The time unit of each datum can be solved so that the water-table depth D_{WT} may be obtained and the traditional dual antenna method can be applied.

CHAPTER 1
INTRODUCTION

1.1 The Advantages of GPR in Water-Table Determination

Hydrologists consider Ground-Penetrating Radar (GPR) to be superior to traditional approaches such as boreholes, piezometers, and observation wells for water-table determination because of the following reasons:

(1). GPR provides a continuous profile of two-dimensional information along the transect direction (Fetter, 1988). The traditional interpolation techniques are no longer required along this continuous line. Watershed boundary delineation becomes easier than before because this continuous transect line may transverse the watershed boundary randomly.

(2). There is no preparation cost before probing performances because it is not necessary to install any sensor or to dig any hole in the field for GPR.

(3). There is no maintainance problem in the observation network itself because there is no contact between the sensor and the target.

(4). The GPR measurements are not necessarily restricted by any predetermined spatial network.

(5). The measurements are not restricted by weather conditions or nightfall.

(6). The GPR measurement is rapid and relatively cheap.

1.2 The Disadvantages of the Graphic Image Produced from the Graphic Recorder for Water-Table Determination

Although GPR has many advantages, the state-of-the-art of GPR application to water-table probing has encountered several problems due to the limitations of the graphic recorder:

(1). Information truncation due to the blackprint threshold of a graphic recorder is serious. The conventional GPR graphic image is formed from hundreds of stylus vertical lines which represented scans of received echo signals. A scan is produced during every few inches of antenna travel along the ground. The graphic recorder converts echo signals into graphic images by printing strong signals as black vertical lines and weak signals as grey ones (Johnson et al., 1979; Shih and Doolittle, 1984; Doolittle, 1987), as shown in Figure 1.1. The threshold of the black line is ±0.5 Volt. Interpretation of the difference in signal strength beyond this threshold is therefore impossible. Since the shape of the blackline image does not directly match the spatial, actual dimension of the interface from which it is reflected,

the accurate size and boundary positions of any interface are not interpretable.

(2). Shallow interfaces can not be estimated due to the existence of a dead zone of measurement in the top surface of the ground. Johnson and his associates (1979) noted that the upper 38 cm of soil were not detectable by any 300 and 900 Mhz antennas because the first strong surface reflection masked any changes in that part of the soils. This means that both of the zero surface positions and the nearest-surface structures are not determinable under natural soil conditions. This disadvantage prevents the direct distinction of the water table from the graphic images, especially under the natural condition of a shallow water table occurring in Florida (McCollum et al., 1976; Shih & Doolittle, 1984; Snyder et al., 1978; Terry et al., 1980).

(3). It is not necessarily true that the water tables are presumed as black images or as the strongest reflection by previous researchers (Asmussen et al., 1986; Doolittle, 1987; Sellmann et al., 1983; Shih et al., 1986). The lack of a distinct record of the water-table interface in the graphic images (Figure 1.1) can be explained through the use of Eq. 1.2.1 (see Chapter 4 for the derivation of this equation).

$$R_r(z, t+2t_r) = \frac{\sqrt{\epsilon_1} - \sqrt{\epsilon_2}}{\sqrt{\epsilon_1} + \sqrt{\epsilon_2}} E_i(z, t) \qquad 1.2.1$$

where ϵ_i is the relative dielectric constant for medium i. Because of the existence of a capillary fringe zone and the close correlation between soil moisture content and relative dielectric constant, the upper and lower counterparts of the water-table interface can be expected to reflect weaker echo signals and hence produce lower values of R(z,t+2tr).

(4). The recording medium is dry electrosensitive paper. Since the sunlight, temperature variation, and folding will cause damages in the graphic images, data quality may not be confident.

1.3 Prospects for Improvement of GPR in the Water-Table Determination

For water-table determination, analyses based on the pretreated, original, real-time, echo-analog signal prior to the graphic recorder would be a potential solution to the information truncation problem, although no research reports have emphasized it to date. By application of this concept, the zero position could be determined, and, consequently, the problem of a dead zone could be solved by proper analysis. The low readout from the water-table interface could be readable.

The existence of a capillary fringe zone can be recognized properly.

1.4 Objectives of Research

The specified objectives of this study are as follows:

(1). To review the principles of GPR detections.

(2). To derive the theoretical expression of the reflection coefficient for the water-table interface.

(3). To develop a procedure to recognize the components of a digital echo signal from the water-table profile.

(4). To characterize the parameters pertaining to various components of a water-table echo signal.

(5). To characterize the response pattern of the water-table interface.

(6). To map the water-table profile along the GPR transect line.

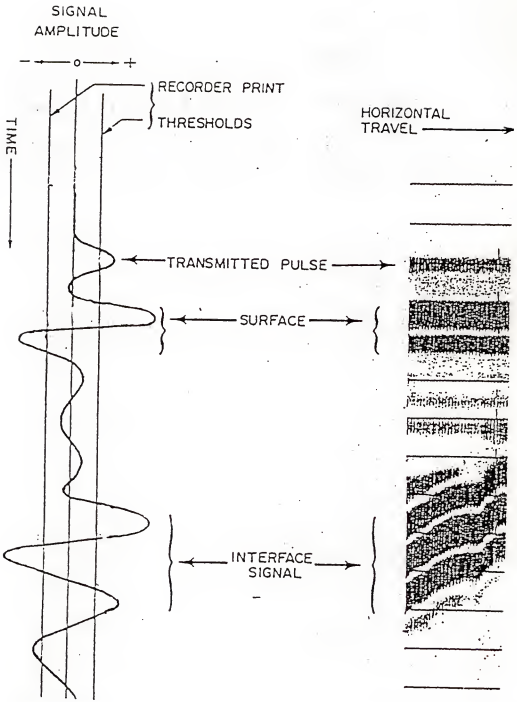

A. The echo signal. B. The graphic image

Figure. 1.1. An example of the graphic representation. (After Johnson et al., 1979).

CHAPTER 2
LITERATURE REVIEW

2.1 GPR Echoes from the Layered Interfaces

The positive proportional relationship of water content (θ_v) to relative dielectric constant (ϵ_r) has been built after numerous studies (Davis, 1975; Davis et al., 1977; Fellner-Feldegg, 1969; Hoekstra & Delaney, 1974; Jesch, 1978; King & Smith, 1981; Lane and Saxton, 1952; Newton et al., 1980; Newton & Rouse, 1976: Njoku & Kong, 1977; Okrasinski et al., 1978; Ra, 1972; Ruault & Tabbagh, 1980; Schmugge, 1980; Selig, 1975; Wang, 1980; Wang & Schmugge, 1980). The typical equation appears as Eq. 2.1.1, which was proposed by Topp and his associates (1980).

$$\epsilon_r = 3.03 + 9.30\ \theta_v + 146.00\ \theta_v^2 - 76.70\ \theta_v^3 \qquad 2.1.1$$

From this equation, the abrupt change in the water content at the interface boundary between two different media can be expected to cause an abrupt change in the relative dielectric constant. The echo strength $R(z,\ t+2t_r)$ becomes stronger (either positive or negative) in response to this abrupt shift of ϵ_r, according to Eq. 1.2.1. This principle has formed the basis of applications involving determination of such parameters as peat thickness (Bjelm, 1980; Shih &

Doolittle, 1984; Ulriksen, 1980, 1983), water-table depth (El-Said, 1956; McCollum et al., 1976; Sellmann et al., 1983; Shih et al., 1986; Zhody et al., 1984), and watershed delineation (Asmussen et al., 1986; Truman et al., 1988a; Truman et al., 1988b). The delineations of subsurface rock features (Cook, 1974; Fowler, 1981; Lundien, 1971; Rubin & Fowler, 1978), mine ore deposits (Cook, 1975; Harrison, 1970; Pittman et al., 1984), slope terrain (Olson & Doolittle, 1985), archaeological sites (Fisher, 1980), and soil microvariation (Collins et al., 1986; Collins & Doolittle, 1987; Doolittle, 1982, 1983) have also been based on this principle. Similar applications have included snow, ice, or permafrost layer (low ϵ_1) above water or a wet soil layer (high ϵ_2) (Acrone et al., 1978; Annan & Davis, 1976, 1977; Campbell & Orange, 1974; Cook, 1960; Evan, 1963; O'Neill & Acrone, 1988; Watts & Wright, 1981).

2.2 The GPR Echo from a Subsurface Cavity

When a subsurface cavity occurs, a boundary between the soil and air exists. From Eq. 4.2.11 and 4.2.8 the propagation velocity (V_a) in air (with ϵ_a=1) is 30 cm/ns. The propagation velocity (V_x) in soil (with relative dielectric constant of ϵ_x) may be computed from Eq. 2.2.1,

$$V_x = \frac{30^{cm/ns}}{\sqrt{e_x}} \qquad 2.2.1$$

The propagation velocity within cavity is two (dry) to six (wet) times faster than within soil. This difference is sufficient to produce a special return of electromagnetic waves (causing denser echoes or stronger echoes). consequently, explorations for cavities or for voids in dams (Silver et al., 1986) and karst terrain (Ballard, 1982; Beck and Wilson, 1988; Gilboy, 1987; Hearn, 1987; Kuhns, 1982; Stangland and Kuo, 1987), and for voids formed by pipes (Doolittle, 1987; Hara et al., 1983; Hearn, 1987; Rubin & Fowler, 1978; Zobeck et al., 1985), and buried containers (Bowder et al., 1982) have been very successful.

2.3 The GPR Echo from a Saline Boundary

A subsurface saline region generally shows a high conductivity in Eq. 2.3.1 (see Chapter 4 for the derivation of this equation),

$$R = \frac{\sqrt{(p^2 - q^2)^2 + (2pq\sin\Phi)^2}}{p^2 + q^2 + 2pq\cos\Phi} e^{j\phi} \qquad 2.3.1$$

wehere p is μ_2/μ_1, q is amplitude, and ϕ is phase.

$$q = \frac{\sqrt{\mu_2 e_2 \sqrt{1^2 + (\frac{\sigma_2}{\omega e_2})^2}}}{\sqrt{\mu_1 e_1 \sqrt{1^2 + (\frac{\sigma_1}{\omega e_1})^2}}} \qquad 2.3.2$$

$$\phi = \tan^{-1}\left(-\frac{\sigma_2}{\omega\varepsilon_2}\right) + \tan^{-1}\left(-\frac{\sigma_1}{\omega\varepsilon_1}\right) \qquad 2.3.3$$

In the case of $\frac{\sigma_1}{\omega\varepsilon_1} << 1$ and $\frac{\sigma_2}{\omega\varepsilon_2} > 1$, a second medium with high conductivity would produce an R value two times or higher than that for a second medium with a $\frac{\sigma^2}{\omega\varepsilon_2} << 1$ which may cause no reflection (Jordan & Balmain, 1968). This higher R value may not be good enough to produce a blackprint in a graphic image because it also may be weak.

Applications of this principle include detection of lake bottoms (Ulriksen, 1987), nuclear waste (Horton & Morey, 1982; Horton et al., 1982), organic waste (Olhoeft, 1986), contaminated sites (Glaccum et al., 1981), concrete damages caused by salt (Ulriksen, 1983), and saline soil layers (Shih, Myhre, and Schellentrager, 1985).

2.4 The GPR As a Monitoring Tool

Since echoes from cavities, layered interfaces, or saline regions are instantly detected, GPR has been suggested as a sensor to monitor land subsidence and cavity enlargement (Benson & Yuhr, 1987), excavating programs (Moffatt et al., 1973), and site investigations (Glaccum et al., 1981; Hara, 1985; Sakayama et al., 1988; Stangland and Kuo, 1987). Moreover, GPR was used in the Apollo 17 mission to probe the lunar soils (Porcello, 1974; Simmons, 1973).

2.5 The Effective Radar Range

The GPR approximate ground exploration depth, D_e, is in the following equation (Hara, 1985):

$$70 - 109\frac{vD_e}{\rho} - 20\log\frac{\lambda R}{D_e} \qquad 2.5.1$$

where v = propagation velocity in the ground, cm/ns,

D_e = maximum exploration depth, m,

ρ = resistivity, Ω. m,

λ = wavelength of electromagnetic waves, m, and

R = reflection coefficient (0.001 or less).

The propagation velocity in the ground varies from 15 cm/ns to 5 cm/ns according to Eq. 2.2.1. For the high resistivity case (dry soil) of 1,000 Ωm with f = 100 MHz and v = 10 cm/ns, D_e ranges from 10 m to 20 m. For the low resistivity case (wet soil) of 100 Ωm, D_e is reduced to 3-4 m.

A more comprehensive quantitative picture of the penetration performance of GPR is shown in Figure 2.1 (Horton et al., 1981; Markt, 1988; Smith, 1988). The attenuation A is approximated by

$$A = 8.68\ \alpha\ (dB/m) \qquad 2.5.2$$

where α is the attenuation coefficient of the medium.

According to Figure 2.1, the penetration depth for a 300 MHz in wet sand could reach 15 m.

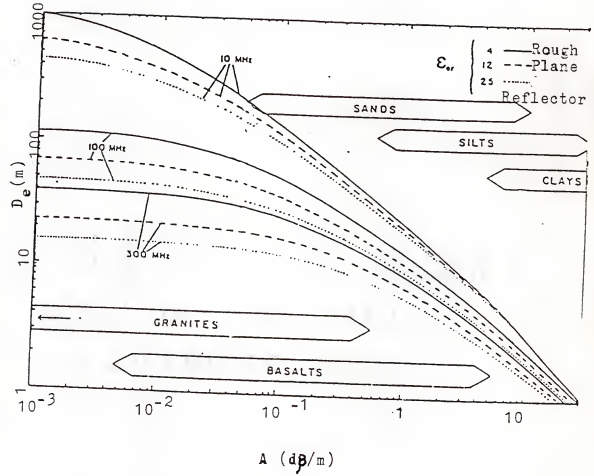

Figure 2.1 Variation of maximum depth (D_e) of penetration as a function of attenuation (A) for different frequencies and of a relative dielectric constants for different earth materials (Horton et al., 1981).

CHAPTER 3
THE ORIGIN AND THE STATE-OF-THE-ART OF GPR

3.1 Tracing Four Patents Chronologically

A patent entitled "Electromagnetic Prospecting Method" was granted to Melton (1937). He described a method, based on the time of travel of echoed waves as obtained by a visual receiver, for locating buried geological formations.

A patent entitled "Underground Prospecting System" was granted to Donaldson (1953). He emphasized the machine system of measurement. A generator migrated electromagnetic pulses into the ground, and the echoed waves were received by an oscilloscope.

A patent entitled "Geophysical Surveying System Employing Electromagnetic Impulses" was granted to Morey (1974). This is the GPR of today and is used in this research. A block diagram of GPR is shown in Figure 3.1.

A similar patent entitled "Ground Radar System" was granted to Lerner (1974). He emphasized that the function of the system was to launch radiation and receive reflections from underground discontinuities which excluded the clutters from both the surface and subsurface. The latter clutters referred to voids or any reflector within 3 M.

3.2 The Echo Signal of GPR and the Graphic Image

Until now, the graphic image, as shown in Figure 1.1, had served as the sole interpretable source of subsurface for GPR researchers. The graphic image was bimasked by grey and black. The black threshold is ± 0.5 voltage and the black image is the only portion of importance to the researchers.

3.3 The Bow-Tie Antenna and the Borehole Probe

After 1972, Geophysical Survey System Inc. in the United States and Oyo Co. in Japan produced GPR systems with the Bow-Tie Antenna (Chan et al., 1981; Church & Webb 1986). This type of GPR may be towed along the ground or may be airborne. According to Church and Webb (1986), during the late 1970s and early 1980s, a borehole probe was developed by the South West Research Institute for the United States Department of the Interior. This type of antenna was restricted to borehole use only. This kind of GPR is applicable for projects involving deeper or lateral subsurface features.

3.4 Multiple Receivers

Oyo Co. in Japan in the 1980s developed a new radar system, Georadar II, with the objective of improving the accuracy of exploration by multiplying the number of receivers by four or six.

3.5 The Underground Pipe Detector

A GAR with a pair of axially aligned transmitting arms was created by Ohio State University (Young and Caldecott, 1976, 1977). This radar was announced to locate the pipes. Later, this kind of GAR was named as Terrascan (Miller, 1986).

3.6 The Elevated Antenna Method

Gudmansen in 1972 (Ulriksen, 1983) suggested that the reflected energy density will become greater as the antenna position is elevated. Ulriksen (1983) suggested that the elevating position of the antenna allowed separation of transmitter loss and surface reflection from echo signals of subsurface interfaces.

3.7 Methods for Locating the Targets

There are two kinds of target--one is the point object target, the other is the layered target. For a point object target, Hogan (1988) suggested the migration method. For a layered target, the dual antenna method is applicable. The dual antenna method is described below:

(1). Two antennas are arranged as shown in Figure 3.2. The basic equation may be written as follows:

$$\sqrt{(\frac{X}{2})^2 + D_{x,r}^2} = \frac{t_{x,r}}{2} \cdot V_{x,r} \qquad 3.5.1$$

where X is the distance between antennas, D_r is the depth to target location as shown in Figure 3.2, and $V_{x,r}$ and $t_{x,r}$ are the average velocity and travel time measured at distance X, respectively. Eq. 3.5.1 may be rewritten as

$$t_{x,r}^2 = \frac{1}{V_{x,r}^2} \cdot X^2 + \frac{4D_{x,r}^2}{V_{x,r}^2} \qquad 3.5.2$$

(2). Several measurements are performed by changing the X distance.

(3). These x^2 values and the corresponding t^2 are plotted as shown in Figure 3.3.

(4). The intercept value $\frac{4D^2}{V^2}$ and slope value $\frac{1}{V^2}$ are obtained to solve the two unknown values D and V.

3.8 Migration of the Personal Computer

Physical data are becoming easier to measure, analyze, manipulate, and control because of the development of relatively inexpensive personal computer hardware and software. For instance, Ulriksen in 1983 used an HP 3437 system voltmeter to integrate the reflection intensity over a specific period and an HP 85 microcomputer, which is a popular microcomputer applied in time-domain measurement of transient radar (Miller, 1986), for storage. Today this may be replaced by installing a data acquisition board into any

personal computer and by using a simple summation program. Therefore, the introduction of the personal computer to GPR applications can result in improvements in the GPR approach. When equipped with a specified board, a computer becomes a data acquisition system that can accept GPR analog data, convert it into digital form, store it, and perform any further mathematical processes on it.

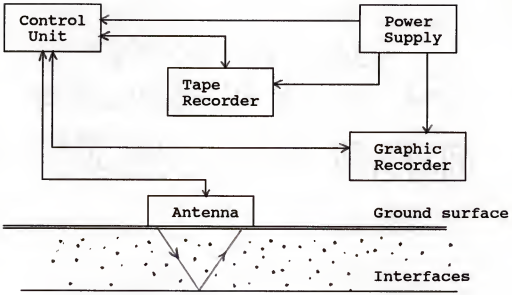

Figure 3.1 Block diagram of GAR

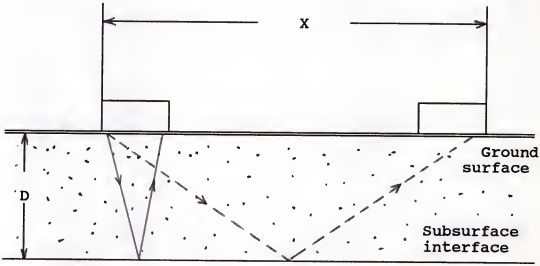

Figure 3.2 The layout of the dual antenna measurement method.

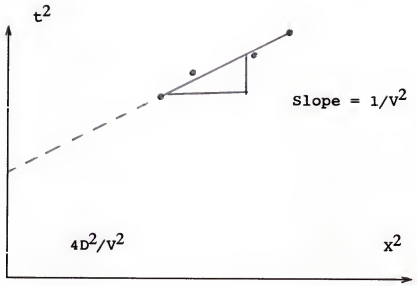

Figure 3.3. Solving V and D for a soil layer.

CHAPTER 4
THE FUNDAMENTAL PRINCIPLES OF THE READOUTS OF GPR

4.1 Governing Equations for Electromagnetic Sine Waves in a Homogeneous Isotropic Conductive Medium

4.1.1 Maxwell's Equation

The electromagnetic field may be described by Maxwell's eqs. as outlined by Jordan and Balmain (1968) as follows:

$$\mathbf{V} \times \mathbf{H} = \dot{\mathbf{D}} + \mathbf{J} \qquad 4.1.1^{*}$$

$$\mathbf{V} \times \mathbf{E} = -\dot{\mathbf{B}} \qquad 4.1.2$$

$$\mathbf{V} \cdot \mathbf{D} = \rho \qquad 4.1.3$$

$$\mathbf{V} \cdot \mathbf{B} = 0 \qquad 4.1.4$$

where $\mathbf{V}\times$ is the curl of a vector--it means differentiation with respect to space and is a vector too; $\mathbf{V}\cdot$ is the divergence of a vector and means the scaler net outflux of a force vector; $\mathbf{E}$ and $\mathbf{H}$ indicate the electric and magnetic strength in the field, respectively; $\dot{\mathbf{D}}$ and $\dot{\mathbf{B}}$ are the partial differentiation with respect to time; and $\mathbf{D}$, $\mathbf{B}$, and $\mathbf{J}$ are the electric (convective), the magnetic, and the conductive

---

* The bold capital letter notes vectors in this research.

strength vectors, respectively. The characteristics of the medium may be subject to the following conditions:

$$\mathbf{D} = \epsilon\mathbf{E} \qquad 4.1.5$$

$$\mathbf{B} = \mu\mathbf{H} \qquad 4.1.6$$

$$\mathbf{J} = \sigma\mathbf{E} \qquad 4.1.7$$

where ϵ (Farady/m), μ (Henry/m), and σ (Mho/m) are the permittivity (also termed as dielectric constant), permeability, and conductivity of the medium, which is assumed to be homogeneous, isotropic, and source-free. A homogeneous medium is one for which the quantities ϵ, μ, σ are constant throughout the medium. The medium is isotropic if ϵ is a scaler constant, so that $\mathbf{D}$ (coulomb/m^2) and $\mathbf{E}$ (volt/m) everywhere have the same direction throughout the medium. Eqs. 4.1.1 and 4.1.2 are for source-free regions in which there are no impressed voltages or currents or generator (Jordan & Balmain, 1968).

4.1.2 In a Conductive Medium

Differentiating with respect to time, Eq. 4.1.5 becomes

$$\dot{\mathbf{D}} = \epsilon\dot{\mathbf{E}} \qquad 4.1.8$$

$$\ddot{\mathbf{D}} = \epsilon\ddot{\mathbf{E}} \qquad 4.1.9$$

From Eqs. 4.1.7, 4.1.8, and 4.1.9, Eq.4.1.1 becomes

$$\nabla \times \mathbf{H} = \epsilon\dot{\mathbf{E}} + \sigma\mathbf{E} \qquad 4.1.10$$

$$\nabla \times \dot{\mathbf{H}} = \epsilon\ddot{\mathbf{E}} + \sigma\dot{\mathbf{E}} \qquad 4.1.11$$

Differentiating Eq. 4.1.6 with respect to time yields

$$\dot{\mathbf{B}} = \mu\dot{\mathbf{H}} \qquad 4.1.12$$

Taking the curl of both sides of Eq. 4.1.2 and applying Eqs. 4.1.11 and 4.1.12,

$$\nabla \times (\nabla \times \mathbf{E}) = -\nabla \times \dot{\mathbf{B}} = -\mu\nabla \times \dot{\mathbf{H}} = -\mu\epsilon\ddot{\mathbf{E}} - \mu\sigma\dot{\mathbf{E}} \qquad 4.1.13$$

Using the vector identity (Davis & Snider, 1987)

$$\nabla \times \nabla \times \mathbf{E} = \nabla (\nabla \cdot \mathbf{E}) - \nabla^2\mathbf{E} \qquad 4.1.14$$

and from Eq. 4.1.5, $\mathbf{E} = \dfrac{\mathbf{D}}{\epsilon}$ 4.1.15

Taking the divergence of Eq. 4.1.15 and of Eq. 4.1.3 yields

$$\nabla \cdot \mathbf{E} = \frac{1}{\epsilon} \nabla \cdot \mathbf{D} = \frac{1}{\epsilon} \cdot \rho \qquad 4.1.16$$

When there is no net charge within a conductor, the charge density equals zero,

$$\nabla \cdot \mathbf{D} = 0 \qquad 4.1.17$$

and Eq. 4.1.16 becomes

$$\nabla \cdot \mathbf{E} = 0 \qquad 4.1.18$$

the right side of Eq. 4.1.14. Thus, it is simplified as

$$\nabla \times (\nabla \times \mathbf{E}) = 0 - \nabla^2\mathbf{E} = - \nabla^2\mathbf{E} \qquad 4.1.19$$

Equating Eqs. 4.1.13 and 4.1.19, the wave equation for $\mathbf{E}$ is obtained as shown in Eq. 4.1.20,

$$\nabla^2\mathbf{E} = \mu\epsilon\ddot{\mathbf{E}} + \mu\sigma\dot{\mathbf{E}} \qquad 4.1.20$$

4.1.3 Sine Wave

The GPR antenna transmits voltages and currents and hence electric and magnetic fields, which vary sinusoidally

with time t. This can be expressed as

$$E(t) = E_0 \cos \omega t \qquad 4.1.21$$

where w=2 f (f is the angular frequency), and E_0 is the amplitude (or strength) of the initial source. Representing Eq. 4.1.21 in phasor form as shown in Figure 4.1,

$$E(r) = Re[E_0 e^{j\omega}] \qquad 4.1.22$$

that is,

$$E(r,t) = Re[E_0(r)\, e^{j\omega t}] \qquad 4.1.23$$

$$E(r,t) = j\omega Re[E_0(r)\, e^{j\omega t}] = j\omega E(r,t) \qquad 4.1.24$$

$$E(r,t) = j^2\omega^2 Re[E_0(r)\, e^{j\omega t}] = -\omega^2 E(r,t) \qquad 4.1.25$$

Introducing Eqs. 4.1.24 and 4.1.25 into Eq. 4.1.20,

$$\nabla^2 \mathbf{E} = -\mu\varepsilon\omega^2 \mathbf{E} + j\mu\sigma\omega\mathbf{E} \qquad 4.1.26$$

Eq. 4.1.25 can be rewritten as

$$\nabla^2 \mathbf{E} + K^2 \mathbf{E} = 0 \qquad 4.1.27$$

where

$$K = \sqrt{\mu\varepsilon\omega^2 - j\sigma\omega} = \omega\sqrt{\mu\varepsilon\left(1-\frac{j\sigma}{\omega\varepsilon}\right)} = \omega\sqrt{\mu\varepsilon\left(1+\frac{\sigma}{j\omega\varepsilon}\right)} \qquad 4.1.28$$

Similarly,

$$\nabla^2 H + K^2 H = 0 \qquad 4.1.29$$

4.2 Solutions and Properties of the Uniform Plane Wave Propagated in Direction Z

Eq. 4.1.27 can be rewritten as

$$\frac{\partial^2 E}{\partial Z^2} = (jk)^2 E \qquad 4.2.1$$

To satisfy the electric field strength as shown in Eq. 4.2.1, one solution (Jordan & Balmain, 1968) of the uniform plane wave travelling in direction z is

$$E(z) = E_0 e^{-jkz} \qquad 4.2.2$$

Referring to Eq. 4.1.23

$$\begin{aligned} E(z,t) &= \mathrm{Re}\{E_0 e^{-jkz+j\omega t}\} \\ &= \mathrm{Re}\{E_0 e^{j(\omega t-kz)}\} \\ &= E_0[\cos(\omega t-kz)+j\sin(\omega t-kz)] \end{aligned} \qquad 4.2.3$$

That is, for plane waves propagated in direction z that veer off in direction x as shown in Figure 4.2, the solution for wave propagation can be obtained as Eqs. 4.2.4 and 4.2.5:

$$E_x = E_0\,[\cos(\omega t-kz)+j\sin(\omega t-kz)] \qquad 4.2.4$$

$$H_y = H_0[\cos(\omega t-kz)+j\sin(\omega t-kz)] \qquad 4.2.5$$

where K is defined as the propagation coefficient.

$$K = \omega\sqrt{\mu\epsilon(1 + \frac{\sigma}{j\omega\epsilon})} \qquad 4.1.28$$

K may be rewritten as

$$K = \beta - j\alpha \qquad 4.2.6$$

where

$$\alpha = \omega\sqrt{\frac{\mu\epsilon}{2}}\sqrt{\sqrt{1^2 + (\frac{\sigma}{\omega\epsilon})^2} - 1} \qquad 4.2.7$$

$$\beta = \omega\sqrt{\frac{\mu\epsilon}{2}}\sqrt{\sqrt{1^2 + (\frac{\sigma}{\omega\epsilon})^2} + 1} \qquad 4.2.8$$

The symbol α is called the attenuation coefficient and β is the phase coefficient. Substituting Eq. 4.2.6 into Eq. 4.2.4,

$$\begin{aligned} E_x &= E_0 e^{j(\omega t - kz)} \\ &= E_0 e^{j[\omega t - (\beta - j\alpha)z]} \\ &= E_0 e^{-\alpha z} e^{j(\omega t - \beta z)} \end{aligned} \qquad 4.2.9$$

Similarly,

$$H_y = H_0 e^{-\alpha z} e^{j(\omega t - \beta z)} \qquad 4.2.10$$

That is, electromagnetic waves in a conductive medium are attenuated as $e^{-\alpha z}$ and are propagated at a velocity in direction z.

$$V = \frac{z}{t} = \frac{\omega}{\beta} \qquad 4.2.11$$

4.3 Reflected Readouts for an Interface Formed by Electromagnetic Waves Directly Incident to Boundaries Between Medium 1 and Medium 2

According to the boundary conditions imposed on Maxwell's equations, when a uniform plane wave in a medium with

constants ϵ_1, μ_1, and σ_1 is normally incident upon a second medium of infinite depth having the constants ϵ_2, μ_2, and σ_2, as shown in Figure 4.3, at the boundary (the surface of discontinuity), continuity of tangential field components demands that Eqs. 4.3.1 and 4.3.2 hold (Jordan & Balmain, 1968),

$$E_i + E_r = E_t \qquad 4.3.1$$

$$H_i + H_r = H_t \qquad 4.3.2$$

where E_i and H_i are the incident strengths, E_r and H_r are the reflected strengths, and E_t and H_t are the transmitted strengths. Rewriting Eqs. 4.1.2, 4.1.12, and 4.1.10 for a homogeneous medium

$$\nabla \times \mathbf{E} = -\mu \frac{\partial \mathbf{H}}{\partial t} \qquad 4.3.3$$

$$\nabla \times \mathbf{H} = \epsilon \frac{\partial \mathbf{E}}{\partial t} + \sigma \mathbf{E} \qquad 4.3.4$$

For a uniform plane wave propagating in the z direction and having only components E_x and H_y, Eqs. 4.3.3 and 4.3.4 may be rewritten as

$$\frac{\partial E_x}{\partial z} + \mu \frac{\partial H_y}{\partial t} = 0 \qquad 4.3.5$$

$$\frac{\partial H_y}{\partial z} - \epsilon \frac{\partial E_x}{\partial t} - \sigma E_x = 0 \qquad 4.3.6$$

From Eq. 4.1.24, Eq. 4.3.6 becomes

$$\frac{\partial H_y}{\partial z} - (\sigma + j\omega\epsilon) E_x = 0 \qquad 4.3.7$$

Similarly, from Eq. 4.1.24, Eq. 4.3.5 becomes

$$\frac{\partial E_x}{\partial z} + (0 + j\omega\mu) H_y = 0 \qquad 4.3.8$$

Differentiating Eqs. 4.3.7 and 4.3.8 yields

$$\frac{\partial^2 E_x}{\partial z^2} - (j\omega\mu)(\sigma+j\omega\epsilon) E_x = 0 \qquad 4.3.9$$

$$\frac{\partial^2 H_y}{\partial z^2} - (j\omega\mu)(\sigma+j\omega\epsilon) H_y = 0 \qquad 4.3.10$$

There are two solutions (Jordan & Balmain, 1968) for Eqs. 4.3.9 and 4.3.10. One possible solution is

$$E = A_1 e^{-j\Gamma z} + B_1 e^{j\Gamma z} \qquad 4.3.11$$

$$H = A_2 e^{-j\Gamma z} + B_2 e^{j\Gamma z} \qquad 4.3.12$$

where $\Gamma^2 = j\omega\mu(\sigma+j\omega\epsilon)$ 4.3.13

The other solution (this is a useful solution according to Jordan & Balmain, 1968) is

$$E = A_1 \cosh \Gamma z + B_1 \sinh \Gamma z \qquad 4.3.14$$

$$H = A_2 \cosh \Gamma z + B_2 \sinh \Gamma z \qquad 4.3.15$$

From the boundary conditions shown in Figure 4.4, $E=E_r$ and $H=H_r$ at $z=0$ and $E=E_s$ and $H=H_s$ at $z=z_1$, the solution is

$$A_1 = E_r \qquad 4.3.16$$

$$B_1 = -\eta H_r = -\sqrt{\frac{j\omega\mu}{\sigma+j\omega\epsilon}}\,.H_r \qquad 4.3.17$$

$$A_2 = H_r \qquad 4.3.18$$

$$B_2 = \frac{E_r}{\eta} = -\sqrt{\frac{\sigma+j\omega\epsilon}{j\omega\mu}}\,.E_r \qquad 4.3.19$$

where

$$\eta = \sqrt{\frac{j\omega\mu}{\sigma+j\omega\epsilon}}$$

is called the characteristic impedance of the medium. When $L=-z_1$, Eqs. 4.3.17 and 4.3.19 become Eqs. 4.3.20 and 4.3.21

$$E_S = E_r \cosh \Gamma L + \eta H_r \sinh \Gamma L \qquad 4.3.20$$

$$H_S = H_r \cosh \Gamma L + \frac{E_r}{\eta} \sinh \Gamma L \qquad 4.3.21$$

If the homogeneous medium 1svery thick, Re{ΓL} will be a large quantity

$$\cosh \Gamma L \approx \frac{e^{\Gamma L}}{2} \approx \sinh \Gamma L \qquad 4.3.22$$

$$\frac{E_s}{H_s} = \eta \qquad 4.3.23$$

Applying Eq. 4.3.23, and referring to Figure 4.3,

$$\eta_1 H_i = E_i \tag{4.3.24}$$

$$\eta_1 H_r = -E_r \tag{4.3.25}$$

$$\eta_2 H_t = E_t \tag{4.3.26}$$

Since E_i is known, the unknown E_r and E_t can be expressed in terms of η.

From Eq. 4.3.1 $\quad E_r - E_t = -E_i$ 4.3.27

From Eq. 4.3.2 $\quad H_r - H_t = -H_i$

$$\Rightarrow -\frac{E_r}{\eta_1} - \frac{E_t}{\eta_2} = -\frac{E_i}{\eta_1} \Rightarrow \frac{E_r}{\eta_1} + \frac{E_t}{\eta_2} = \frac{E_i}{\eta_1} \tag{4.3.28}$$

The solutions of Eqs. 4.3.27 and 4.3.28 are

$$\frac{E_r}{E_i} = \frac{\eta_2 - \eta_1}{\eta_2 + \eta_1} \tag{4.3.29}$$

$$\frac{E_t}{E_i} = \frac{2\eta_2}{\eta_1 + \eta_2} \tag{4.3.30}$$

Similarly, for the magnetic field,

$$\frac{H_r}{H_i} = \frac{\eta_1 - \eta_2}{\eta_2 + \eta_1} \tag{4.3.31}$$

$$\frac{H_t}{H_i} = \frac{2\eta_1}{\eta_2 + \eta_1} \tag{4.3.32}$$

Eq. 4.3.29 is defined as the reflection coefficient, which can be represented by R as Eq. 4.3.33

$$R = \frac{E_r}{E_i} = \frac{\eta_2 - \eta_1}{\eta_2 + \eta_1} = \frac{\sqrt{\frac{j\omega\mu_2}{\sigma_2+j\omega e_2}} - \sqrt{\frac{j\omega\mu_1}{\sigma_1+j\omega e_1}}}{\sqrt{\frac{j\omega\mu_2}{\sigma_2+j\omega e_2}} + \sqrt{\frac{j\omega\mu_1}{\sigma_1+j\omega e_1}}}$$

$$= (\mu_2 - \mu_1 n)/(\mu_2 + \mu_1 n) \qquad 4.3.33$$

where the relative reflection ratio n is represented by Eq. 4.3.34

$$n = \frac{\sqrt{\mu_2 (e_2 + \frac{\sigma_2}{j\omega})}}{\sqrt{\mu_1 (e_1 + \frac{\sigma_1}{j\omega})}} = \frac{k_2}{k_1} = q.e^{j\phi} \qquad 4.3.34$$

the magnitude q is expressed as

$$q = \frac{\sqrt{\mu_2 e_2 \sqrt{1^2 + (\frac{\sigma_2}{\omega e_2})^2}}}{\sqrt{\mu_1 e_1 \sqrt{1^2 + (\frac{\sigma_1}{\omega e_1})^2}}} \qquad 4.3.35$$

and the phase Φ is expressed as

$$\phi = \tan^{-1}(\frac{\frac{-\sigma_2}{\omega e_2}}{1}) + \tan^{-1}(\frac{\frac{-\sigma_1}{\omega e_1}}{1}) = \tan^{-1}(\frac{-\sigma_2}{\omega e_2}) + \tan^{-1}(\frac{-\sigma_1}{\omega e_1}) \qquad 4.3.36$$

From Eq. 4.3.34, Eq. 4.3.33 may be rewritten as

$$R = \frac{\mu_2 - \mu_1 q e^{j\phi}}{\mu_2 + \mu_1 q e^{j\phi}} = \frac{p - q e^{j\phi}}{p + q e^{j\phi}} \qquad 4.3.37$$

where $p = \frac{\mu_2}{\mu_1}$ = magnetic permeability ratio 4.3.38

and Eq. 4.3.37 may be rewritten as

$$R = \frac{p-(q\cos\phi+jq\sin\phi)}{p+(q\cos\phi+jq\sin\phi)} = \frac{p^2-q^2-2jpq\sin\phi}{p^2+q^2+2jpq\cos\phi} \quad 4.3.39$$

Eq. 4.3.39 may be further rewritten as

$$R = \frac{\sqrt{(p^2-q^2)^2+(2pq\sin\phi)^2}\cdot e^{j\phi}}{p^2+q^2+2pq\cos\phi} \quad 4.3.40$$

Therefore, the reflection readout may be expressed as

$$E_r(z,t+2t_r) = R(z,\ t+2t_r)\ \cdot\ E_i(z,t)$$

$$= \frac{\sqrt{(p^2-q^2)^2+(2pq\sin\phi)^2}\ e^{j\phi}}{p^2+q^2+2pq\cos\phi}\cdot E_i(z,t) \quad 4.3.41$$

where $2t_r$ means travelling time including back and forth paths, E_i is the incident electric strength, and E_r is the reflected electric strength.

4.4 The Reflected Readouts for Various Subsurface Interfaces

4.4.1 Conductors and Dielectrics

In electromagnetics, materials are divided roughly into two classes: Conductors and dielectrics (insulator). From Eqs. 4.1.1, 4.1.8, and 4.1.23, Eq. 4.4.1 is obtained as

$$\nabla \times H = \underbrace{\sigma E}_{\text{Conduction current density}} + \underbrace{j\omega\epsilon E}_{\text{Displacement current density}} \qquad 4.4.1$$

The ratio of $\sigma/\omega\epsilon$ represents the ratio of conduction current density to displacement current density, and $\frac{\sigma}{\omega\epsilon}=1$ may be considered to mark the dividing line between conductors and dielectrics (Jordan & Balmain, 1968). For good conductors (such as metals), $\sigma/\omega\epsilon >> 1$. For instance, copper at 30,000 MHz has $\sigma/\omega\epsilon = 3.5 \times 10^8$. For good dielectrics, $\sigma/\omega\epsilon << 1$, for example, mica has $\sigma/\omega\epsilon = 0.0002$.

4.4.2 Case 1

When $\frac{\sigma_1}{\omega\epsilon_1} << 1$ and $\frac{\sigma_2}{\omega\epsilon_2} << 1$, the upper and lower layers are close to being nonconductors for the incident plane wave. From Eq. 4.3.38, Eq. 4.3.35 becomes

$$q = \sqrt{\frac{\mu_2\epsilon_2}{\mu_1\epsilon_1}} - \sqrt{p\frac{\epsilon_2}{\epsilon_1}} \qquad 4.4.2$$

The permeability of all known insulators is not appreciably different from that of free space, $\mu_1 = \mu_2 = \mu_v$. Therefore,

$$p = 1 \qquad 4.4.3$$

Eq. 4.4.2 is thus

$$q = \sqrt{\frac{\epsilon_2}{\epsilon_1}} \qquad 4.4.4$$

From Eq. 4.4.2 is thus

$$\phi = 0 \qquad 4.4.5$$

It follows that cos ϕ = 1 and $e^{j\phi}$ = 1 and Eq. 4.3.40 becomes

$$E_r(z, t+2t_r) = \frac{\sqrt{(p^2-q^2)^2}}{p^2+q^2+2pq} E_i(z, t) = \frac{\sqrt{\epsilon_1} - \sqrt{\epsilon_2}}{\sqrt{\epsilon_1} + \sqrt{\epsilon_2}} R_i(z, t) \qquad 4.4.6$$

Reflection, therefore, mainly depends on the dielectric constants in the first and second layers. In this case, if the contrast between layers of differing dielectric constants is high, a strong reflection readout will be obtained according to Eq. 4.4.6. The difference in dielectric constants may be due to moisture content or cavities as mentioned in Chapter 2.

4.4.3 Case 2

When $\frac{\sigma_1}{\omega\epsilon_1} << 1$, and $\frac{\sigma_2}{\omega\epsilon_2} >> 1$, the upper layer is resistive and the lower layer is conductive. Reflection depends on both the dielectric constant and the conductivity. In this case, Eq. 4.3.40 is used directly.

4.4.4 Case 3

When $\frac{\sigma_1}{\omega\epsilon_1} >> 1$, and $\frac{\sigma_2}{\omega\epsilon_2} >> 1$, the upper and the lower layers are conductive, ϕ is a small value, $e^{j\phi} \approx 1$, $1^2 + (\frac{\sigma}{\omega_\epsilon})^2 \approx \sigma^2$. Thus,

$$q = \sqrt{\frac{\sigma_2}{\sigma_1}} \qquad 4.4.7$$

$$R = \frac{p-q}{p+q} = \frac{\sqrt{\sigma_1}-\sqrt{\sigma_2}}{\sqrt{\sigma_1}+\sqrt{\sigma_2}} \qquad 4.4.8$$

$$E(z_1 t+2t_r) = \frac{\sqrt{\sigma_1}-\sqrt{\sigma_2}}{\sqrt{\sigma_1}+\sqrt{\sigma_2}} E_i(z,t) \qquad 4.4.9$$

Reflections are mainly dependent on the difference between the conductivities of layers 1 and 2. In this case, no reflected wave can be picked up because the damping factor in the first layer is large (Jordan & Balmain, 1968).

4.4.5 Case 4

When $\frac{\sigma_1}{\omega\epsilon_1} >> 1$, $\frac{\sigma_2}{\omega\epsilon_2} << 1$, the upper layer is conductive, the lower layer is resistive, and reflection depends on the dielectric constant and the conductivity. In this case, no reflected wave can be picked up because the damping factor in the first layer is large (Jordan & Balmain, 1968).

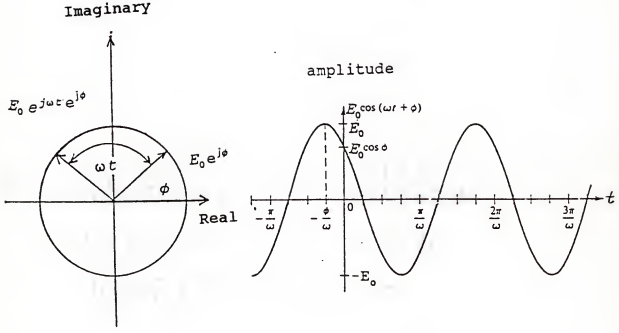

Figure 4.1 Relationship between time-varying and phasor quantities.

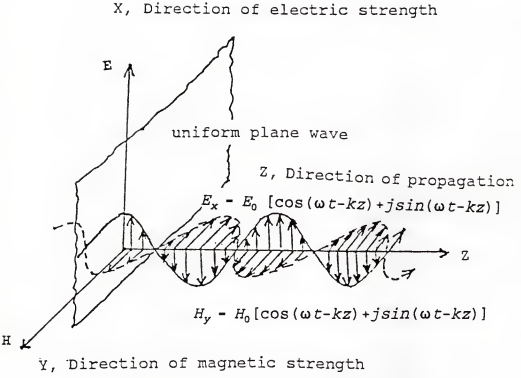
X, Direction of electric strength
E
uniform plane wave
Z, Direction of propagation
$E_x = E_0 [\cos(\omega t - kz) + j\sin(\omega t - kz)]$
Z
$H_y = H_0 [\cos(\omega t - kz) + j\sin(\omega t - kz)]$
H
Y, Direction of magnetic strength

Figure 4.2 Propagation of the electromagnetic wave.

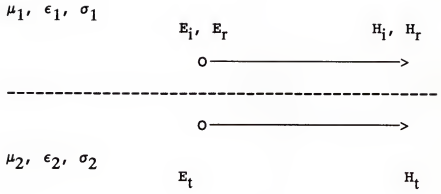

Figure 4.3 Reflection and transmission at a boundary between two conductive media.

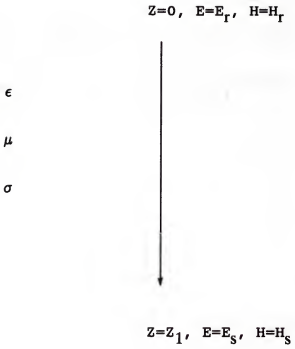

Figure 4.4 Boundary conditions for solving A_i and B_i in a homogeneous medium.

CHAPTER 5
DATA ACQUISITION APPROACH FOR GPR

5.1 The Personal Computer-Based Data Acquisition Approach

The echo signal is an analog curve representing real-time information for a specific site point at depths from the antenna position to the penetration depth, which correspond to the soil profile. The amplitude is recorded in voltage units as shown in Figure 1.1. It is necessary for a system to perform sampling at regular time intervals to allow for the conversion of the continuous-time signals into a discrete-time representation (Mindell, 1989). The digitizing system consists of a personal computer plus a data acquisition board as shown in Figure 5.1. This approach has several advantages.

(1). Reduction of system weight.

(2). Reduction of system cost.

(3). Increasing resolution, processing power, storing capacity, and retrieval capability.

5.2 DAS-50 and Real-Time Programming

The important specifications of the data acquisition board include the number of channels, sampling rate,

resolution, range, gain, accuracy, and nonlinearity (Beizer et al., 1975; Dailey, 1988; MetraByte Co., 1989; Mindell, 1989; Taylor, 1981). The quantity and quality of the digitized signals are controlled by the above-mentioned parameters. The important specifications are listed in Table 5.1. Since the GPR antenna is towed along the ground at speeds equal to or larger than 8Km/h, the allowable time interval of a trace (a trace means a series of samples taken at a specific site point) should be as short as 0.04 sec. or less if one trace is sampled at each 10 Cm interval.

The sampling rate for each datum in the trace must adequately represent the analog signal (Beizer et al., 1975; MetraByte Co., 1989; Mindell, 1989; Tamimoto, 1987) along the vertical direction of the soil profile. A high-speed on-board buffer of a MetraByte DAS-50 data acquisition board was used to meet this requirement. This on-board memory buffer is called DRAM (direct random access memory). DRAM provides on-board memory to store the transferred data. It is best to have a way of transferring data without involving the processor and system memory so that it is optimized for extremely high-speed performance (higher than 1 MHZ) with its own internal track and hold amplifier. Such an on-board memory buffer allows the data to be held locally until such time that it is required by the system (MetraByte Co., 1989).

For such a DRAM data acquisition board, a real-time program, running continuously and reacting to the

spontaneously changing inputs (Heller, 1987), is required to sequentially handle the on-board memory before any transfer of the data files. This real-time program, rather than a batch program (in which inputs are predetermined and prepacked before the program is run), is used to handle the external files. Transfer of the recorded data files commences after data acquisition is completed. The program used is listed in Appendix A, and a sample data file is listed in Appendix B. The programmed sample size of 400 is designated as N_P.

5.3 Fourier Transformation and Effective Echo Frequencies

In order to perform sampling, the optional range of sample size corresponding to the sampling rate of the DAS-50 card and the machine parameters of GPR must be determined. Several combinations of machine factors and sampling parameters were performed to determine the effective echo frequencies and the optimal sampling rate in this study (see Table 5.2). This section deals with the effective echo frequencies. The optimal sampling rate will be treated in the next section. The theoretical sample size (N_T) in Table 5.2 is given by the following equation:

$$N_T \text{ (sample/scan)} = \frac{\text{sampling rate}}{\text{scanning rate}} \qquad 5.3.1$$

According to Eqs. 4.2.7 and 4.2.8 and conditions of $\sigma/\omega\epsilon \ll 1$ and no appreciable difference of the μ value for the soil environment, the frequency information would reflect the propagation through the soil environment as described in Eqs. 5.3.2 and 5.3.3.

$$\alpha \sim f(\omega) \qquad 5.3.2$$

$$\beta \sim f(\omega) \qquad 5.3.3$$

In order to detect the frequency range of information from the GPR echo signal under specific sampling conditions, the Fourier Transformation was employed to transform the time domain series, X_t, into the frequency-domain series, $R_p(\omega_p)$ or $R_p^2(f_p)$, as described in Eqs. 5.3.4 and 5.3.5.

$$X_t = A_0 + \sum_{p=1}^{N/2-1} \left[A_p \cos\left(\frac{2\pi pt}{N}\right) + B_p \sin\left(\frac{2\pi pt}{N}\right)\right] + A_N \cos\pi t \qquad 5.3.4$$

where,

$t=1,2,\ldots, N,\ p=1,\ldots,N/2-1,$

$$A_0 = \bar{X}_t$$

$$A_N = \Sigma(-1)^t \frac{X_t}{N}$$

$$A_p = \frac{2}{N}\left[\Sigma X_t \cos\left(\frac{2\pi pt}{N}\right)\right], \text{ and}$$

$$B_p = \frac{2}{N}\left[\Sigma X_t \sin\left(\frac{2\pi pt}{N}\right)\right] \qquad 5.3.5$$

For the p^{th} harmonic,

$$\text{let frequency } \omega_p = \frac{2\pi p}{N} \quad \text{and}$$

$$R_p \text{Cos}(\omega_p t + \text{Tan}^{-1} \frac{-B_p}{-A_p}) = A_p \text{Cos}\, \omega_p t + B_p \text{Sin}\, \omega_p t,$$

Eq. 5.3.6 is obtained for amplitude R_p and phase ϕ_p,

$$R_p = \sqrt{(A_p^2 + B_p^2)}$$

$$\phi_p = \text{Tan}^{-1} (-B_p / A_p) \qquad 5.3.6$$

When $A_0 = 0$, i.e. the mean of X_t is removed, the sum of the ordinates equals the sum of the squared data values (Chatfield, 1984). Anderson (1971) suggested the term spectrogram to describe the plot of the spectrum ordinate, R_p^2, as plotted against ω_p. Since $\omega_p = 2\pi f_p$, the R_p^2 vs f_p plot as shown in Figure 5.2 is designated as the spectrogram in this research.

From Figure 5.2, the three operation positions of antenna ground, (H), and (2H) show that the important information in the echo signals comes mainly from frequencies between 200 and 2,000 Hz and between 6,000 and 8,000 Hz, and that the dominant sources consist of a few large peaks.

The first large peaks from both 120 MHz (A,B, and C) and 300 MHz (D, E, and F) antenna systems for ground, H, and 2H probing positions occur at 650, 1,000, and 950 Hz, respectively. The second large peaks for ground, (H), and (2H) positions occur at 1,000, 650, and 650 Hz, respectively. The peak ratios of 120 Mhz to 300 Mhz antenna for the first

large peak of three probing positions are 1.28 (A:D), 0.73 (B:E), and 0.53 (C:F), respectively, and for the second large peak, are 0.39 (A:D), 0.38 (B:E), and 0.41 (C:F), respectively. Another significant response is the variation of the multiple-peak pattern and the shift of the tail peak. For the echo signal of the 120 MHz antenna, the double (A), triple (B), and quaternary (C) peaks appeared for ground, (H), and (2H) positions, respectively. The tail peak moves to 7,300 Hz for the (H) position and moves to 6,000 Hz for the (2H) position of the 120 Mhz antenna. The scale of variation occurring in the case of the 300 MHz antenna ones (D, E, and F) is smaller. These variations, both in high frequency (6,000 ~ 8,000 Hz) and in low frequency (< 2,000 Hz) indicate that the sampling rate of 20,000 Hz would provide meaningful data for further analysis.

The phase change ϕ_c due to the tail peak located at the p^{th} harmonic is computed as

$$\phi_c = \phi_p - \phi_{p-1} \qquad 5.3.7$$

The ϕ_p of the tail peak of the echoes in Figure 5.2 reaches 180°. Figure 5.3 shows that a 180° phase change results in a vertical reflection of the travelling waves. Such a vertical reflection will only return to the receiver if the corresponding interface is deep in the soil profile position. It reveals the important fact that the tail peak contributes to the reflection record of a subsurface interface.

Both locations and ordinates of large peaks evidently varied with various probing positions and antenna types at the sampling rate of 20,000 Hz. Therefore, sampling rates no greater than 20,000 Hz were used in this research.

5.4 Double Mass Analysis and Actual Sample Size

The reliability of the sampled data should be assessed after calibrations of the data acquisition board have been performed. One way to test the reliability of DAS-50 records is based on the double mass analysis of two consecutive sampling traces.

The sampled data series of each trace of various sampling conditions concerned is accumulated chronologically (Σx_t) and plotted coordinately as Figure 5.4 to test whether the first trace $(\Sigma x_t)_1$ is similar to the second trace $(\Sigma x_t)_2$. If each point formed from these paired values is identical, the predicting function is

$$(\Sigma x_t)_1 = (\Sigma x_t)_2 \qquad 5.4.1$$

If a discrepancy occurs, the linear regression becomes as

$$(\Sigma x_t)_1 = c + d\left[(\Sigma x_t)_2 - \frac{\Sigma (\Sigma x_t)_2}{N}\right] \qquad 5.4.2$$

where

$$c = \frac{\Sigma (\Sigma x_t)_1}{N} \qquad 5.4.3$$

$$d = \frac{\Sigma\left[(\Sigma x_t)_1 (\Sigma x_t)_2\right] - \frac{\left[\Sigma (\Sigma x_t)_1\right]\left[\Sigma (\Sigma x_t)_2\right]}{N}}{\Sigma (\Sigma x_t)_2^2 - \frac{\left[\Sigma (\Sigma x_t)_2\right]^2}{N}} \qquad 5.4.4$$

and the interpretation percentage R^2 (Eq. 5.4.1) is computed as

$$R = \frac{d\left\{\Sigma\left[(\Sigma x_t)_1 (\Sigma x_t)_2\right] - \frac{\left[\Sigma (\Sigma x_t)_2\right]\left[\Sigma (\Sigma x_t)_1\right]}{N}\right\}}{\Sigma (\Sigma x_t)_1^2 - \frac{\left[\Sigma (\Sigma x_t)_1\right]^2}{N}} \qquad 5.4.5$$

When R^2 is close to a value of 1, trace 1 and trace 2 will fit into a straight line (Draper and Smith, 1966), as described in Eq. 5.4.2, and therefore these two traces are considered substitutively because the data point in each trace is regarded as the same value. Tables 5.3 and 5.4 verity that the DAS-50 is a reliable data acquisition unit because of the high value of R^2 throughout a large range of sampling rates from 20,000 to 900 Hz. Such information demonstrates that the DAS-50 is reliable.

Considering the GPR application requirements of the high scanning rate of the control unit, the high sampling rate of the data acquisition board, and the short-time interval allowed for a trace, the advantage of a small sample size is obvious. Therefore, the combination of a 20,000 Hz sampling rate and a 51.2 scan/sec scanning rate are chosen as the optimal sampling condition for this study.

Under such data standards, after the initial and end values of the scan signals were removed, the actual sample sizes (N_A) (shown in Tables 5.3 and 5.4) ranged from 377 to 359. The relationship between N_T, N_P, N_A, and the scanning signals is shown in Figure 5.5.

Table 5.1 Important specifications of DAS-50.

Channel: 4 single-ended

Ranges: ±2.5V ~ ±10V

Resolution: 12 bit

Conversion rate: 1/μ sec

Accuracy:

- Overall ~ 2 LSB max
- Differential ~ 1 LSB max
- Integral ~ 1.5 LSB max
- No missing codes

Temperature Drift:

- Offset coefficient: 15 pp m/°C
- Gain coefficient: 25 pp m/°C
- Differential linearity: 1.5 pp m/°C

Table 5.2 The theoretical sample sizes (N_T) for various combinations of machine factors and sampling parameters using the DAS-50 card.

Sampling rate	Machine factor (scan/sec)		
(Hz)	51.2	25.6	6.4
80,000	1,563	3,124	12,500
50,000	976	1,953	7,813
30,000	586	1,172	4,688
20,000	390	781	3,125
10,000	196	390	1,563
7,000	137	274	1,094
4,000	78	157	625
1,500	30	59	235
900	18	36	141

Table 5.3 The R^2 and N_A values for various GPR performance conditions using a 300 MHz antenna.

Ceiling height	Sampling rate	machine factor, scan/sec.					
		51.2		25.6		6.4	
	(Hz)	N_A	R^2	N_A	R^2	N_A	R^2
G	20,000	377	99.97	-	-	-	-
	10,000	188	99.95	376	99.99	-	-
	7,000	132	99.94	263	99.99	-	-
	4,000	75	99.95	150	99.99	-	-
	1,500	x	-	57	99.10	225	99.98
	900	x	-	x	-	135	99.95
H	20,000	375	99.99	-	-	-	-
	10,000	187	99.95	374	99.99	-	-
	7,000	130	99.95	261	99.99	-	-
	4,000	74	99.16	149	99.96	-	-
	1,500	x	-	56	99.78	225	99.98
	900	x	-	x	-	134	99.94
2H	20,000	371	99.99	-	-	-	-
	10,000	186	99.98	372	99.95	-	-
	7,000	130	99.71	260	99.93	-	-
	4,000	74	99.14	148	99.92	-	-
	1,500	x	-	55	99.73	220	99.98
	900	x	-	x	-	133	99.92

Note: X means not found
- means not available

Table 5.4 The R^2 and N_A values for various GPR performance conditions using a 120 MHz antenna.

Ceiling height	Sampling rate	machine factor, scan/sec.					
		51.2		25.6		6.4	
	(Hz)	N_A	R^2	N_A	R^2	N_A	R^2
G	20,000	369	99.98	-	-	-	-
	10,000	184	99.97	369	99.99	-	-
	7,000	129	99.90	259	99.99	-	-
	4,000	74	99.85	148	99.99	-	-
	1,500	x	-	55	99.25	220	99.99
	900	x	-	x	-	131	99.99
H	20,000	367	99.98	-	-	-	-
	10,000	183	99.97	367	99.99	-	-
	7,000	128	99.96	257	99.98	-	-
	4,000	73	99.75	146	99.96	-	-
	1,500	27	97.57	55	99.69	220	99.99
	900	x	-	x	-	131	99.98
2H	20,000	366	99.98	-	-	-	-
	10,000	183	99.98	366	99.99	-	-
	7,000	128	99.90	256	99.96	-	-
	4,000	73	99.72	146	99.95	-	-
	1,500	x	-	55	98.36	219	99.97
	900	x	-	x	-	132	99.91

Note: X means not found
- means not available

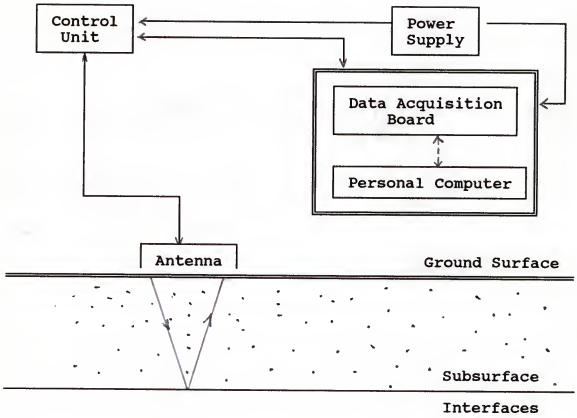

Figure 5.1 The personal computer-based data acquisition approach.

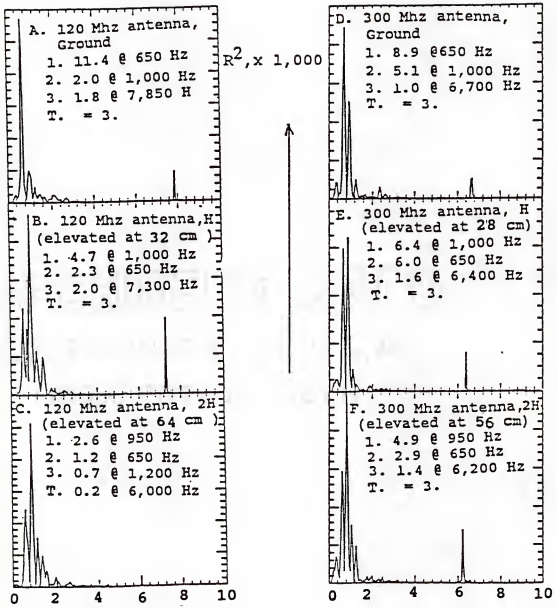
A. 120 Mhz antenna, Ground
1. 11.4 @ 650 Hz
2. 2.0 @ 1,000 Hz
3. 1.8 @ 7,850 H
T. = 3.
B. 120 Mhz antenna,H (elevated at 32 cm)
1. 4.7 @ 1,000 Hz
2. 2.3 @ 650 Hz
3. 2.0 @ 7,300 Hz
T. = 3.
C. 120 Mhz antenna, 2H (elevated at 64 cm)
1. 2.6 @ 950 Hz
2. 1.2 @ 650 Hz
3. 0.7 @ 1,200 Hz
T. 0.2 @ 6,000 Hz
R2,x 1,000
D. 300 Mhz antenna, Ground
1. 8.9 @650 Hz
2. 5.1 @ 1,000 Hz
3. 1.0 @ 6,700 Hz
T. = 3.
E. 300 Mhz antenna, H (elevated at 28 cm)
1. 6.4 @ 1,000 Hz
2. 6.0 @ 650 Hz
3. 1.6 @ 6,400 Hz
T. = 3.
F. 300 Mhz antenna,2H (elevated at 56 cm)
1. 4.9 @ 950 Hz
2. 2.9 @ 650 Hz
3. 1.4 @ 6,200 Hz
T. = 3.
0 2 4 6 8 10
0 2 4 6 8 10
Frequency, Khz

Figure 5.2 The frequency spectrum shows the information sources of echo signals of experimental site.

1. First large peak 2. Second large peak
3. Third large peak T. Tail peak

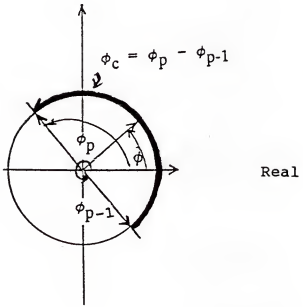

Figure 5.3 The meaning of phase change ϕ_c.

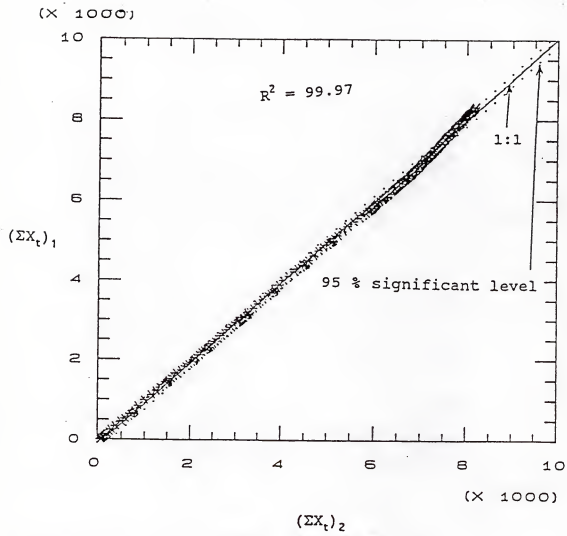

Figure 5.4 Double mass analysis on two consecutive traces $(\Sigma X_t)_1$ and $(\Sigma X_t)_2$ using a 300 MHz antenna.

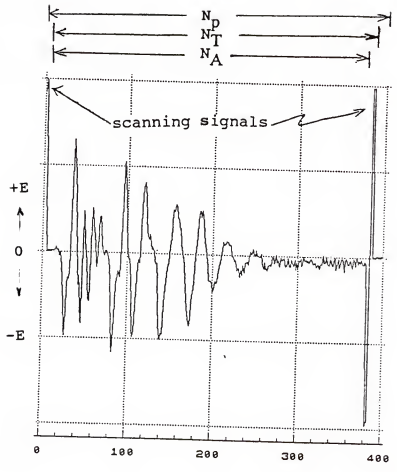

Figure 5.5 Schematic relationship of N_T, N_A, N_P, and the scanning signals.
N_P ~ sample size programmed,
N_T ~ theoretical sample size,
N_A ~ actual sample size.

CHAPTER 6
COMPONENTS OF THE DIGITAL ECHO SIGNAL

6.1 The Separation Technique Used in This Research

The GPR system receives a three-portion signal as shown in Figure 1.1. These portions include the transmitted impulse (due to transmitter loss to receiver, it is abbreviated as TL in this research), the portion of surface (due to the reflection from the ground surface, it is abbreviated as SR in this research), and the portion of interface signal (due to the reflections from subsurface interfaces, it is abbreviated as SI in this research). The triple band recognized in the graphic image was interpreted as a characteristic record of a single interface (Johnson et al., 1979). Ulriksen (1983) suggested the separation of the above-mentioned portions by the elevated antenna method in which the measurements are performed at a position above the ground. He used a unit impulse of a three-half-period which corresponds to the triple band in the graphic image to obtain a synthetic signal. The synthetic signal indicated the location due to the contribution of this triple band. However, he only obtained good results in a few cases.

In this research, a reversed procedure is proposed in which a separation process is used. When one specified signal portion is removed, the corresponding spectrogram as described in Section 5.3 reveals the measurable changes. These changes are used as a signature to indicate the presence of this specified signal portion source in the time-domain series.

A digital echo signal obtained from a good reflector, obtained by placing a steel plate beneath the 300 MHz antenna, will serve as a data set for an example of the separation technique. There are two sets of four-cycle components and residual weak signals in this time-domain plot (shown in Figure 6.1.A). The first four-cycle component is recognized as transmitter loss TL, the second four-cycle component is regarded as surface reflection SR, the residuals SI are weak compared to the previous components.

The characteristics in the frequency domain, as shown in the corresponding spectrogram (Figure 6.1.B), are described in Table 6.1. When the first TL portion (the black portion in Figure 6.1.B) ending at E_{TL}=60 is removed, the corresponding spectrogram as shown in Figure 6.1.C indicates several significant facts.

(1). The location of the tail peak is not moved.

(2). The phase change ϕ_c due to the tail peak is maintained at approximately 180°.

(3). The area ΣR_{p2} of the tail peak was reduced from 7.9% to 5.9% of the full spectrogram.

(4). The area ΣR_{p2} due to the peak 1,500 and 1,850 Hz is shown to decay rapidly.

These facts lead to the conclusion that the peaks of 1,500 and 1,850 Hz mainly contribute to TL.

When the second four-cycle ending at E_{SR}=124 is removed, the tail peak becomes the dominant peak, as shown in Figure 6.1.D. The significant facts in the spectrogram response to this removal include:

(1). The peaks at 1,500 and 1,850 Hz have disappeared.

(2). The ratio of tail peak to the full spectrogram (ΣR_p^2) does not decay significantly.

(3). The phase change ϕ_c remained approximately 180°.

These facts lead to the conclusion that the contribution of the tail peak is due to the reflection from subsurface interface. Therefore, the sole tail peak is the typical spectrogram pattern for SI.

The ratio of the area ΣR_p^2 of the three components of this example is 0.6:0.3:0.1. The SI portion is shown to be weak.

6.2 The Portion of Transmitter Loss TL

Six echo signals represent six different performance conditions of the 300 MHz antenna as shown in Figure 6.2. One

identical four-cycle pattern is recognized in all these six echo signals as described in Table 6.2. The end point E_{TL} that separate the TL and SR is visibly determined by measuring the first four-cycle.

The spectrograms of the full traces (TL+SR+SI) are given in Figure 6.3.A and those without TL are given in Figure 6.3.B. Several significant facts evident from comparison of the results from the inclusion and exclusion of the first four-cycle TL include:

(1). The peaks disappear at 400 and 1,200 Hz.

(2). Ratios of the tail peak did not change much except in the case of long grass ground cover with a water-table depth of 95 cm.

(3). The phase change ϕ_c of the tail peak remained approximately 180°.

The detailed descriptions of the characteristics of portion TL are given in Tables 6.3 to 6.8 for each condition. Conditions A, B, C, and D are the experiment sites shown in Figure 6.4.A, B, C, and D. Condition A was a dry profile condition; condition B was wet; condition C was dry with a water bag at 80 cm below the ground surface; condition D was wet with the water table at 75 cm below the ground surface; condition E was a site with a 3 cm grass cover (cut) and a natural water table 79 cm below the ground surface as shown in Figure 6.4.E; and condition F is a site with a 6 cm grass

cover (cut) and a natural water table 96 cm below the ground surface as shown in Figure 6.4.F.

6.3 The Portion of Surface Reflection SR

Since the end point of surface reflection E_{SR} is not visible for the six conditions, the frequency-domain plots accompanied with the separation of peaks must be used to determine it. Therefore, when the typical spectrogram with only a tail peak appears, the portion of surface reflection SR is supposed to have been removed as shown in Figure 6.4. The results of such performances are described in Tables 6.9 to 6.14.

The conclusions from these six tables are given as follows:

(1). The contribution of peaks from 600 to 800 Hz is the main resource of SR.

(2). The decay of the tail peak is not significant in sequential removals.

(3). The phase change due to the tail peak is approximately 180°.

In the time-domain series, the end points of E_{SR} are 162, 123, 191, 138, and 96 for conditions A, B, D, E, and F, respectively. The portion of SR for condition C was not determined due to the lack of a no capillary fringe zone (fresh water was placed in a plastic bag). The capillary

fringe zone in a soil is believed to reduce the interaction between the incident and reflected waves. The portions of SR may have a single period, double period, or triple period, as described in Table 6.15 and Figure 6.2.

6.4 The Portion of Subsurface Interface SI

This portion contains all peaks after the end point E_{SR} of the SR portion. In comparison to the previous two components, it is weak. Table 6.16 describes the weight of TL, SR, and SI in the frequency-domain spectrogram. The portion SI contains only 5% to 15% of the total R_p^2 area, but the tail peak shares 50% to 70% of the portion SI. This means that 50% to 70% of the total R_p^2 of SR contributes to the tail peak (which comes from the deeper interfaces based on the information of $\phi_c \approx 180°$).

6.5 Probing with the 120 MHz Antenna

In order to locate the end point of SR, E_{SR} for echo signals from different frequency antennas, a 120 MHz antenna was used to perform measurements for conditions B and D. The time-domain plot of this measurement, as shown in Figure 6.6, and the corresponding results of the frequency-domain analysis for condition D (condition D is a better result from these two

examples), as shown in Table 6.17, do not succeed in accomplishing this aim. That is, the 120 MHz antenna was not found to be satisfactory for the purpose of this research and was not considered any further.

6.6 The Elevated Antenna Method

The elevated antenna method has been found useful in separating various source components from a strong reflector (Ulriksen, 1983). This method was found impractical for the natural water-table condition (tested in condition F). The TL portion is observed in the time-domain plot as shown in Figure 6.7. The SR and SI portions, however, were not separable. Therefore, the elevated antenna method was not applied further in this research. Special attention was also paid to the decay pattern of peaks in the full spectrogram as shown in Figure 6.7.B, the ground position of an antenna on a long uninterrupted decay envelope starting at 800 MHz into a high frequency (ending at 3,000 Hz), the (H) position (28 cm above the ground, medium, and the (2H) position (56 cm above the ground), a short one. These significant characteristics may be further restated as Figure 6.8. The full spectrogram from the antenna placed on the ground is a single decay pattern of an envelope curve (Figure 6.8A), the (H) position, double decay pattern; the (2H) position, triple decay pattern.

Table 6.1 The characteristics of a digital echo signal obtained from a good reflector in a frequency-domain analysis.

Components		TL+SR+SI	SR+SI	SI
Sample size		384	324	260
Total R_p^2		269,367	97,815	30,364
Peak #1	f_p, (Hz)	1,500	1,500	
	ΣR_p^2, (%)	25.0	6.3	NN
	ϕ_p, (°)	309	295	
Peak #2	f_p, (Hz)	1,850	1,850	
	ΣR_p^2, (%)	40.0	9.5	NN
	ϕ_p, (°)	303	338	
Tail peak	f_p, (Hz)	8,850	8,850	8,850
	ΣR_p^2, (%)	7.9	5.9	5.1
	ϕ_p, (°)	175	177	182

Note: f_p ~ Location of peak, Hz

ΣR_p^2 ~ area % of peak located at f_p to total area of full spectrogram in Figure 6.1.B, %

ϕ_c ~ phase change due to the peak at p^{th} harmonic, °

NN ~ negligible (< .1%)

TL ~ The portion of transmitter loss

SR ~ The portion of surface reflection

SI ~ The portion of subsurface interface

Table 6.2 The characteristics of TL portion in time domain plot.

Performance condition	N_A	End point	Full four-period pattern
A	375	71	yes
B	370	70	yes
C	375	71	yes
D	370	70	yes
E	364	67	yes
F	364	67	yes

* A. ~ Dry soil profile

B. ~ Wet soil profile

C. ~ Dry soil profile with a water bag

D. ~ Wet soil profile with a water table

E. ~ Water-table site with 3 cm grass

F. ~ Water-table site with 6 cm grass

N_A ~ Actual sampled size

Table 6.3 The characteristics of TL portion in frequency domain for condition A (dry soil).

Components		TL+SR+SI	SR+SI
Sample size		375	304
Total R_p^2		153,409	87,543
Peak #1	f_p, (Hz)	400	
	ΣR_p^2, (%)	7.4	NN
	ϕ_c, (°)	309	
Peak #2	f_p, (Hz)	600	600
	ΣR_p^2, (%)	43.0	37.7
	ϕ_c, (°)	287	315
Peak #3	f_p, (Hz)	1,000	
	$\Sigma R2_p^2$, (%)	20.9	NN
	ϕ_c, (°)	312	
Tail peak	f_p, (Hz)	7,500	7,500
	ΣR_p^2, (%)	13.9	11.8
	ϕ_c, (°)	168	168

Note: f_p - Location of peak, Hz

ΣR_p^2 - area % of peak located at f_p to total area of full spectrogram in Figure 6.3.A, %

ϕ_c - phase change due to the peak at p^{th} harmonic, °

NN - negligible (< .1%)

TL - The portion of transmitter loss

SR - The portion of surface reflection

SI - The portion of subsurface interface

Table 6.4 The characteristics of TL portion in frequency domain for condition B (wet soil).

Components		TL+SR+SI	SR+SI
Sample size		370	301
Total R_p^2		222,695	198,239
Peak #1	f_p, (Hz)	700	700
	$\Sigma R2_p^2$, (%)	41.4	68.1
	ϕ_c, (°)	292	324
Peak #2	f_p, (Hz)	1,200	
	ΣR_p^2, (%)	18.1	NN
	ϕ_c, (°)	306	
Tail peak	f_p, (Hz)	6,500	6,500
	ΣR^2_p, (%)	8.9	8.0
	ϕ_c, (°)	171	187

Note: f_p ~ Location of peak, Hz

ΣR_p^2 ~ area % of peak located at f_p to total area of full spectrogram in Figure 6.3.A, %

ϕ_c ~ phase change due to the peak at p^{th} harmonic, °

NN ~ negligible (< .1%)

TL ~ The portion of transmitter loss

SR ~ The portion of surface reflection

SI ~ The portion of subsurface interface

Table 6.5 The characteristics of TL portion in frequency domain for condition C (dry soil + water bag).

Components		TL+SR+SI	SR+SI
Sample size		375	306
Total R_p^2		285,165	211,722
Peak #1	f_p, (Hz)	600	600
	ΣR_p^2, (%)	54.3	55.8
	ϕ_c, (°)	230	285
Tail peak	f_p, (Hz)	7,500	7,500
	ΣR_p^2, (%)	6.7	5.5
	ϕ_c, (°)	176	181

Note: f_p ~ Location of peak, Hz

ΣR_p^2 ~ area % of peak located at f_p to total area of full spectrogram in Figure 6.3.A %

ϕ_c ~ phase change due to the peak at p^{th} harmonic, °

NN ~ negligible (< .1%)

TL ~ The portion of transmitter loss

SR ~ The portion of surface reflection

SI ~ The portion of subsurface interface

Table 6.6 The characteristics of TL portion in frequency domain for condition D (wet soil + water table).

Components		TL+SR+SI	SR+SI
Sample size		370	301
Total R_p^2		311,644	198,269
Peak #1	f_p, (Hz)	700	700
	ΣR_p^2, (%)	60.4	48.2
	ϕ_c, (°)	276	297
#2	f_p, (Hz)	1,200	
	ΣR_p^2, (%)	16.2	NN
	ϕ_c, (°)	309	
Tail peak	f_p, (Hz)	6,500	6,500
	ΣR_p^2, (%)	6.4	5.7
	ϕ_c, (°)	186	198

Note: f_p ~ Location of peak, Hz

ΣR_p^2 ~ area % of peak located at f_p to total area of full spectrogram in Figure 6.3.A, %

ϕ_c ~ phase change due to the peak at p^{th} harmonic, °

NN ~ negligible (< .1%)

TL ~ The portion of transmitter loss

SR ~ The portion of surface reflection

SI ~ The portion of subsurface interface

Table 6.7 The characteristics of TL portion in frequency domain for condition E (water-table depth = 79 cm).

Components		TL+SR+SI	SR+SI
Sample size		364	297
Total R_p^2		180,390	77,820
Peak #1	f_p, (Hz)	800	800
	ΣR_p^2, (%)	34.7	14.4
	ϕ_c, (°)	285	309
Peak #2	f_p, (Hz)	600	
	ΣR_p^2, (%)	5.6	NN
	ϕ_c, (°)	290	
Tail peak	f_p, (Hz)	6,000	6,000
	ΣR_p^2, (%)	11.7	9.5
	ϕ_c, (°)	180	183

Note: f_p ~ Location of peak, Hz

ΣR_p^2 ~ area % of peak located at f_p to total area of full spectrogram in Figure 6.3.A, %

ϕ_c ~ phase change due to the peak at p^{th} harmonic, °

NN ~ negligible (< .1%)

TL ~ The portion of transmitter loss

SR ~ The portion of surface reflection

SI ~ The portion of subsurface interface

Table 6.8 The characteristics of TL portion in frequency domain for condition F (water-table depth = 96 cm).

Components		TL+SR+SI	SR+SI
Sample size		364	297
Total R_p^2		188,750	79,121
Peak #1	f_p, (Hz)	800	800
	ΣR_p^2, (%)	19.1	4.9
	ϕ_c, (°)	316	337
Peak #2	f_p, (Hz)	1,200	
	ΣR_p^2, (%)	25.1	NN
	ϕ_c, (°)	307	
Tail peak	f_p, (Hz)	6,000	6,000
	ΣR_p^2, (%)	22.0	11.7
	ϕ_c, (°)	170	186

Note: f_p ~ Location of peak, Hz

ΣR_p^2 ~ area % of peak located at f_p to total area of full spectrogram in Figure 6.3.A, %

ϕ_c ~ phase change due to the peak at p^{th} harmonic, °

NN ~ negligible (< .1%)

TL ~ The portion of transmitter loss

SR ~ The portion of surface reflection

SI ~ The portion of subsurface interface

Table 6.9 The characteristics of SR portion in frequency domain for condition A (dry soil).

Components		SR+SI	SI
Sample size		304	213
Total $R2_p^2$		87,543	17,782
Peak #2	f_p, (Hz)	600	
	ΣR_p^2, (%)	37.7	NN
	ϕ_c, (°)	315	
Tail peak	f_p, (Hz)	7,500	7,500
	$\Sigma R2_p^2$, (%)	13.9	11.6
	ϕ_c, (°)	168	171

Note: f_p ~ Location of peak, Hz

ΣR_p^2 ~ area % of peak located at f_p to total area of full spectrogram, %

ϕ_c ~ phase change due to the peak at p^{th} harmonic, °

NN ~ negligible (< .1%)

TL ~ The portion of transmitter loss

SR ~ The portion of surface reflection

SI ~ The portion of subsurface interface

Table 6.10 The characteristics of SR portion in frequency domain for condition B (wet soil).

Components		SR+SI	SI
Sample size		301	247
Total R_p^2		198,239	23,449
Peak #1	f_p, (Hz)	700	
	ΣR_p^2, (%)	68.1	NN
	ϕ_c, (°)	324	
Tail peak	f_p, (Hz)	6,500	6,500
	ΣR_p^2, (%)	8.0	6.7
	ϕ_c, (°)	187	197

Note: f_p ~ Location of peak, Hz

ΣR_p^2 ~ area % of peak located at f_p to total area of full spectrogram, %

ϕ_c ~ phase change due to the peak at p^{th} harmonic, °

NN ~ negligible (< .1%)

TL ~ The portion of transmitter loss

SR ~ The portion of surface reflection

SI ~ The portion of subsurface interface

Table 6.11 The characteristics of SR portion in frequency domain for condition C (dry soil + water bag).

Components		SR+SI	SI?	
Sample size		306	213	185
Total R_p^2		211,722	81,307	47,833
Peak #1	f_p, (Hz)	600	600	600
	ΣR_p^2, (%)	55.8	18.7	9.8
	ϕ_c, (°)	285	270	271
Tail peak	f_p, (Hz)	7,500	7,500	7,500
	ΣR_p^2, (%)	5.5	3.8	3.5
	ϕ_c, (°)	181	171	177

Note: f_p ~ Location of peak, Hz

ΣR_p^2 ~ area % of peak located at f_p to total area of full spectrogram, %

ϕ_c ~ phase change due to the peak at p^{th} harmonic, °

NN ~ negligible (< .1%)

TL ~ The portion of transmitter loss

SR ~ The portion of surface reflection

SI ~ The portion of subsurface interface

? ~ No answer

Table 6.12 The characteristics of SR portion in frequency domain for condition D (wet soil + water table).

Components		SR+SI	SI
Sample size		301	179
Total R_p^2		198,269	13,875
Peak #1	f_p, (Hz)	700	
	ΣR_p^2, (%)	48.2	NN
	ϕ_c, (°)	297	
Tail peak	f_p, (Hz)	6,500	6,500
	ΣR_p^2, (%)	5.7	2.7
	ϕ_c, (°)	198	184

Note: f_p - Location of peak, Hz

ΣR_p^2 - area % of peak located at f_p to total area of full spectrogram, %

ϕ_c - phase change due to the peak at p^{th} harmonic, °

NN - negligible (< .1%)

TL - The portion of transmitter loss

SR - The portion of surface reflection

SI - The portion of subsurface interface

Table 6.13 The characteristics of SR portion in frequency domain for condition E (water-table site with 3 cm grass ground cover).

Components		SR+SI	SI
Sample size		297	216
Total R_p^2		77,820	22,790
Peak #1	f_p, (Hz)	800	
	ΣR_p^2, (%)	14.4	NN
	ϕ_c, (°)	309	
Tail peak	f_p, (Hz)	6,000	6,000
	ΣR^2_p, (%)	9.5	7.1
	ϕ_c, (°)	183	185

Note: f_p - Location of peak, Hz

ΣR_p^2 - area % of peak located at f_p to total area of full spectrogram, %

ϕ_c - phase change due to the peak at p^{th} harmonic, °

NN - negligible (< .1%)

TL - The portion of transmitter loss

SR - The portion of surface reflection

SI - The portion of subsurface interface

Table 6.14 The characteristics of SR portion in frequency domain for condition F (water-table site with 6 cm grass ground cover).

Components		SR+SI	SI
Sample size		297	278
Total R_p^2		79,121	34,425
Peak #1	f_p, (Hz)	800	
	ΣR_p^2, (%)	4.9	NN
	ϕ_c, (°)	337	
Tail peak	f_p, (Hz)	6,000	6,000
	ΣR_p^2, (%)	11.7	11.0
	ϕ_c, (°)	186	190

Note: f_p ~ Location of peak, Hz

ΣR_p^2 ~ area % of peak located at f_p to total area of full spectrogram, %

ϕ_c ~ phase change due to the peak at p^{th} harmonic, °

NN ~ negligible (< .1%)

TL ~ The portion of transmitter loss

SR ~ The portion of surface reflection

SI ~ The portion of subsurface interface

Table 6.15 The characteristics of SR portion in time-domain plot

Performance condition	E_{SR}	Number of periods removed for SR
A	162	3
B	123	2
C	>220?	>5?
D	191	4
E	138	3
F	96	1

* A. ˜ Dry soil profile

B. ˜ Wet soil profile

C. ˜ Dry soil profile with a water bag

D. ˜ Wet soil profile with a water table

E. ˜ A water-table site with 3 cm grass ground

F. ˜ A water-table site with 6 cm grass ground

? ˜ There is no answer even the consecutive removal of data is performed until the data sequence of 220 or the 5 periods.

Table 6.16 Weight of ΣR_p^2 of each component.

Components	A	B	D	E	F
TL	42.9	44.0	40.8	63.9	67.4
TL_o	13.0	8.6	6.4	11.0	9.8
TL_x	(30.3)	(19.5)	(2.5)	(17.2)	(14.5)
SR	45.5	45.5	54.7	22.4	18.3
SR_o	11.7	7.9	5.3	8.6	9.1
SR_x	(25.7)	(17.4)	(9.7)	(38.4)	(49.7)
SI	11.6	10.5	4.5	13.7	14.3
SI_o	8.2	6.7	2.7	7.3	9.0
SI_x	(70.7)	(63.8)	(60.0)	(50.0)	(63.0)

Note: Subscript o means weight of tail peak relative to overall spectrogram.
Subscript x means weight of tail peak relative to individual portion.

Table 6.17 The characteristics of frequency domain for condition D by using 120 MHz antenna.

Components		TL+SR+SI	SI
Sample size		368	196
Total R_p^2		434,107	28,315
Peak #1	f_p, (Hz)	500	500
	ΣR_p^2, (%)	56.5	0.2
	ϕ_c, (°)	280	301
Peak #2	f_p, (Hz)	1,000	
	ΣR_p^2, (%)	3.0	NN
	ϕ_c, (°)	295	
Tail peak	f_p, (Hz)	6,500	6,500
	ΣR_p^2, (%)	4.3	3.0
	ϕ_c, (°)	173	199

Note: f_p ~ Location of peak, Hz

ΣR_p^2 ~ area % of peak located at f_p to total area of full spectrogram, %

ϕ_c ~ phase change due to the peak at p^{th} harmonic, °

NN ~ negligible (< .1%)

TL ~ The portion of transmitter loss

SR ~ The portion of surface reflection

SI ~ The portion of subsurface interface

? ~ No answer

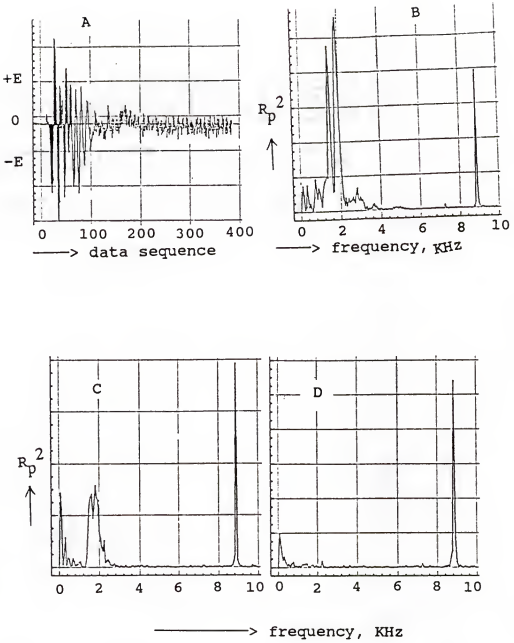

Figure 6.1 Digital echo-signal plots obtained from a strong reflector.
A. Time-domain plot
B. Spectrogram consisting of TL, SR, and SI
C. Spectrogram consisting of SR and SI
D. Spectrogram consisting of SI only

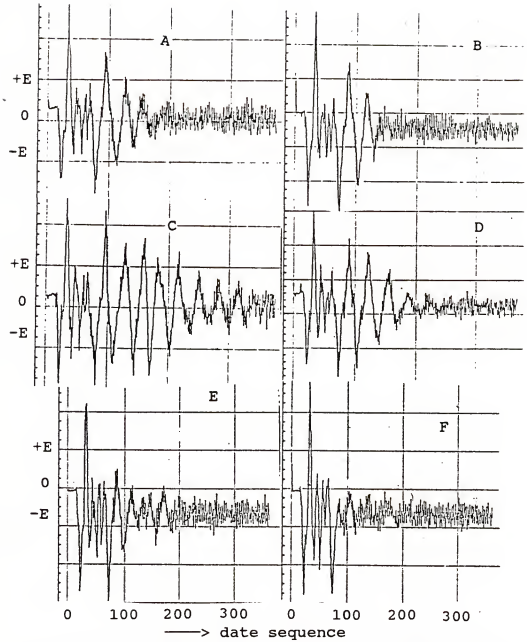

Figure 6.2 Time-domain plot of six different soil conditions.

A. Dry soil profile
B. Wet soil profile
C. Dry soil profile with a water bag
D. Wet soil profile with a water table
E. Water-table site with 3 cm grass (cut)
F. Water-table site with 6 cm grass (cut)

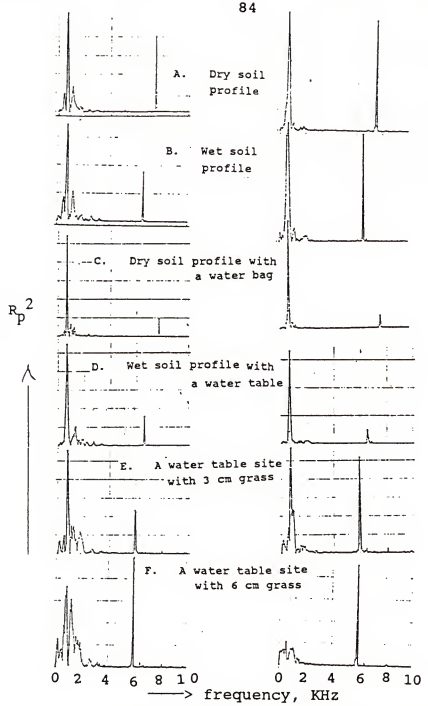
A. Dry soil profile
B. Wet soil profile
C. Dry soil profile with a water bag
D. Wet soil profile with a water table
E. A water table site with 3 cm grass
F. A water table site with 6 cm grass
R_p^2
0 2 4 6 8 10
0 2 4 6 8 10
frequency, KHz

Figure 6.3 Frequency-domain spectrograms before and after the removal of TL.
A. Dry soil profile
B. Wet soil profile
C. Dry soil profile with a water bag
D. Wet soil profile with a water table
E. Water-table site with 3 cm grass (cut)
F. Water-table site with 6 cm grass (cut)

A. Dry soil profile

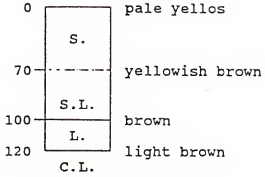

B. Wet soil profile

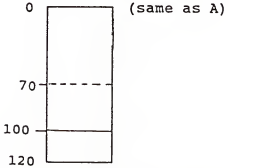

C. Dry soil profile with a water bag

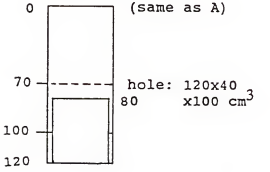

D. Wet soil profile with a water-table

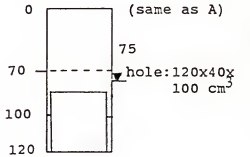

E. A water-table site with 3 cm grass

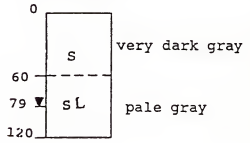

F. A water-table site with 6 cm grass

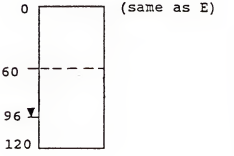

▼ water table

Figure 6.4 Various sites measured with 300 MHz antenna.

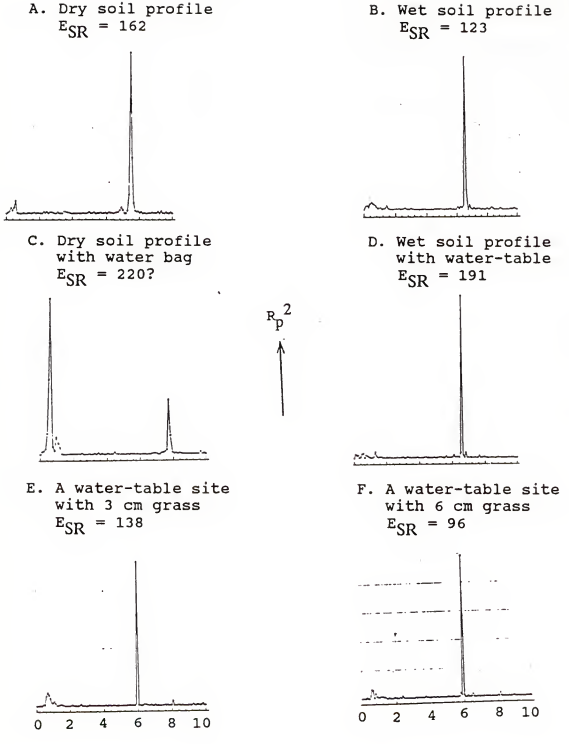

Figure 6.5 Spectrogram for searching E_{SR}.

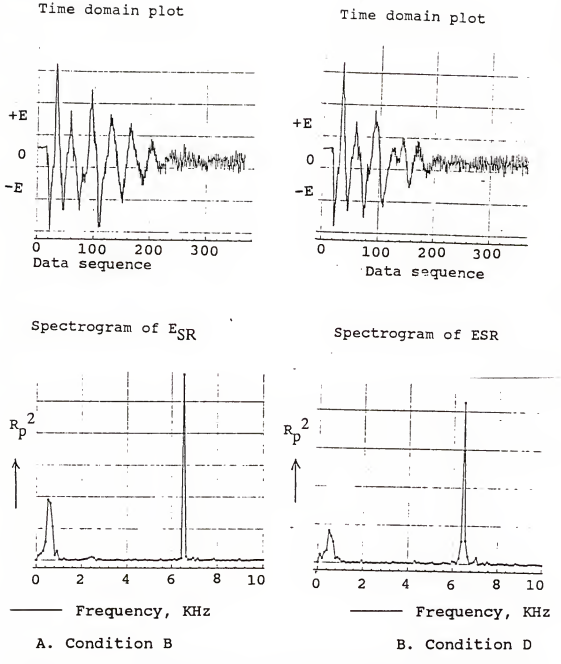

Figure 6.6 Measurements of conditions B and D with the 120 MHz antenna.

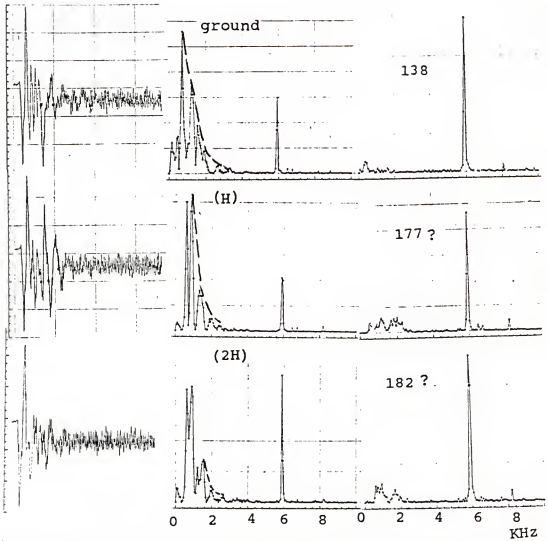

A. Time domain plot B. Full spectrogram C. Spectrogram of SI?

Figure 6.7 Time-domain plot and spectrograms of condition F (natural water site with 6 cm grass) for elevated positions of 300 MHz antenna.

* ? means no answer
--- an uninterrupted decay envelope

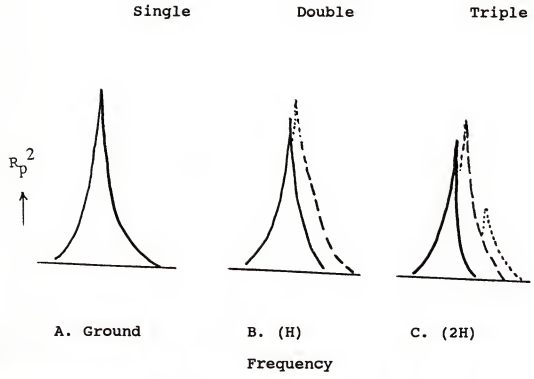

Figure 6.8 Decay pattern of the envelope curve from elevated position of 300 MHz antenna.

CHAPTER 7
CHARACTERISTICS OF ECHO SIGNALS FROM THE WATER TABLE

7.1 The Characteristics of the Full Spectrograms and Their Corresponding Time-Domain Series

The actual sample size N_A and the position of the end point of the first four cycles E_{TL} of echo signals from the 39 GPR transect sites (given in Appendix C) are listed in Table 7.1. The characteristics of the spectrogram include phase change ϕ_c, ΣR_p^2, and frequency of peaks f_p. The values of ϕ_c (given in Appendix D) are near 180°, 75% of them are within 180°± 10°. The $\%\Sigma R_p^2$ values and locations of important peaks are also given in Table 7.1. The important peaks are located at 800, 1,200, 1,600 and 6,000 Hz. There are smaller peaks located at 200, 400 and 2,000 Hz.

7.2 Location of Zero Surface Position in Echo Signal of a 4-M Transect Line

7.2.1 The E_{SR} Values for 39 GPR Transect Sites

The end point of the SR portion, E_{SR}, is the separation point between SR and SI portions; therefore, it represents the

ground surface and is defined as the zero surface position in the digital echo signal. The digital echo signals from 39 measurement sites were treated by the separation technique described in Chapter 6. The E_{SR} values and the important peaks are shown in Table 7.2. The peaks occurring at 400, 1,200, and 2,000 Hz disappear when the TL portion is removed. However, the separation procedure is inapplicable to condition C (Figure 6.4), comprised of a subsurface interface formed by sandy loam and a water bag, which has a very high reflection coefficient of -0.64 but has no capillary fringe zone.

7.2.2 The Ground Condition and Echo Signal of SR

There are two E_{SR} locations corresponding to long grass and short grass ground cover conditions (Table 7.2). At the long grass site, grass is cut to a height of 4 to 7 Cm, whereas at the short grass site, it is cut to a height of 2 to 3 Cm. In the time-domain series, the second peak of the SR portion for the long grass site is abruptly weakened, and the end of this half-period indicates the location of E_{SR}. The second peak of the SR portion is sharp for the short grass site, and the SR portion contains at least three half-periods.

In the spectrogram, a tail-peak characteristic [ϕ_c] represented the difference between the ϕ_c value before (termed as ϕ_f) and after (termed as ϕ_{SI}) the portions of TL and SR are removed. This value responses the topographic variation of

the ground. The negative value of $[\phi_c]$ only occurs when the ground surface is inclined downward as shown in Figure 7.1.

7.3 The SI Portion from Water-Table Profile

7.3.1 The Typical Pattern and the Tail Peak

The spectrograms of the SI portion of all water-table sites have only one tail peak. The unique characteristics of this spectrogram are the existence of the single peak and the meaningful value of phase change due to this tail peak. This spectrogram is regarded as the typical pattern and consists of only the subsurface interfaces as shown in Figures 6.5.E and 6.5.F. The phase change of this tail peak from the water-table profile is approximately 180°. Seventy-five percent of ϕ_f values are within 180°±10°, whereas ϕ_{SI} has 80% as listed in Appendix D. The increase of 5% of the phase change within 180°±10° indicates the increase of the contribution of deeper subsurfaces due to the removal of portions of TL and SR.

7.3.2 The Water Content of a Medium

For a given site, the location of index peaks is fixed at a specified frequency in the spectrograms, even if the

TL and SR portions are removed sequentially. For seven ground-truth sites, the frequency of the tail peak ranges from 6,000 Hz to 8,850 Hz, as shown in Appendix E. Figure 7.2 shows the relationship between the location of the tail peak (f_t) and the average volumetric water content (θ_v). The frequency of the tail peak is inversely proportional to the average water content in the region above the reflected interface, as described in the following equation:

$$f_t = 8769.62 - 273.137\ \theta_v$$

$$r = -0.9816 \qquad 7.3.1$$

The average water content in the steel plate is assumed as zero. The tail peak of the echo signal from this zero water content condition is located at 8,850 Hz. As the water content of the medium increases, the tail peak shifts to lower frequency due to the decrease in travelling velocity. This confirms the theoretical relationship described in Eq. 4.2.11 in which the travelling velocity is proportional to the frequency of an electromagnetic wave.

7.4 Computation of Water-Table Depth

7.4.1 Time Scaling in the Time-Domain Series

Since a GPR echo signal datum in the time domain is a two-dimensional point, the time axis should be scaled to a

standard time unit. The zero sampled data point is the end of the scan signal. The 17^{th} sampled data point corresponds to the beginning of the transmitter loss portion. The average distance between the transmitter and the receiver is 46 Cm. It takes 1.5 ns to travel this distance through the air. Therefore, the unit time of a data point at a sampling rate of 20 KHz is 0.08824 ns. For ground truth site 0M+0Cm, the value of E_{TL} is 66, so that the surface reflection SR returns to become a significant peak at the time of 5.8 ns. For E_{SR} = 93, the echo signal from the subsurface interface becomes a significant period in the time domain-series at the time of 8.2 ns, as shown in Figure C.1.

7.4.2 Computation of Water-Table Depth

The profile information from the four ground truth sites is given in Appendix F. The interface between the soil and water table is not the location of the highest reflection coefficient along the profiles of these sites. Therefore, the echo signal from the water table does not necessarily correspond to the highest amplitude peak as previous researchers assumed (see Chapter 1).

In order to locate the starting data point of the water table, B_{WT}, a three-point moving average is plotted for the SI portion to match the variation of reflection coefficients, as shown in Figures 7.3 to 7.6. The location of the B_{WT} is

the point indicating the existence of a water table within the SI portion. The water-table interface is located behind the highest reflection coefficient point for one or two half-periods. The portion of the water-table interface WT is shown in the figures. The starting point of the WT portion is B_{WT}. A linear relationship between water-table depth D_{WT} versus B_{WT} for ground truth sites indicates that B_{WT} was determined to be very close. This linear relationship is described as the following equation,

$$D_{WT} = 12.24 + 2.09332\ B_{WT}$$

$$r = 0.9917 \qquad 7.4.2$$

Therefore, there are two ways to calculate the water-table depth based on the known unit time and the value of B_{WT}. Once B_{WT} is obtained, the location of the water table is found. The receiving time of the water-table interface is computed as $0.08824 \times B_{WT}$ ns. The other way is to locate the water-table interface by the traditional dual antenna method (described in Chapter 3).

7.5 The Pattern and Decay of Echo Signals from Water-Table Interface

7.5.1 Reflection Coefficients from Water-Table Interface

The reflection coefficients R_r of the 39 GPR transect sites ranges from -0.05 to -0.11, according to computation

results for four ground truth sites as shown in Table 7.4. The reflection coefficients (described in Appendix F) are plotted in Figures 7.3 to 7.6. It obtained by applying Eqs. 2.1.1 and 4.4.6 to the data in Appendix E.

7.5.2 Decay and Pattern

From Figures 7.3 to 7.6, the WT portion starting from B_{WT} is basically a three half-period pattern, but in most cases it has just one half-period because of weak returns.

Table 7.1 Actual sample size N_A, end point location E_{TL}, and the important peaks for a 4-M GPR transect line.

Site	N_A	E_{TL}	peaks #1 Location Hz	#1 $\%ER_p^2$	#2 Location Hz	#2 $\%\Sigma ER_p^2$	Tail Location Hz	Tail $\%ER_p^2$	ΣER_p^2
0M + 0Cm	365	66	800	40.0	1,600	10.2	6,000	12.0	205,750
0M + 10Cm	365	66	800	23.3	1,600	9.8	6,000	14.6	203,656
0M + 20Cm	365	66	800	24.5	1,600	7.6	6,000	12.7	195,129
0M + 30Cm	365	66	800	22.7	1,600	8.5	6,000	5.6	195,474
0M + 40Cm	365	66	800	20.1	1,600	5.8	6,000	5.0	201,331
0M + 50Cm	365	73	800	40.6	1,600	15.7	6,000	10.0	201,304
0M + 60Cm	365	73	800	30.3	1,600	13.4	6,000	8.5	192,851
0M + 70Cm	365	74	800	25.6	1,600	12.7	6,000	9.2	188,885
0M + 80Cm	365	74	800	24.9	1,600	13.0	6,000	11.8	185,368
0M + 90Cm	365	71	800	25.1	1,600	10.8	6,000	10.2	180,814
1M + 0Cm	365	72	800	20.5	1,600	8.5	6,000	10.7	172,737
1M + 10Cm	365	70	800	16.7	1,600	10.2	6,000	11.5	176,703
1M + 20Cm	365	70	800	17.5	1,600	9.2	6,000	11.7	175,626
1M + 30Cm	365	67	800	23.5	1,600	7.4	6,000	12.0	166,446
1M + 40Cm	365	66	800	22.4	1,600	7.6	6,000	10.2	165,495
1M + 50Cm	364	66	800	21.3	1,200	7.7	6,000	9.2	162,651
1M + 60Cm	364	66	800	32.4	1,200	6.1	6,000	6.7	177,435
1M + 70Cm	364	66	800	27.2	1,200	6.9	6,000	12.8	182,844
1M + 80Cm	364	66	800	26.1	1,600	7.5	6,000	13.4	182,664
1M + 90Cm	364	66	800	35.0	1,700	8.3	6,000	11.5	185,687
2M + 0Cm	364	67	800	32.1	1,000	5.7	6,000	11.6	199,045
2M + 10Cm	364	67	800	34.7	1,200	5.6	6,000	11.7	180,390
2M + 20Cm	364	67	800	26.7	1,200	25.5	6,000	20.5	159,117
2M + 30Cm	364	67	800	20.1	1,200	20.9	6,000	20.3	152,196
2M + 40Cm	364	67	800	18.3	1,200	8.7	6,000	18.5	151,359
2M + 50Cm	364	67	800	18.7	1,200	10.3	6,000	17.7	149,519
2M + 60Cm	364	67	800	18.6	1,200	16.4	6,000	18.1	157,864
2M + 70Cm	364	67	800	21.9	1,200	18.2	6,000	20.1	156,885
2M + 80Cm	364	66	800	24.3	1,200	19.7	6,000	18.1	167,221
2M + 90Cm	364	67	800	23.4	1,200	18.8	6,000	19.1	171,573
3M + 0Cm	364	67	800	19.1	1,200	25.1	6,000	22.0	188,750
3M + 10Cm	364	67	800	25.4	1,200	20.1	6,000	14.8	165,304
3M + 20Cm	364	66	800	27.1	1,200	20.1	6,000	15.0	163,954
3M + 30Cm	364	66	800	32.4	1,200	15.1	6,000	14.2	164,808
3M + 40Cm	364	66	800	18.6	1,200	10.2	6,000	9.9	165,529
3M + 50Cm	364	66	800	15.8	1,200	10.2	6,000	7.6	179,749
3M + 60Cm	364	67	800	16.7	1,200	10.9	6,000	6.9	185,326
3M + 70Cm	364	68	800	25.7	1,600	11.4	6,000	5.8	188,643
3M + 80Cm	364	67	800	25.8	1,200	10.2	6,000	7.6	190,045

Note: N_A - Actual sample size

E_{TL} - End point of portion transmitter loss

$\%ER_p^2$ - Area % of peak located at f_p, based on total area of full spectrogram ER_p^2

Table 7.2 End point Location E_{SR} and the important peaks after TL is removed for a 4-M GPR transect line.

Site	E_{SR}	Height of grass cm	Peak #1		Peak Tail	
			Location Hz	$\%\Sigma R_p^2$	Location Hz	$\%\Sigma R_p^2$
0M + 0Cm	131	3	800	15.2	6,000	8.5
0M + 10Cm	96	5	800	6.5	6,000	10.5
0M + 20Cm	105	4	800	5.8	6,000	12.1
0M + 30Cm	110	4	800	6.2	6,000	10.3
0M + 40Cm	100	4	800	3.8	6,000	14.1
0M + 50Cm	100	5	800	4.5	6,000	11.2
0M + 60Cm	113	6	800	8.5	6,000	10.5
0M + 70Cm	112	6	800	10.5	6,000	10.2
0M + 80Cm	99	6	800	3.9	6,000	14.2
0M + 90Cm	100	7	800	4.5	6,000	13.1
1M + 0Cm	114	5	800	7.6	6,000	11.0
1M + 10Cm	112	4	800	6.2	6,000	10.6
1M + 20Cm	118	4	800	5.9	6,000	12.0
1M + 30Cm	118	3	800	6.5	6,000	10.9
1M + 40Cm	116	4	800	7.0	6,000	10.2
1M + 50Cm	91	5	800	3.6	6,000	13.1
1M + 60Cm	95	6	800	4.5	6,000	12.6
1M + 70Cm	93	3	800	4.7	6,000	12.9
1M + 80Cm	94	2	800	4.8	6,000	13.2
1M + 90Cm	122	2	800	4.0	6,000	9.2
2M + 0Cm	122	4	800	11.6	6,000	9.9
2M + 10Cm	138	4	800	14.4	6,000	9.5
2M + 20Cm	118	6	800	12.1	6,000	10.0
2M + 30Cm	137	7	800	14.8	6,000	8.6
2M + 40Cm	94	6	800	3.4	6,000	13.6
2M + 50Cm	93	5	800	3.5	6,000	14.5
2M + 60Cm	97	6	800	3.7	6,000	14.0
2M + 70Cm	95	5	800	3.8	6,000	12.7
2M + 80Cm	94	5	800	4.0	6,000	14.6
2M + 90Cm	96	5	800	3.6	6,000	11.9
3M + 0Cm	96	4	800	4.9	6,000	11.7
3M + 10Cm	100	5	800	5.0	6,000	11.5
3M + 20Cm	96	6	800	4.3	6,000	10.0
3M + 30Cm	109	4	800	6.5	6,000	9.5
3M + 40Cm	104	4	800	4.9	6,000	10.6
3M + 50Cm	115	3	800	7.8	6,000	9.8
3M + 60Cm	118	2	800	8.9	6,000	8.9
3M + 70Cm	118	2	800	8.6	6,000	9.6
3M + 80Cm	120	3	800	10.4	6,000	7.9

Note: $\%\Sigma_p^2$ - Area % of peak located at f_p, based on total area of full spectrogram.

Table 7.3 B_{WT}, T_{WT}, and the water-table depth evaluated for a 4-M GPR transect line.

Site	Water-table depth interpolated cm	B_{WT}	T_{WT} ns	Number of peak after E_{SR}
0M + 0Cm	65.0*	146	12.88	2
0M + 10Cm	66.0			
0M + 20Cm	66.5			
0M + 30Cm	67.1			
0M + 40Cm	67.5			
0M + 50Cm	67.0			
0M + 60Cm	68.3			
0M + 70Cm	68.0			
0M + 80Cm	66.5			
0M + 90Cm	67.6			
1M + 0Cm	68.0			
1M + 10Cm	67.5			
1M + 20Cm	68.0			
1M + 30Cm	67.0			
1M + 40Cm	66.5			
1M + 50Cm	66.2			
1M + 60Cm	68.0			
1M + 70Cm	70.0			
1M + 80Cm	72.1			
1M + 90Cm	75.0			
2M + 0Cm	78.2			
2M + 10Cm	79.2*	184	16.24	4
2M + 20Cm	83.0			
2M + 30Cm	85.0			
2M + 40Cm	87.3			
2M + 50Cm	88.0			
2M + 60Cm	89.0			
2M + 70Cm	89.5			
2M + 80Cm	90.5			
2M + 90Cm	93.0			
3M + 0Cm	96.4*	208	18.35	3
3M + 10Cm	95.0			
3M + 20Cm	98.0			
3M + 30Cm	97.5			
3M + 40Cm	99.9			
3M + 50Cm	102.0			
3M + 60Cm	104.7			
3M + 70Cm	107.0			
3M + 80Cm	109.1*	243	21.44	4

* Ground truth sites

Table 7.4 Reflection coefficient R_r calculated from sites with various soil conditions.

GPR probing site	Subsurface Interface	Relative dielectrical constant upper layer	lower layer	R_r
	condition A (dry profile) L vs CL	4.37	5.34	-0.05
	condition B (wet profile) L vs CL	4.37	5.34	-0.05
Figure 6.4	condition C SL vs water bag	3.85	8.10	-0.64
	condition D S vs water table	10.12	8.10	-0.48
ground truth point in probing transect site	0M + 0Cm SL vs water table	11.96	18.44	-0.11
	2M + 10Cm SL vs water table	10.71	16.87	-0.11
	3M + 0Cm SL vs water table	11.30	13.97	-0.05
	3M + 80Cm SL vs water table	13.97	17.66	-0.06

Note: L: loam
CL: clay loam
SL: sandy loam

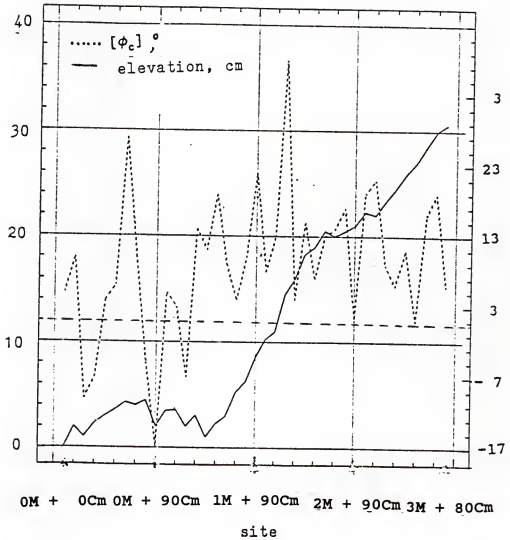

Figure 7.1 Topographic variation versus [ϕ_c] in 39 sites of the 4-M GPR transect line.

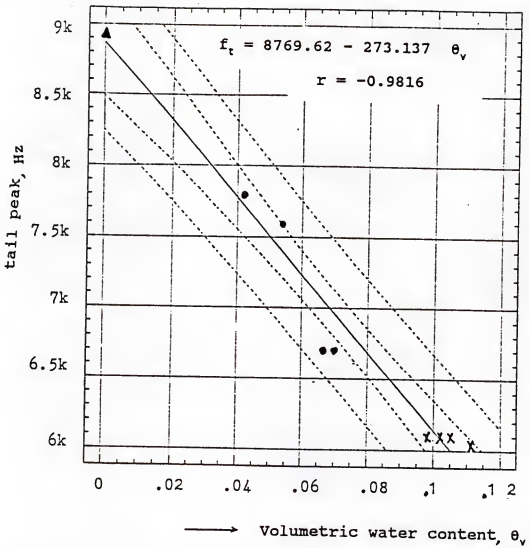

Figure 7.2 Relationship between the tail peak and average volumetric water content in the region above the reflected interface.

▲ - Tail peak formed from steel plate
● - Tail peak from echo signals in Figure 6.4
X - Tail peak from 13-ft GPR transect line

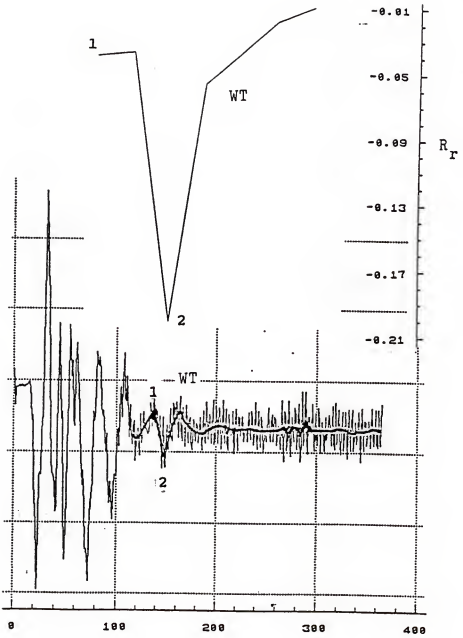

Figure 7.3 The smoothed curve and the corresponding reflection coefficients of SI portion for site 0'+0".

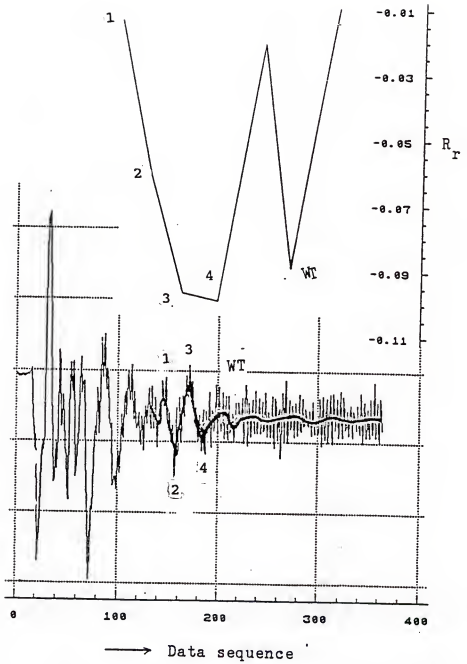

Figure 7.4 The smoothed curve and the corresponding reflection coefficients of SI portion for site 7'+0".

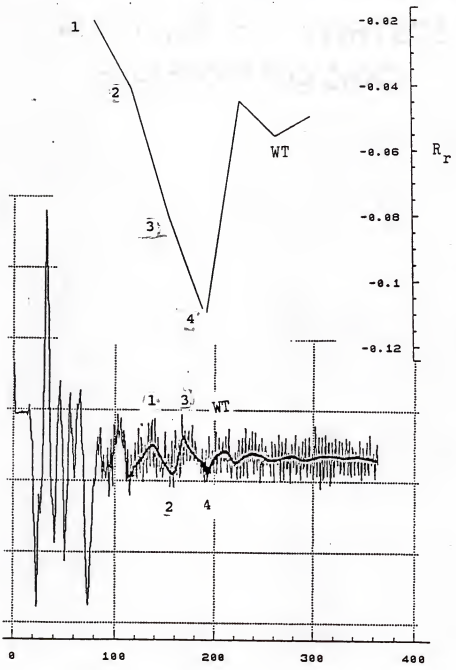

Figure 7.5 The smoothed curve and the corresponding reflection coefficients of SI portion for site 10'+0".

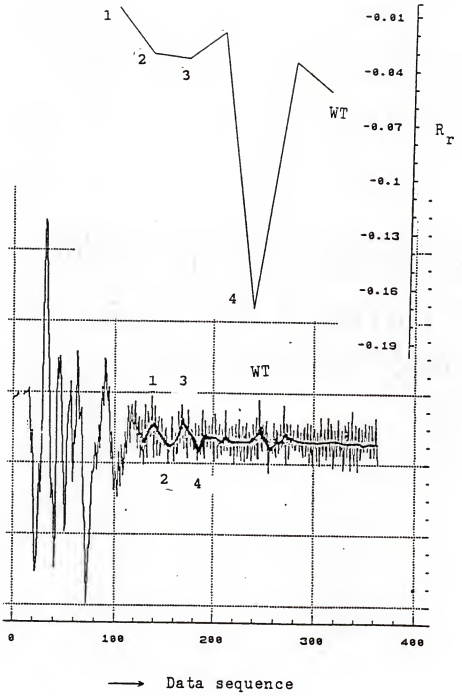

Figure 7.6 The smoothed curve and the corresponding reflection coefficients of SI portion for site 12'+8".

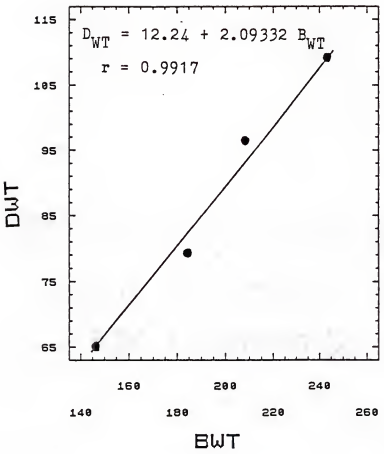

Figure 7.7 The relationship between B_{WT} and ground truth water-table depth D_{WT}.

CHAPTER 8
MAPPING THE WATER TABLE

8.1 Procedure for Mapping the Water Table

The procedure for mapping the water table by the separation technique is illustrated in the flow chart shown in Figure 8.1, which is based on the use of a 300 MHz antenna in the GPR probing. There are some important characteristics in the time and frequency domains for each step. Those characteristics belonging to the time-domain series are abbreviated as T_i, and those characteristics belonging to the frequency-domain spectrogram are abbreviated as F_i.

8.2 Sampling by DAS-50

The DAS-50 or any equivalent data acquisition board with on-board memory should be used to meet the requirements of continuous high-speed sampling. The important characteristics are described as follows:

T1: The actual sample size N_A is restricted by machine parameter (scan speed) and is less than the total sample size N_T and the programmed sample size N_p because of the existence of scan signals.

F1: The important peaks in the full spectrogram occur at 400, 600-800, 1,2000-1,600, and 6,000-8,000 Hz.

F2: The tail peak has a value of ϕ_c near 180° in the full spectrogram.

8.3 Removal of Transmitter Loss TL

The important characteristics are as follows:

T2: The portion of TL that is visible has a four-cycle pattern. The end point of TL, E_{TL}, is always located at the end of the fourth period of a full echo signal. The value of E_{TL} ranges from 66 to 74.

F3: The tail peak has a value of ϕ_c near 180° in the spectrogram without TL.

F4: The important peaks in the spectrogram occur at 800, and 6,000 Hz after TL is removed.

8.4 Removal of Surface Reflection SR and Replacement of Ground Elevation Data

The important characteristics are as follows:

T3: The basic pattern of SR has four cycles. It may be reduced to one, two, or three cycles due to attenuation caused by surface conditions. On a long grass site it has just one or two cycles, whereas on a short grass site

it has three or four cycles. The end point of SR, E_{SR}, ranges from 93 to 138.

T4: For a short grass site the portion of SR has a high second peak, whereas for a long grass site there is an abrupt reduction of the second peak.

T5: The E_{SR} is the location of zero surface, therefore, this value is replaced by elevation data.

F5: The tail peak in the spectrogram of the SI portion has a value of ϕ_c near 180°.

F6: The peak located at 800 Hz disappered after SR is removed.

F7: The difference value ,$[\phi_c]$, between the value of ϕ_c before (termed as ϕ_f) and after (termed as ϕ_{SI}) the portions of TL and SR are removed corresponds to topographic variation. A positive increase in elevation compared to that of the previous site produces a positive value of $[\phi_c]$; a decrease one may has a minus value of $[\phi_c]$.

F8: The location of E_{SR} is found when the spectrogram has a typical pattern containing a single peak. This is an important criterion in determining E_{SR} from the time-domain series. The residual portion coming after E_{SR} in the time-domain series is the SI portion.

8.5 Computation of Water Table

T6: The SI portion contains all information from the subsurface. The readouts of various interfaces correspond to the reflection coefficients of the computations. The highest peak in the SI portion indicates the location of the capillary fringe zone. The beginning data point of the water-table portion B_{WT} comes after the highest reflection coefficient by 15-30 cm.

T7: The receiving time of the water-table interface signal T_{WT} is obtained from 0.08824 ns x B_{WT}.

T8: The B_{WT} is a reliable parameter because of its good linearship with water-table depth D_{WT} as shown in Figure 7.7. The D_{WT} is counted as the distance from the ground surface to the location of B_{WT} as shown in Figure 8.2.

T9: Since the GPR is towed along the ground surface after the E_{SR} value is replaced by the elevation data of the ground surface, water-table depth D_{WT} relative to a reference is computed as follows:

D_{WT} = water-table elevation + ground elevation

This water-table depth also can be obtained by the traditional dual method based on the known unit time of 0.08824 ns in the time-domain series from B_{WT}.

8.6 Mapping the Water Table

T10: The water-table elevation and the elevation data are plotted along the transect line as shown in Figure 8.3.

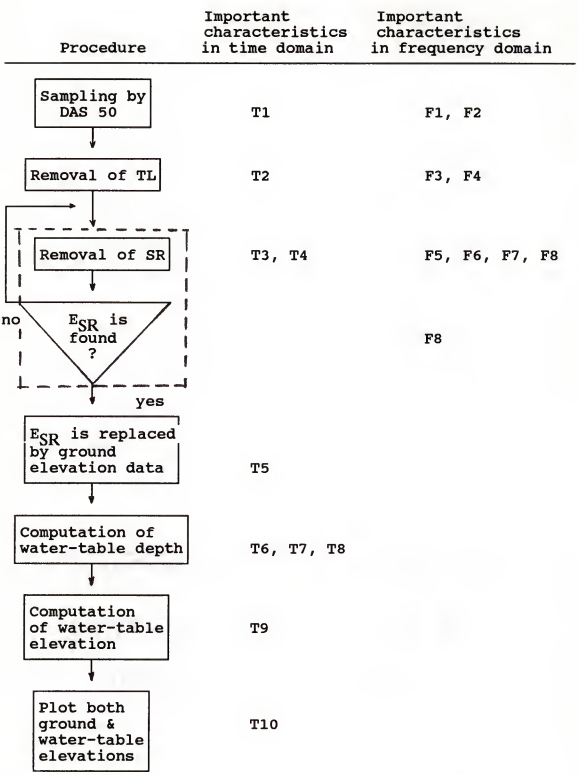

Figure 8.1 Flow chart for mapping water table from a digital echo signal.

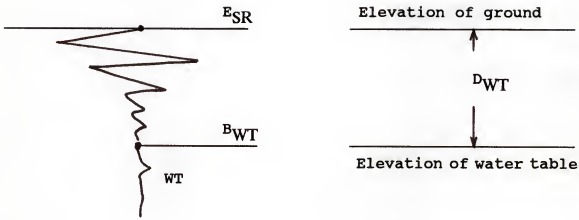

A. Zero surface E_{SR} and the beginning data point B_{WT} of water-table portion

B. Definition of water-table depth

Figure 8.2 Sketch of water-table depth in digital echo signal.

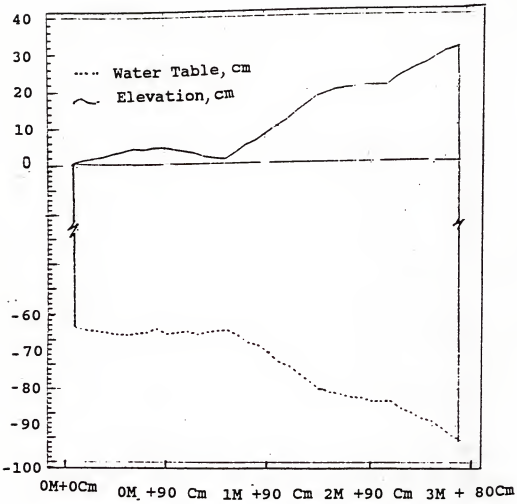

Figure 8.3 Mapping the water table.

CHAPTER 9
CONCLUSIONS AND SUGGESTIONS

9.1 Conclusions

This research demonstrates the theoretical derivation of readouts of GPR echo signals. The reason for water-table interface detection has been expressed in terms of dielectric constants. Although the reason for the ability of GPR to detect a water table is that the dielectric constants bounding the water-table interface have an abrupt change, a high readout of the reflection coefficient in the time-domain series of this echo signal may indicate a capillary fringe zone rather than the location of a water table.

A digital echo-signal record of GPR may be obtained by installing a data-acquisition board in a personal computer. This type of data-acquisition approach has many advantages. It is relatively inexpensive, light in weight, convenient to use, large in storage capacity, and high in processing power.

The convertible relationship between the time-domain series and the frequency-domain spectrogram is employed in this research to distinguish the water-table portion of the digital echo signal. The useful characteristics in the

spectrogram include frequency, amplitude, peak pattern, and phase change, whereas those in the time-domain series include the data sequence and peak pattern. The separation technique described in this research isolates the three components of a digital echo signal--transmitter loss (TL), surface reflection (SR), and subsurface interface reflection (SI). The TL portion in the time-domain series is a four-cycle pattern (when using a 300 MHz antenna). It is distinct enough to allow separation of TL from SR. The contribution of this TL portion is revealed in peaks corresponding to frequencies of less than 600 Hz and 1,200-1,600 Hz in the spectrogram. The SR portion takes into account the functions of topography of the ground surface and ground cover. The contribution of this portion is found in the peaks at frequencies of 800-1,200 Hz in the spectrogram. The separation of SR from SI is based on the appearance of an typical pattern containing an tail peak located at 6,000 to 8,850 Hz.

The SI portion exhibits a sharp definition because it forms only a single peak, located between 6,000 and 8,850 Hz in the spectrogram. The location of this tail peak is modified by the water content of the soil profile above the reflected interface. If the soil is dry, the frequency of the tail peak is high; if it is wet, the frequency of the tail peak is low. The phase change ϕ_c of the tail peak is maintained at approximately 180°.

Since the SI portion is the only useful signal to GPR users, the advantage of isolatable SI is significant. A digital data file consisting of only the SI portion needs a smaller memory size than the one of the full time-domain series. Any further processing becomes easier because of no disturbance and interaction from the TL and SR portions.

The maximum reflection coefficient in the SI portion indicates the existence of the capillary fringe zone. The water-table interface, beginning with the value B_{WT}, occurs 15-30 cm behind the capillary fringe zone. The basic pattern of the water-table interface is three half-periods but most cases are attenuated to one half-period. The time interval per data point in the time-domain series (obtained at a sampling rate of 20 KHz with scanning speed of 51.2 scan/sec) is 0.08824 ns. This known value allows the calculation of water-table depth directly from the digital data series by the traditional dual antenna method or by measuring B_{WT}.

9.2 Suggestions

(1). The PC-based data acquisition approach is a prospective method to improve the disadvantage of information truncation of the graphic recorder.

(2). A new and compact digital data file can be obtained by applying the important discoveries in this research. The digital data file contains the only subsurface

interfaces informatiom. Since such a file does not include the portions of TL and SR the required memory size become economical and the further analyses become easier. Either software or hardware approaches can be further developed in order to fully take these advantages of this technique.

(3) The computation of the water-table depth from a single antenna measurement is possible because of the existence of precursor of water-table interface. The reflected readout of water-table interface is not the highest one. The highest readout comes from the capillary fringe zone and thus it can be treated as the precursor to indicate that the next peak readout is the water-table interface.

APPENDIX A
DATA ACQUISITION PROGRAM FOR USING DAS-50

```
{$R-}    {Range checking off}
{$I-}
{$B+}    {Boolean complete evaluation on}
{$S+}    {Stack checking on}
{$N-}    {No numeric coprocessor}
{$M 65500,16384,655360} {Turbo 3 default stack and heap}
{$O+}

(*************************************************************************)
(***       DAS-50 Data Acquisition and Logging program                 ***)
(***         For a Trace-After Trigger to sample channel 0             ***)
(***                      TURBO PASCAL 5.5 -XT-                        ***)
(***         COPY RIGHT : Sheng lewis Liang  3-20-1999                 ***)
(***                    A ANALOG TRIGGER IN CHANNEL 0                  ***)
(*************************************************************************)

program finaldas;

uses  Dos, Crt, printer;

type
      sample = array[1..400] of integer;
      data=^sample;
      StringOne = string[255] ;
      StringTwo = string[32]  ;
       xstring  = string[4];
       ystring  = string[15];
var
      Regs                                          : Registers ;
      LogFile,DASIN,DASOUT                          : text      ;
      AString,Bstring                               : StringOne ;
      TMString,CHString                             : StringTwo ;
      EN,SMString,VString                           : StringTwo ;
      pop,head                                      : xstring   ;
      filename                                      : ystring   ;
      CString,ChannelA,ChannelB,Channelc,Clock      : integer   ;
      Status,Channel,Trigger,Range,I,II,y,yy        : integer   ;
      Key                                           : char      ;
      Hour,Minute,Second,Second100,date             : word      ;
      year,month,day,Day_of_week                    : word      ;
      d,dx                                          :data ;
procedure clearscreen ;
begin
   Regs.ah := 6 ;
   Regs.al := 0 ;
   Regs.bh := 7 ;
   Regs.ch := 0 ;
   Regs.cl := 0 ;
   Regs.dh := 24 ;
   Regs.dl := 79 ;
   intr(16,Regs) ;
end ;

procedure sampley(y:integer;head:xstring);

(* Read a Key from the Keyboard - getkey *)
(* read a command from the batch file -getword *)

 FUNCTION GetKey : char ;
   var TempKey : char ;
   BEGIN
     TempKey := ReadKey ;
     if(Tempkey = #0) THEN TempKey := ReadKey ;
     GetKey := TempKey ;
   END;
```

```
  FUNCTION GetWord : char; (* a text file y.dat of only one y is provided *)
  var TempKey : char;
      ReadFile    : File of Char;
  Begin
    Assign(Readfile,'Y.DAT');
    Reset(ReadFile);
    Read(ReadFile,TempKey);
    Close(ReadFile);
    if(TempKey=#0) Then TempKey := ReadKey;
    Getword :=TempKey;
  END;

(* OutPut a string to the DAS-50 device driver *)
FUNCTION D50Output(Str:StringTwo):integer ;
BEGIN
  writeln(DASOUT,Str);
  D50Output := IOResult ;
END;

(* Read the Current Status of the DAS-50 as a string *)
(* and convert the string to an integer.  This is    *)
(* a useful way to control routines that act on the  *)
(* Status output                                     *)

FUNCTION D50InputInt (var Number:integer):integer ;
var  NumString : string[32] ;
var  Result    : integer    ;
var  Code      : integer    ;
BEGIN
   ReadLn(DASIN,NumString) ;
   Result := IOResult ;
   if     (Result <> 0) then D50InputInt := 1      (* Error in Read *)
   else   Begin
          val(NumString,Number,Code) ;
          if   (Code <> 0) then D50InputInt := 1
          else                  D50InputInt := 0 ;
          END;
END;

FUNCTION D50InputString(var Stw:StringTwo):integer ;
var  Result                              :integer ;
BEGIN
   ReadLn(DASIN,Stw) ;
   Result := IOResult ;
   if (Result <> 0) then D50InputString := 1 (* Error in Read *)
   else
          D50InputString := 0 ;
END ;

PROCEDURE D50InString ;
BEGIN
   readln(DASIN,EN);
   readln(DASIN,AString);
   readln(DASIN,BString);
end ;

PROCEDURE GetError  ;
BEGIN
    clearscreen ;
    GotoXY(6,27);
    D50InString ;
    writeln(char(7));
    writeln('Driver Error Has Occurred !!');
    writeln('DAS-50 Error Number => ',EN);
    writeln('Error => ',BString);
    writeln('On Command Line of => ',Astring);
    Halt ;
end;
```

```
BEGIN
new(d);
 str(y,head);
 for II:=1 to 1 do
 begin
   str(II,pop);
   filename :='w'+head+'w'+pop+'.58';
 Assign(LogFile,filename);
 Assign(DASIN  ,'$DAS50'); (* Open Device Driver for Input *)
 Assign(DASOUT ,'$DAS50'); (* Open Device Driver for Output *)
 Reset(DASIN);             (* Input, PASCAL has no read/write text files *)
 Rewrite(DASOUT);          (* Output, see above *)
 ClearScreen ;             (* Use BIOS scroll to clear screen *)
 GotoXY(1,7);              (* Set cursor to Row 1, Col 7 *)
 WRITELN('  DAS-50 Data Acquisition and Logging Program lian50',II,'.pas');
 WRITELN ;
 WRITELN ;
 WRITELN ;
 WRITELN('     This Program provides a simple sample for the acquisition ');
 WRITELN('of 400 samples from channel 0 in the  Trace-After-Trigger mode.');
 WRITELN('The DAS-50 is set up and controlled by the software driver with');
 WRITELN('the data being stored in the DAS-50 buffer memory. The data can');
 WRITELN('then be logged to a disk file called dytn For This ex-');
 WRITELN('ample, the channel data is logged sequentially.');
 WRITELN ;
 WRITELN('Connect inputs to Channel 0 in the range of  +/- 10 volts.');
 WRITELN('When you have done this, press ''Enter'' to start the DAS-50.');
 WRITELN('Pressing ''Esc'' will abort this program');
 WRITELN ;
 WRITELN ;
 WRITELN ;
 WRITELN ;
 WRITELN ;
 WRITELN(CHR(7)) ;  (* BELL *)
 WRITELN('Press any key to continue . . .');
 Key := GetKey; ) (* GetKey Takes Care of Two Digit Function Keys *)
 if(D50Output('Clear') <> 0) then GetError;  (* Output command to *)
                          (* Clear Device      *)

 (* ------------------------------------------------------------*)
 (* Set up the DAS-50 to take 400 samples, direct from channel *)
 (* 0, in the Trace-After Trigger mode.  Note that*)
 (* all the following Print statements could be abbreviated    *)
 (* and put into one print statement                           *)
 (*------------------------------------------------------------*)

 if (D50Output('Set Channels=0    ') <> 0) then GetError ;
 if (D50Output('Set Samples=400   ') <> 0) then GetError ;
 if (D50Output('Set Range= +-10v  ') <> 0) then GetError ;
 if (D50Output('Set Trigger Mode=0') <> 0) then GetError ;
 if (D50Output('Set Start=After   ') <> 0) then GetError ;
 if (D50Output('Set Rate = Int 2e4') <> 0) then GetError ;

 (*------------------------------------------------------------*)
 (* Command the DAS-50 to Acquire the Data                     *)
 (*------------------------------------------------------------*)

 if (D50Output('Acquire') <> 0) then GetError ;

{ writeln(' now finish file ', II);

 ELSE)
 end;  (loop for II)

 Status := 0 ;  (* Device Clears Bits 3 & 4 upon completion of *)
              (* Data Acquisition *)
```

```
  while ((Status AND $018) <> $018) DO (* While Bits 3 & 4 Clear *)
  BEGIN              (* Device Still Gathering Data *)
       IF (D50OutPut('Get Status') <> 0) then GetError ;
       IF (D50InputInt(Status) <> 0) then GetError ;
  END ;
(*-------------------------------------------------------------*)
(* End the Data Acquisition Portion of the Program            *)
(*-------------------------------------------------------------*)

  ClearScreen ;
  GotoXY(27,4);
  WRITELN('Data Acquisition Complete');
  GotoXY(6,10);

  (*-------------------------------------------------------------*)
  (* PROMPT FOR LOGGED DATA FILE OR NOT                        *)
  (*-------------------------------------------------------------*)

  WRITELN('Do You Wish to Log the Acquired Data to Disk (Y or N)');
  Key := GetKey ;
  if ((Key <> 'Y') AND (Key <> 'y')) Then Halt ;
  Rewrite(LogFile) ;

  (*       TITLE OF FILE       *)

  WriteLn(LogFile,'DAS-50 Log Program w',y,'w',II);

  (*       TIME OF DAY         *)
  GetDate(Year,Month,Date,Day_of_week);
  GetTime(Hour,Minute,Second,Second100) ;
  write(LogFile,'Date and Time  ');

  case day_of_week of

  0 : begin
      write(LogFile,'sun');
      end;

  1 : begin
      write(LogFile,'mon');
      end;
  2 : begin
      write(LogFile,'tue');
      end;
  3 : begin
      write(LogFile,'wed');
      end;
  4 : begin
      write(LogFile,'thr');
      end;
  5 : begin
      write(LogFile,'fri');
      end;
  6 : begin
      write(LogFile,'sat');
      end;
end;


 write(LogFile,Month:3,'M ');
  write(LogFile,Day:2,' ');
  if (Hour < 10) Then write(LogFile,'0',Hour:1,':')
     else             write(LogFile,Hour:2,':');
  if (Minute < 10) Then write(LogFile,'0',Minute:1,':')
     else             write(LogFile,Minute:2,':');
  if (Second < 10) Then write(LogFile,'0',Second:1,'.')
     else             write(LogFile,Second:2,'.');
  if (Second100 <10) Then write(LogFile,'0',Second100:1,'-')
     else             write(LogFile,Second100:2,'-');
```

```
writeln(LogFile,year:4);

(*       START MODE          *)

if (D500utput('Get StartMode') <> 0) then GetError ;
if (D50InputInt(Status) <> 0)        then GetError ;

if        (Status = 0) then writeln(LogFile,'Trace          Before Trigger')
else  if  (Status = 1) then writeln(LogFile,'Trace          About  Trigger')
else                        writeln(LogFile,'Trace          After  Trigger') ;

(*     TRIGGER MODE      *)

if (D500utput('Get TM') <> 0)  then GetError ;
if (D50InputInt(Trigger) <> 0) then GetError ;

(*     OutPut Correct Trigger Mode To Log File     *)

if ( Trigger = 0 ) then
       writeln(LogFile,'Trigger        Internal')
else if (Trigger = 1) then
       writeln(LogFile,'Trigger        External Digital - Positive Level')
else if (Trigger = 2) then
       writeln(LogFile,'Trigger        External Digital - Negative Level')
else if (Trigger = 3) then
       writeln(LogFile,'Trigger        External Analog - positive Level')
else writeln(LogFile,'Trigger       External Analog - Negative Level') ;

(*       CHANNEL       *)

if (D500utput('Get Channel') <> 0) then GetError ;
if (D50InputInt(Channel) <> 0) then GetError ;
Case Channel of
  0 : BEGIN
       WriteLn(LogFile,'Channel        0');
       Channel := 0 ;
      END ;
  1 : BEGIN
       WriteLn(LogFile,'Channel        1');
       Channel := 1 ;
      END ;
  2 : BEGIN
       WriteLn(LogFile,'Channel        2');
       Channel := 2 ;
      END ;
  3 : BEGIN
       WriteLn(LogFile,'Channel        3');
       Channel := 3 ;
       END ;
  4 : BEGIN
       WriteLn(LogFile,'Channel        0&1');
       ChannelA := 0 ;
       ChannelB := 1 ;
      END ;
  5 : BEGIN
       WriteLn(LogFile,'Channel        0&2');
       ChannelA := 0 ;
       ChannelB := 2 ;
      END ;


6 : BEGIN
       WriteLn(LogFile,'Channel        0&3');
       ChannelA := 0 ;
       ChannelB := 3 ;
      END ;
  7 : BEGIN
       WriteLn(LogFile,'Channel        1&2');
       ChannelA := 1 ;
```

```
            ChannelB := 2 ;
      END ;
```



```
  8 : BEGIN
        WriteLn(LogFile,'Channel        1&3');
        ChannelA := 1 ;
        ChannelB := 3 ;
      END ;
  9 : BEGIN
        WriteLn(LogFile,'Channel        2&3');
        ChannelA := 2 ;
        ChannelB := 3 ;
      END ;
 10 : BEGIN
        WriteLn(LogFile,'Channel      1,2&3');
        ChannelA := 1 ;
        ChannelB := 2 ;
        channelc := 3 ;
      END;
END ; (* CASE of Channel *)

(*      RANGE      *)

if (D500utput('Get Range!') <> 0) then GetError ;
if (D50InputInt(Range) <> 0)     then GetError ;

Case Range of
   0 : writeln(LogFile,'RANGE:          +/- 2.5 Volt');
   1 : writeln(LogFile,'RANGE:          +/- 5.0 Volt');
   2 : writeln(LogFile,'RANGE:          +/- 10.0 Volt');
   3 : writeln(LogFile,'RANGE:          0.0 - 5.0 Volt');
   4 : WRITELN(LOGFILE,'RANGE:          0.0 -10.0 VOLT');
End ;    (* Case of Range *)

if (D500utput('Get Samples') <> 0) then GetError ;
if (D50InputString(VString) <> 0)  then GetError ;
WriteLn(LogFile,'Samples        ',VString);

(*     CLOCK     *)

if (D500utput('Get Clk') <> 0) then GetError ;
if (D50InputInt(Clock) <> 0)   then GetError ;
if (Clock = 0) then writeln(LogFile,'Clock          Internal')
else                writeln(LogFile,'Clock          External') ;

(*     RATE      *)

if (D500utput('Get Rate') <> 0)      then GetError ;
if (D50InputString(VString) <> 0)    then GetError ;
WriteLn(LogFile,'RATE (Hz)     ',Vstring) ;

if (D500utput('Set Address 0') <> 0) then GetError ;

(* IMPORTANT: Send Transfer Parameters in Correct Order    *)
(* Leave Spaces Between Parameters in Command String !!   *)
(* For This Example :                                     *)
(* Command                                                *)
(* Segment of Data Array                                  *)
(* Offset  of Firs Data Array Location                    *)
(* Number of Samples To Take                              *)
(* Auto-Increment Value (1,2 or 4)                        *)
(array is the only data format for trasfer command)
WriteLn(DASOUT,'Transfer ',SEG(D^),' ',Ofs(D^[1]),' ','400',' ','1') ;

if (IOResult <> 0) then GetError ;  (*  Check for Device I/O Error  *)
(*  Write Header for Data Records to Be Written *)
writeln(LogFile,'DATA (Trigger-Relative-Sample,Channel,Value)') ;
```

```
    I := 1 ;
  While ( I < 401 ) do
  begin
     write(logfile,I:6);
     write(LogFile,' ');
     write(LogFile ,channel:5 );
     write(LogFile,' ');
     writeln(LogFile, d^[I]:5  );
    I := I + 1; {for 1 channel}
  end ;
  Close(LogFile);      (* REMEMBER To Close File Here *)
  ClearScreen ;       (* OtherWise, Some Data May Not Be Written *)
  WriteLn ;
  WriteLn ;
  WriteLn('Data Has Been Sequentially Parsed');
  WriteLn('and transfer to disk is complete.');
  WriteLn ;
  WriteLn('ex50_y.ch0 may be examined by using the TYPE command') ;
  WriteLn('                when at the DOS prompt');
  WriteLn ;
  WRITELN('DAS50.EXE FINISHED');
  writeln('Do you want to process ex50_y.ch0 ?');
  delay(1000);

end;    {II}

end;
begin
        clearscreen;
        gotoxy(25,10);
      writeln(' THIS IS THE SAMPLE SET');
      readln(yy);
           sampley(yy,heed);
END.
```

APPENDIX B
AN EXAMPLE OF THE SAMPLED DATA FILE BY DAS-50

The unit of value: x 0.005 Volt.

```
DAS-50 Log Program g8001g1
Date and Time  tue  5M 2577 18:37:23.32-1990
Trace          After  Trigger
Trigger        External Analog - positive Level
Channel        0
RANGE:         +/- 10.0 Volt
Samples         0000400
Clock          Internal
RATE (Hz)      20.000E3
DATA (Trigger-Relative-Sample,Channel,Value)
     1      0    204
     2      0    213
     3      0    210
     4      0     20
     5      0     14
     6      0     15
     7      0     14
     8      0     16
     9      0     16
    10      0     15
    11      0     16
    12      0     16
    13      0     15
    14      0      8
    15      0     17
    16      0     16
    17      0     18
    18      0     18
    19      0     19
    20      0      0
    21      0     -7
    22      0    -11
    23      0     -8
    24      0    -56
    25      0    -84
    26      0    -83
    27      0    -77
    28      0    -47
    29      0    -21
    30      0    -27
    31      0    -35
    32      0     -8
    33      0     57
    34      0     94
    35      0    122
    36      0    122
    37      0     82
    38      0     44
    39      0     21
    40      0    -15
    41      0    -39
    42      0    -41
```

43	0	-37
44	0	-70
45	0	-76
46	0	-17
47	0	35
48	0	52
49	0	42
50	0	18
51	0	-31
52	0	-76
53	0	-84
54	0	-102
55	0	-79
56	0	-16
57	0	11
58	0	37
59	0	60
60	0	65
61	0	40
62	0	25
63	0	21
64	0	9
65	0	10
66	0	34
67	0	28
68	0	16
69	0	5
70	0	-11
71	0	-35
72	0	-38
73	0	-45
74	0	-50
75	0	-58
76	0	-33
77	0	-42
78	0	-36
79	0	-22
80	0	-11
81	0	-32
82	0	-43
83	0	-27
84	0	-42
85	0	-51
86	0	-35
87	0	-32
88	0	-52
89	0	-40
90	0	-12
91	0	-38
92	0	-30
93	0	-3
94	0	-9

95	0	-22
96	0	0
97	0	-3
98	0	-19
99	0	-13
100	0	3
101	0	-12
102	0	-13
103	0	9
104	0	-3
105	0	-6
106	0	8
107	0	11
108	0	5
109	0	-4
110	0	13
111	0	-13
112	0	-15
113	0	1
114	0	-7
115	0	-14
116	0	-14
117	0	-1
118	0	-18
119	0	-19
120	0	-6
121	0	-16
122	0	-24
123	0	-2
124	0	-6
125	0	-16
126	0	-5
127	0	8
128	0	-2
129	0	-10
130	0	12
131	0	10
132	0	-7
133	0	17
134	0	14
135	0	-1
136	0	-3
137	0	5
138	0	-4
139	0	-10
140	0	9
141	0	0
142	0	-21
143	0	-4
144	0	-11
145	0	-21
146	0	-25

147	0	-15
148	0	-20
149	0	-21
150	0	-9
151	0	-12
152	0	-16
153	0	5
154	0	0
155	0	-15
156	0	-9
157	0	5
158	0	-5
159	0	-20
160	0	10
161	0	15
162	0	-6
163	0	-3
164	0	11
165	0	-5
166	0	-12
167	0	11
168	0	-3
169	0	-15
170	0	9
171	0	-8
172	0	-11
173	0	-6
174	0	7
175	0	-12
176	0	-10
177	0	9
178	0	-13
179	0	-13
180	0	6
181	0	-10
182	0	-27
183	0	-19
184	0	-4
185	0	-10
186	0	-15
187	0	-3
188	0	-7
189	0	-15
190	0	-4
191	0	2
192	0	-17
193	0	-13
194	0	1
195	0	-5
196	0	-15
197	0	6
198	0	-1

199	0	-13
200	0	-20
201	0	-2
202	0	-10
203	0	-12
204	0	0
205	0	-9
206	0	-16
207	0	9
208	0	-1
209	0	-10
210	0	-2
211	0	6
212	0	-7
213	0	-6
214	0	1
215	0	-3
216	0	-7
217	0	3
218	0	-6
219	0	-20
220	0	-8
221	0	-3
222	0	-17
223	0	-11
224	0	4
225	0	-8
226	0	-16
227	0	-6
228	0	-4
229	0	-12
230	0	-14
231	0	0
232	0	-2
233	0	-16
234	0	2
235	0	3
236	0	-8
237	0	-3
238	0	7
239	0	-14
240	0	-12
241	0	8
242	0	-6
243	0	-17
244	0	3
245	0	-4
246	0	-15
247	0	-3
248	0	3
249	0	-19
250	0	-12

251	0	4
252	0	-13
253	0	-12
254	0	-1
255	0	-2
256	0	-24
257	0	-6
258	0	2
259	0	-12
260	0	-20
261	0	-6
262	0	-9
263	0	-16
264	0	-6
265	0	-3
266	0	-13
267	0	-15
268	0	1
269	0	-12
270	0	-10
271	0	13
272	0	-5
273	0	-13
274	0	-9
275	0	-4
276	0	-11
277	0	-17
278	0	7
279	0	-17
280	0	-22
281	0	-1
282	0	-1
283	0	-14
284	0	-5
285	0	4
286	0	-16
287	0	-10
288	0	5
289	0	-14
290	0	-13
291	0	4
292	0	-5
293	0	-22
294	0	-1
295	0	1
296	0	-17
297	0	-9
298	0	3
299	0	-10
300	0	-14
301	0	3
302	0	0

303	0	-22
304	0	-16
305	0	9
306	0	-16
307	0	-16
308	0	0
309	0	-7
310	0	-16
311	0	1
312	0	0
313	0	-18
314	0	-5
315	0	10
316	0	-14
317	0	-16
318	0	3
319	0	-7
320	0	-12
321	0	-6
322	0	5
323	0	-19
324	0	-8
325	0	9
326	0	-4
327	0	-17
328	0	2
329	0	-7
330	0	-16
331	0	-4
332	0	-5
333	0	-7
334	0	-17
335	0	3
336	0	-7
337	0	-21
338	0	-4
339	0	-1
340	0	-12
341	0	-6
342	0	0
343	0	-12
344	0	-13
345	0	4
346	0	-12
347	0	-18
348	0	-2
349	0	-1
350	0	-20
351	0	-11
352	0	3
353	0	-16
354	0	-17

355	0	5
356	0	-1
357	0	-14
358	0	-2
359	0	0
360	0	-17
361	0	-10
362	0	2
363	0	-12
364	0	-18
365	0	1
366	0	-4
367	0	-14
368	0	-153
369	0	-180
370	0	-180
371	0	190
372	0	213
373	0	213
374	0	22
375	0	16
376	0	16
377	0	16
378	0	15
379	0	17
380	0	15
381	0	15
382	0	15
383	0	16
384	0	15
385	0	17
386	0	16
387	0	19
388	0	18
389	0	13
390	0	-11
391	0	-14
392	0	1
393	0	-20
394	0	-42
395	0	-76
396	0	-90
397	0	-92
398	0	-49
399	0	-24
400	0	-39

APPENDIX C
THE TIME-DOMAIN PLOTS OF A WATER-TABLE TRANSECT OF 4-M BY USING 300 MHZ ANTENNA

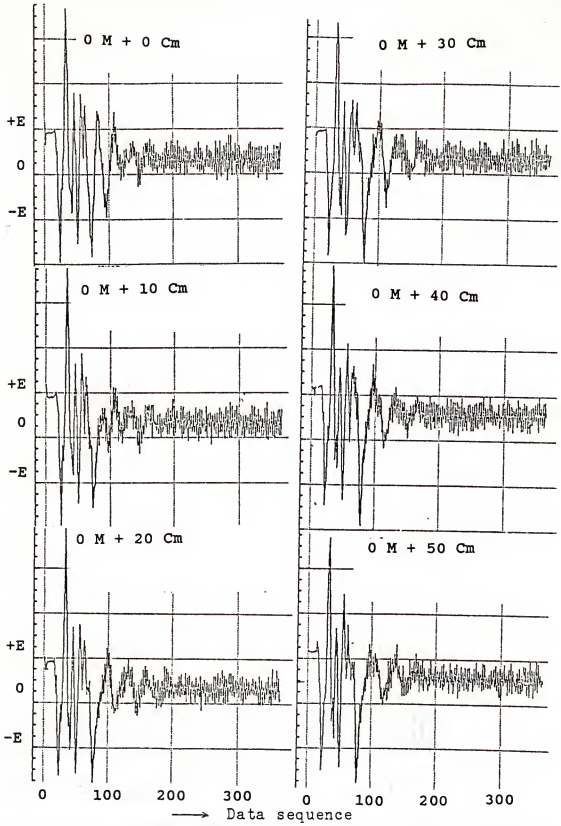

Figure C.1. Time domain plots of echo signal from sites 0 M + 0 Cm - 0 M + 60 Cm.

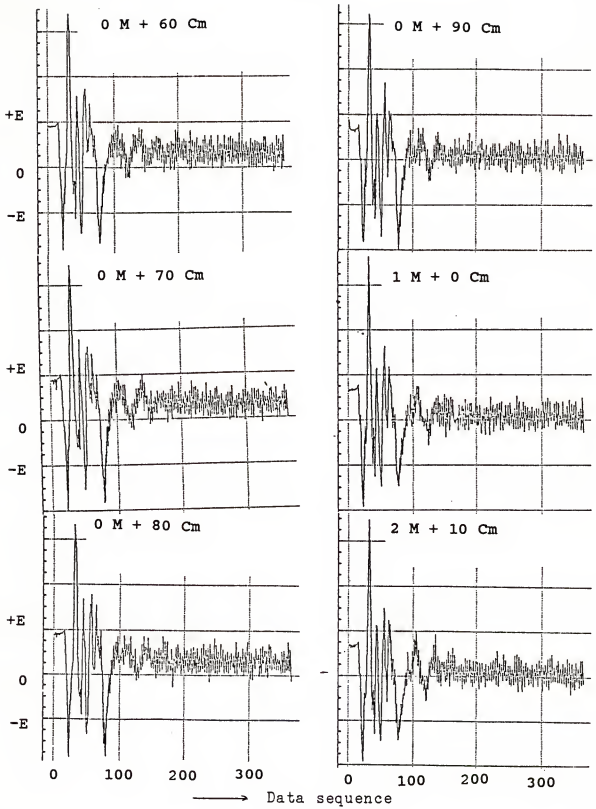

Figure C.2. Time domain plots of echo signal from sites 0 M + 60 Cm ~ 1 M + 10 Cm.

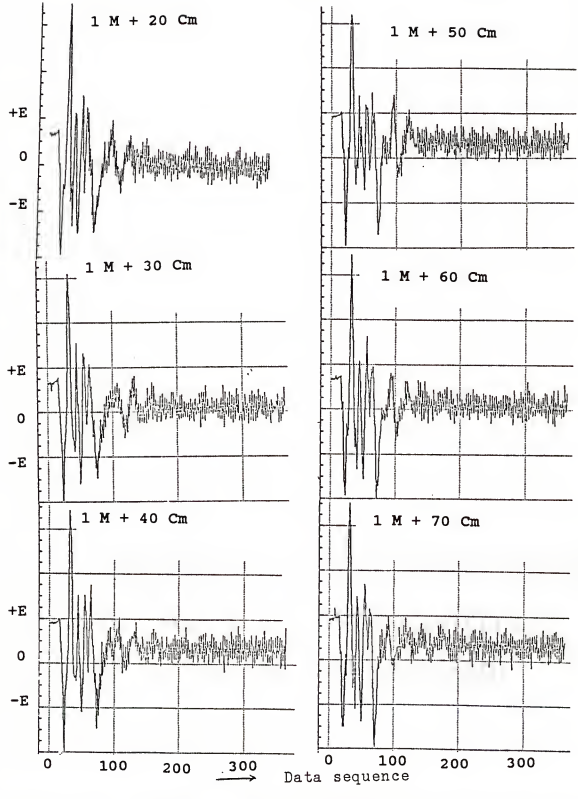

Figure C.3. Time-domain plots of echo signal from sites 1 M + 20 Cm ~ 1 M + 70 Cm.

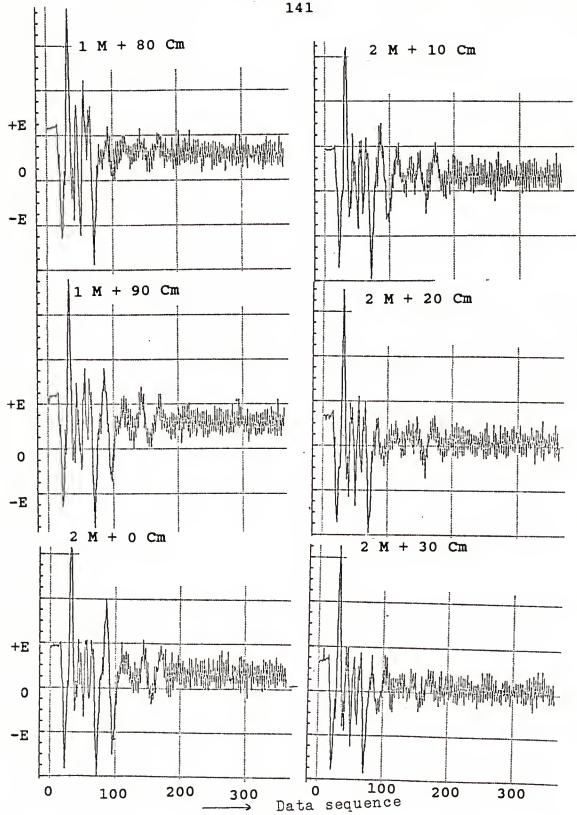

Figure C.4. Time-domain plots of echo signal from sites 1 M + 80 Cm ~ 2 M + 30 Cm.

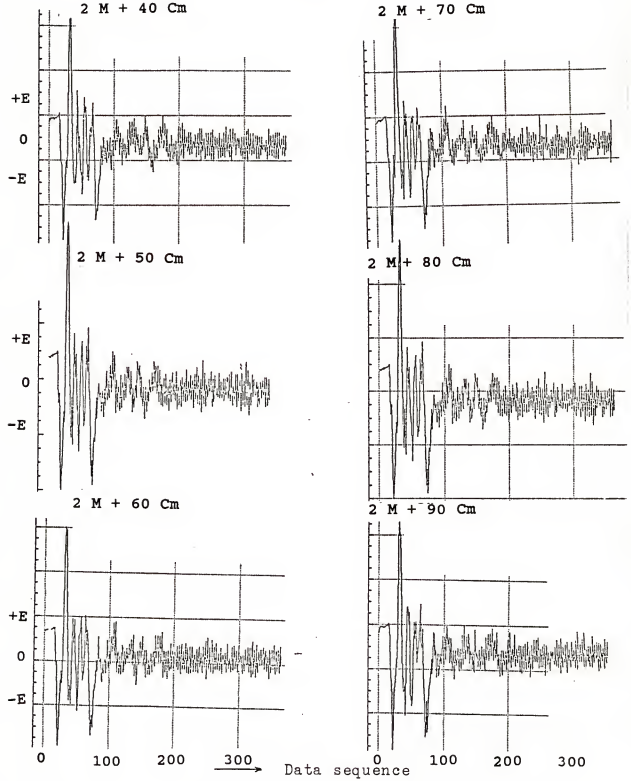

Figure C.5. Time-domain plots of echo signal from sites 2 M + 40 Cm ~ 2 M + 90 Cm.

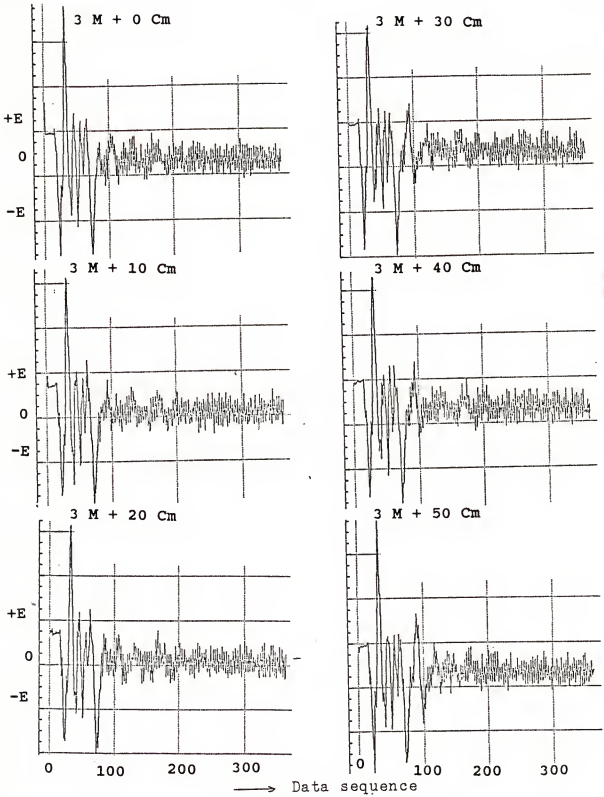

Figure C.6. Time-domain plots of echo signal from sites 3 M + 0 Cm - 3 M + 50 Cm.

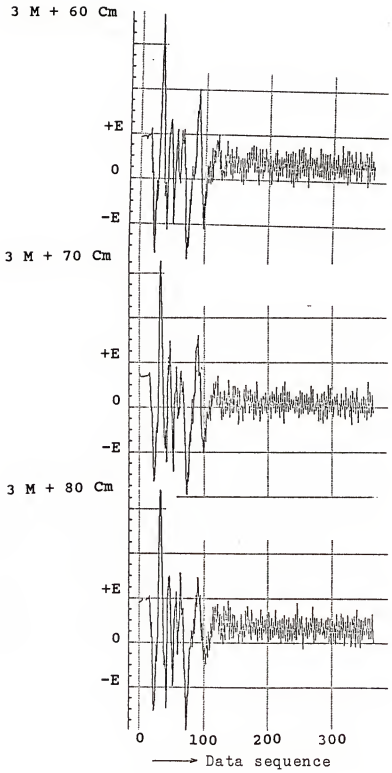

Figure C.7. Time-domain plots of echo signal from sites 3 M + 60 Cm ~ 3 M + 80 Cm.

APPENDIX D
THE PHASE CHANGE ϕ_c OF THE 39 MEASURING SITES FROM A 4-M GPR TRANSECT LINE

Table D.1 The phase change ϕ_c of the 39 measuring sites from a 4-M GPR transect line.

Site	In full spectrogram $\phi_f(^\circ)$	In spectrogram staring From E_{SI} $\phi_{SI}(^\circ)$	Difference of $[\phi_c](^\circ)$
0M +0 Cm	161	166	+ 5
0M +10 Cm	174	184	+10
0M +20 Cm	183	173	-10
0M +30 Cm	189	179	- 7
0M +40 Cm	170	174	+ 4
0M +50 Cm	173	179	+ 6
0M +60 Cm	169	196	+27
0M +70 Cm	180	190	+10
0M +80 Cm	186	181	- 5
0M +90 Cm	187	170	-17
1M +0 Cm	170	175	+ 5
1M +10 Cm	178	181	+ 3
1M +20 Cm	173	166	- 7
1M +30 Cm	172	186	+14
1M +40 Cm	160	171	+11
1M +50 Cm	167	186	+19
1M +60 Cm	177	186	+ 9
1M +70 Cm	171	175	+ 4
1M +80 Cm	172	182	+10
1M +90 Cm	177	199	+22
2M +0 Cm	179	187	+ 8
2M +10 Cm	180	185	+5
2M +20 Cm	176	204	+38
2M +30 Cm	178	182	+ 4
2M +40 Cm	172	187	+15
2M +50 Cm	163	170	+ 7
2M +60 Cm	163	188	+13
2M +70 Cm	171	185	+14
2M +80 Cm	169	186	+17
2M +90 Cm	181	182	+ 1
3M +0 Cm	170	190	+20
3M +10 Cm	164	185	+21
3M +20 Cm	171	180	+ 9
3M +30 Cm	176	182	+ 6
3M +40 Cm	175	186	+11
3M +50 Cm	179	180	+ 1
3M +60 Cm	171	155	+16
3M +70 Cm	176	195	+19
3M +80 Cm	174	180	+ 6

APPENDIX E
WATER CONTENTS OF SOIL PROFILES AND LOCATION OF TAIL PEAK FOR GPR PROBING SITES

Table E.1 Volumetric water content of soil profiles and location of tail peak in spectrogram for the ground truth sites.

Depth (cm)	Soil condition							
	Figure 6.4				GPR transect site			
	A	B	C	D	0M+ 0Cm	2M+ 10Cm	3M+ 0Cm	3M+ 80Cm
0-15	0.02	0.065	0.021	0.062	0.028	0.015	0.013	0.006
16-30	0.032	0.070	0.031	0.071	0.061	0.032	0.032	0.025
31-45	0.052	0.065	0.054	0.061	0.089	0.076	0.062	0.057
46-60	0.053	0.058	0.057	0.054	0.225	0.137	0.112	0.086
61-75	0.076	0.080	0.045	0.010	0.276	0.205	0.183	0.105
76-90	0.067	0.068	0.045	-	0.316	0.225	0.216	0.194
91-105	0.063	0.065	-	-	0.342	0.300	0.261	0.242
106-120	0.072	0.068	-	-	0.325	0.312	0.306	0.314
Mean	0.054	0.067	0.042	0.067	0.102	0.098	0.105	0.111
Tail prak (KHz)	7.5	6.6	7.7	6.6	6.0	6.0	6.0	5.95

APPENDIX F
REFLECTION COEFFICIENTS FROM VARIOUS REGIONS ALONG GROUND TRUTH SOIL PROFILES

Table F.1 Reflection coefficients from various regions along ground truth soil profiles.

Depth	site			
	0 M + 0 Cm	2 M +10Cm	3 M +0 Cm	3 M +80 Cm
1-15 & 16-30	-0.048	-0.020	-0.023	-0.020
16-30 & 31-45	-0.046	-0.067	-0.044	-0.045
31-45 & 46-60	-0.210	-0.102	-0.083	-0.047
46-60 & 61-75	-0.065*	-0.104	-0.114	-0.032
61-75 & 76-90	-0.046	-0.025*	-0.048	-0.183
76-90 & 91-105	-0.027	-0.093	-0.058*	-0.047
91-105 & 105-120	-0.018	-0.013	-0.053	-0.063*

* Location of water-table interface.

APPENDIX G
CALIBRATION RELATIONSHIP BETWEEN WATER ELEVATION FROM GROUND SURFACE AND THE DISTANCE FORM THE WATER BODY

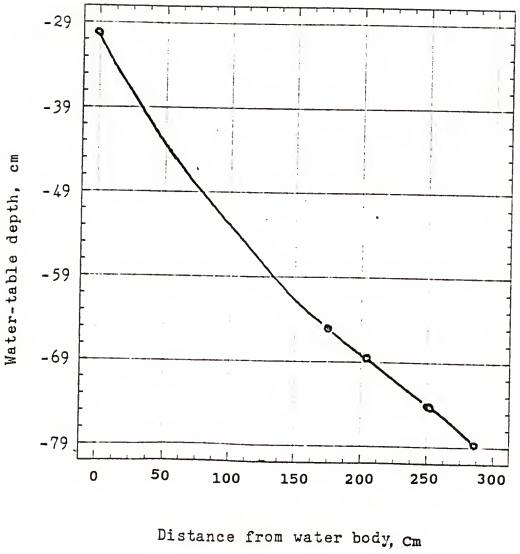

Figure G. 1. Calibration curve of water-table VS distance from water in 4-M transect line.

APPENDIX H
THE MISCELLANEOUS

Table H.1 The operation condition of GPR in this research

Range: Adj - 178

Multiply - X1

Gain - 0.65

Filter: H

Sensitivity: 100

Signal position: Auto

Function: Dir Prnt

Scans/sec: 51.2

Monitor: Out

Graphic sync: on

Tape: none

Motion: Run

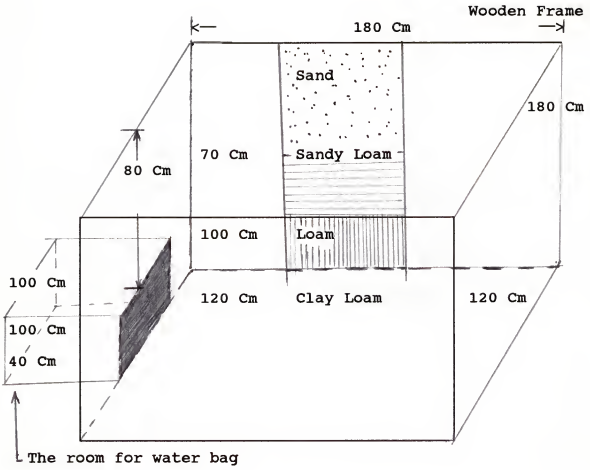

Figure H.1 The control experimental site for the artificial interfaces.

REFERENCES

Acrone, S.A., P.V. Sellmann, and A.J. Delaney. 1978. "Shallow Electromagnetic Investigations of Permafrost." In Poceedings of the Third International Conference on Permafrost, edited by R.J Brown, 501-507. Ottawa, Ontario: National Research Council of Canada.

Anderson, T.W. 1971. The Statistical Analysis of Time Series. New York: Wiley.

Annan, A.P., and J.L. Davis. 1976. "Impulse Radar Sounding in Permafrost." Radio Science 2: 383-394.

Annan, A.P., and J.L. Davis. 1977. Radar Range Analysis for Geological Materials. Report of Activities, Geological Survey of Canada, Paper 77-113, 117-124.

Asmussen, L.E., H.F. Perkins, and H.D. Allison. 1986. Subsurface Descriptions by Ground Penetrating Radar for Watershed Delineation. Georgia Agricultural Experiment Stations, College of Agriculture, University of Georgia. Research Bulletin No. 340.

Ballard, R.F., Jr. 1982. "Cavity Detection." IEEE Digest 2, IGARSS Humick, P. TA-2: 4.1-4.6.

Baranyi, E., O.G. Jensen, and R.T. Lafleche. 1987. "Inverse Solution Modeling of Complex-valued, Frequency Dependent Electrical Properties of Natural Geologic Materials." Radio Science 22(4): 511-519.

Beck, B.F., and W.L. Wilson. 1988. "Interpretation of Ground Penetrating Radar Profiles in Karst Terrace." In Proceedings of the Second Conference on Environmental Problems in Karst Terraces and Their Solutions Conference, Orlando, Florida, 6-13 March 1988, 199-206.

Beizer, J., A.G. Holzman, and A. Kent. 1975. "Analog Digital Conversion." In Encyclopedia of Computer Science Technology, 157-162. New York: McGraw-Hill.

Benson, R.C., and L.B. Yuhr. 1987. "Assessment and Long Term Monitoring of Localized Subsidence Using Ground Penetrating Radar." In Proceedings of the Second Multidisciplinary Conference on Sinkholes and the Environmental Impacts of Karst, Orlando, Florida, 9-11 February 1987, 161-169.

Bjelm, L. 1980. Geologic Interpretation of SIR Data from a Peat Deposit in Northern Sweden. Professional paper. Lund Institute of Technology, Department of Engineering Geology, Lund, Sweden.

Bjelm, L., S.G.W. Follin, and C. Svensson. 1983. "A Radar in Geological Subsurface Investigation." Paris: Bulletin of the International Association of Engineering Geology. 26/27: 10-14.

Bowder, J.J., Jr., R.K. Koerner, and A.E. Lord, Jr. 1982. "Buried Container Detection Using Ground-Probing Radar." Journal of Hazardous Materials 7: 1-17.

Campbell, K.J., and A.S. Orange. 1974. "A Continuous Profile of Sea and Ice and Fresh Water Ice Thickness by Impulse Radar." Polar Record 17(106): 31-41.

Chan, L.C., L. Peters, Jr., and D.L. Moffatt. 1981. "Improved Performance of a Subsurface Radar Target Identification System Through Antenna Design." IEEE Transactions on Antennas and Propagation AP-29(2): 307-311.

Chatfield, C. 1984. The Analysis of Time Series--An Introduction. 3d ed. New York: Chapman and Hall.

Church, R.H., and W.E. Webb. 1986. Evaluation of a Ground-Penetrating-Radar System for Detecting Subsurface Anomalies. United States Department of the Interior, RI-9004, Bureau of Mines.

Collins, M.E., G.W. Schellentrager, J.A. Doolittle, and S.F. Shih. 1986. "Using Ground-Penetrating Radar to Study Changes in Soil Map Unit Composition in Selected Histosols." Journal of the Soil Science Society of America 50(2): 408-412.

Collins, M.E., and J.A. Doolittle. 1987. "Using Ground-Penetrating Radar to Study Soil Microvariability." Journal of the Soil Science Society of America 51(2): 491-493.

Cook, J.C. 1960. "Proposed Monocycle-pulse VHF Radar for Airborne Ice and Snow Measurement." AIEE Communication and Electronics. 51: 588-594.

Cook, J.C. 1974. "Status of Ground-Probing Radar and Some Recent Experience." In Proceedings of the Engineering Conference on Subsurface Exploration for Excavations and Heavy Construction, edited by N.H. Henniker, 175-193, New York: American Society of Civil Engineering.

Cook, J.C. 1975. "Radar Transparencies of Mine and Tunnel Rocks." Geophysics 40: 865-875.

Daily, D.J. 1988. Small Computer Theory and Applications. New York: McGraw-Hill.

Davis, H. F., and A. D. Snider. 1987. Introduction to Vector Analysis. 5th ed. Boston: Allyn and Bacon.

Davis, J.L. 1975. "Relative Permittivity Measurements of Sand and Clay Soil in Situ." Geological Survey of Canada, Paper 75-1c, 361-365.

Davis, J.L., G.C. Topp, and A.P. Annan. 1977. Measuring Soil Water Content in Situ Using Time Domain Reflectrometry Techniques. Geological Survey of Canada, Paper 77-1B, 33-36.

Dolphin, L.T., Jr., R.L. Bollen, and G.C. Oetzel. 1974. "An Underground Electromagnetic Sounder Experiment." Geophysics 39(1): 49-55.

Donaldson, C.A. 1953. Underground Prospecting System. U.S. Patent No. 2,657,380.

Doolittle, J.A. 1982. "Characterizing Soil Map Units with the Ground-Penetrating Radar." Soil Survey Horizons 23(4): 3-10.

Doolittle, J.A. 1983. "Investigating Histosols with the Ground-Penetrating Radar." Soil Survey Horizons 24(3): 23-28.

Doolittle, J.A. 1987. "Using Ground-Penetrating Radar to Increase the Quality and Efficiency of Soil Surveys." In Soil Survey Techniques. edited by W.U. Reybold and G.W. Peterson. Soil Science Society of American Special Publication No. 20, 11-32.

El-Said, M.A.H. 1956. "Geophysical Prospecting of Underground Water in the Desert by Means of Electromagnetic Interference Fringes." In Proceeding, International Rock Engineering 23-30, New York.

Evan, S. 1963. "Radio Technique for the Measurement of Ice Thickness." The Polar Record 2: 406-410, 795.

Fetter, C.W. 1988. Applied Hydrogeology. 2d ed. New York: Merrill.

Fellner-Feldegg, H. 1969. "The Measurement of Dielectrics in the Time Domain." Journal of Physics Chemistry 73(3): 616-623.

Fisher, P.M. 1980. " Applications of Technical Devices in Archaeology: The Use of X-rays, Microscopes, Electrical, and Electromagnetic Devices, and Subsurface Interface Radar Studies in the Mediterranean." Archaeology 63: 1-64.

Fowler, J.C. 1981. "Subsurface Reflection Profiling Using Ground-Probing-Radar." Mining Engineering 8: 1266-1270.

Gilboy, A.E. 1987. "Ground Penetrating Radar: Its Application in the Identification of Subsurface Solution Features -- A Case Study in West-Central Florida." In Proceedings of the Second Multidisciplinary Conference on Sinkholes and the Environmental Impacts of Karst, Orlando, Florida, 9-11 February 1987, 197-203.

Glaccum, R., R. Benson, and M. Noel. 1981. "Improving Accuracy and Cost-Effectiveness of Hazardous Waste Site Investigation with a New Generation of Geophysical Methods." Presented at the National Water Well Association Education Session, Kansas City, Missouri.

Hara, T. 1985. "The Applicability of Ground Probing Radar to Site Investigations." Oyo Technical Note-51, (or RP-4159), Oyo Co., Tokyo, Japan.

Hara, T., H. Ohkubo, Y. Kanesaki, and R. Coldwell. 1983. "An Application of Ground Probing Radar to Detect Cavities in Limestone." Oyo Technical Note-43 (or Rp-4143), Oyo Co., Tokyo, Japan.

Harrison, C.H. 1970. "Reconstruction of Subglacial Relief from Radio Sounding Echoes." Geophysics 35: 1099-1115.

Hearn, D.J. 1987. The Application of Ground Penetrating Radar to Geologic Investigations in Karst Terrace. M.S. Thesis, University of Florida.

Heller, P. 1987. Real-Time Soft Ware Design. Birhauser, Boston.

Hoekstra, P., and A. Delaney. 1974. "Dielectric Properties of Soils at UHF and Microwave Frequencies." Journal of Geophysical Research. 79(11): 1699-1708.

Hogan, G. 1988. "Migration of Ground Penetrating Radar Data: A Technique for Locating Subsurface Targets." In Second International Symposium on Geotechnical Applications of Ground Penetrating Radar, Gainesville, Florida, 6-10 March 1988, 164-179.

Horton, K.A., and R.M. Morey. 1982. A Ground Penetrating Radar Survey of the Maxey Flats Low-Level Nuclear Waste Disposal Site. Fleming County, Kentucky. U.S. Nuclear Regulator Commission, Rep. NUREG/CR-2589.

Horton, K.A., R.M. Morey, R.H. Beers, V.J. Jordan, S.S. Sandler, and L. Isaacs. 1982. An Evaluation of Ground Penetrating Radar for Assessment of Low Level Nuclear Waste Disposal Sites. Geo-centers, Inc., Newton Centre, Massachusetts, Republication NUREG/CR-2212.

Jesch, R.L. 1978. Dielectric Measurements of Five Different Soil Textural Types as Functions of Frequency and Moisture Content. National Bureau of Standards Report No. 78-896. Boulder, Colorado.

Johnson, R.W., R. Glaccum, and R. Wojtasinski. 1979. "Application of Ground Penetrating Radar to the Soil Survey." Soil and Crop Science Society of Florida Proceedings 39: 68-72.

Jordan, E. C., and K. G. Balmain. 1968. Electromagnetic Waves and Radiating Systems. 2d ed. Concord, New Jersey: Prentice-Hill,

King, R.W.P., and G.S. Smith. 1981. Antennas in Matter. Cambridge: MIT Press.

Kuhns, G.L. 1982. Application of Ground Penetrating Radar to Detection of Subsurface Cavities. M.S. thesis, University of Central Florida, Orlando.

Lane, J., and J. Saxton. 1952. "Dielectric Dispersion in Pure Liquids at Very High Radio Frequencies." Proceedings of the Royal Society. A12: 400-408.

Lerner, R.M. 1974. Ground Radar System (MIT). U.S. Patent No. 3,831,173.

Lundien, J.R. 1971. Terrain Analysis by Electromagnetic Means. U.S. Army Engineer Waterways Experiment Station, Vicksburg, Mississippi, Technical Report No. 3-693.

Markt, G. 1988. "Subsurface Characterization of Hazardous Waste Sites Using Ground Penetrating Radar." In Second International Symposium on Geotechnical Applications of Ground Penetrating Radar, 6-11 March 1988, Gainesville, Florida. 61-111.

McCollum, S.H., V.W. Carlisle, and B.G. Volk. 1976. "Historical and Current Classification of Organic Soils in the Florida Everglades." Soil and Crop Science Society of Florida Proceedings 35: 173-177.

Melton. B.S. 1937. Electromagnetic Prospecting Method. U.S. Patent No. 2,077,707.

MetraByte Co. 1989. Data Acquisition and Control. Volum 21.

Miller, E.K. 1986. Time-Domain Measurements in Electromagnetics. New York: Van Nostrand Reinhold.

Mindell, D.A. 1989. "Dealing with a Digital World." Btye (August): 246-256.

Moffatt, D.L., and R.J. Puskar. 1976. "A Subsurface Electromagnetic Pulse Radar." Geophysics 41(3): 506-518.

Moffatt, D.L., R.J. Puskar, and L. Peters, Jr. 1973. Electromagnetic Pulse Sounding for Geological Surveying with Application in Rock Mechanics and the Rapid Excavation Program. Ohio State University Electro Science Laboratory, Report 3408-2.

Morey, R.M. 1974. Geological Survey System. U.S. Patent No. 214,933.

Mulders, M.A. 1987. Remote Sensing in Soil Science, New York: Elsevier. Developments in Soil Science 15.

Newton, R.W. 1976. Microwave Remote Sensing and Its Application to Soil Moisture Detection. Technical Report RSC-81, Remote Sensing Center, Texas A&M University, College Station, Texas.

Newton, R.W., and J.W. Rouse, Jr. 1980. "Microwave Radiometer Measurements of Soil Moisture Constant." IEEE Trans. Ant. Prop., Ap-28, 680-686.

Njoku, E.G., and J.A. Kong. 1977. "Theory of Passive Sensing of Near-Surface Soil Moisture." Journal of Geophysical Research 82: 3108-3118.

Okrasinski, T.A., R.M. Koerner, and A.E. Lord, Jr. 1978. "Dielectric Constant Determination of Soils at L Band Microwave Frequencies." Geotechnical Testing Journal, GTJODJ 1: 134-140.

Olhoeft, G.R. 1986. "Direct Detection of Hydrocarbons and Organic Chemicals with the Ground Penetrating Radar and Complex Resistivity." In Proceeding of the National Water Well Association Conference on Petroleum Hydrocarbons and Organic Chemicals in Groundwater, 1-22. Houston, Texas.

Olson, C.G., and J.A. Doolittle. 1985. "Geophysical Techniques for Reconnaissance Investigations of Soils and Surficial Deposits in Mountainous Terrain." Journal of the Soil Science Society of America 49: 1490-1498.

O'Neill, K., and S. Acrone. 1988. Airborne Surveying of Ice Covers and Water Bodies Using Short Pulse Radar. Cold Regions Research & Engineering Laboratory, Hanover, New Hampshire.

Pittman, W.E. Jr., R.H. Church, W.E. Webb, and J.T. Mclendon. 1984. Ground-penetrating Radar: A Review of Its Application in the Mining Industry. United States Department of the Interior, Bureau of Mines Information Circular. 8964. Washington, D.C: U.S. Government Printing Office.

Procello, L.J. 1974. "The Apollo Lunar Sounder Radar System." Proceedings of the IEEE 62(6): 769-783.

Ra, P.S. 1972. "Broadband Complex Refractive Indexes of Ice and Water." Applied Optics 11: 1836-1844.

Rao, N.N. 1987. Elements of Engineering Electromagnetics. New York: Prentice-Hall.

Rubin, L.A., and J.C. Fowler. 1978. "Ground-Probing Radar for Delineation of Rock Features." In Near Surface Underground Opening Design edited by W.R. Judd, Engineering Geology 12: 163-170.

Sakayama, T., and K. Kanezaki. 1988. "Development of the Georadar System and Basic Experiments." In Second International Symposium on Geotechnical Applications of Ground-Penetrating Radar, Gainesville, Florida, 6-10 March 1988, 122-138.

Sakayama, T., M. Osada, T. Kanemori, and S. Ohya. 1988. "Electro-Magnetic Wave Velocity and Its Application to Civil Engineering Investigations of Soil Layers." In Second International Symposium on Geotechnical Applications of Ground-Penetrating Radar, Gainesville, Florida, 6-10, March 1988, 27-30.

Saxton, J.A., and J.A. Lane. 1952. "Electrical Properties of Sea Waters." Wireless Engineers 29: 269-275.

Schmugge, T.J. 1980. "Effect of Soil Texture on the Microwave Emission from Soil." IEEE Transactions Geoscience and Remote Sensing, GE-18: 353-361.

Selig, E.T., and S. Mansukhani. 1975. "Relationship of Soil Moisture to the Dielectric Property." Journal Geotechnical Engineering Division, Proceeding ASCE 101, GT8: 755-770.

Sellmann, P.V., S.A. Acrone, and A.J. Delaney. 1983. Radar Profiling of Buried Reflectors and the Groundwater Table. U.S. Army Corps of Engineers, Cold Regions Research and Engineering Laboratory Report 83-11.

Shih, S.F., and J.A. Doolittle. 1984. "Using Radar to Investigate Organic Thickness in the Florida Everglades." Soil Science Society of America Journal 48(3): 651-656.

Shih, S.F., J.A. Doolittle, D.L. Myhre, and G.W. Schellentrager. 1986. "Using Radar for Groundwater Investigation." Journal of Irrigation and Drainage Engineering, ASCE 112(2): 110-118.

Shih, S.F., J.A. Doolittle, and G.W. Schellentrager. 1985. "Sampling Design for Radar Application in the Everglades Agricultural Area." Soil and Crop Science Society of Florida Proceedings 44: 199-203.

Shih, S.F., D.L. Myhre, and G.W. Schellentrager. 1985. "Using Radar to Improve Soil Salinity Management." 1985 Winter Meeting of the American Society of Agricultural Engineers, Paper No. 85-2611.

Silver, M.L., P.S. Fisk, and A.L. Greenman. 1986. "Grouting a Sand Dam." Civil Engineering (December): 34-36.

Simmons, G. 1973. Apollo 17 Experiments: Electromagnetic Probing of the Moon. MIT & MSC/NASA Paper URSI/G-AP Meeting, Boulder, Colorado.

Smith, D.V. 1988. "Propagation of Ground Penetrating Radar Signals in Soils." In Second International Symposium on Geotechnical Applications of Ground-Penetrating Radar, Gainesville, Florida, 6-10 March 1988, 31-56.

Snyder, G.H., H.W. Burdine, J.R. Crockett, G.J. Gascho, D.S. Harrison, G.Kidder, J.W. Mishoe, D.L. Myhre, F.M. Pate and S.F. Shih. 1978. Water Table Management for Organic Soil Conservation and Crop Production in the Florida Everglades. Bulletin 801, Agricultural Experiment Stations, IFAS, University of Florida.

Stangland, H.G., and S.S. Kuo. 1987. "Use of Ground-Penetrating Radar Techniques to Aid in Site Selection for Land Application Sites." In Second Multidisciplinary Conference on Sinkholes and the Environmental Impacts of Karst, Orlando, Fl.orida, 9-11 FEbruary 1987, 170-178..

Swain, P.H., and S.M. Davis (eds). 1978. Remote Sensing: The Quantitative Approach. New York: McGraw-Hill.

Tanimoto, S.L. 1987. "Version." The Elements of Artificial Intelligence. New York: Computer Science Press Inc.

Tanaka, A., K. Tamura, T. Toshioka, and S. Ohya. 1988. "Surveys of Cavity and Buried Object by Ground-Probing Radar." In Second International Symposium on Geotechnical Application of Ground-Penetrating Radar, Gainesville, Florida, 6-10 March 1988, 111-117.

Taylor, J.L. 1981. Fundamentals of Measurement Error. Berkeley, California: NEFF Instrument Co.

Terry, R.E., G.J. Gascho, and S.F. Shih. 1980. "Effect of Depth to Water Table on the Quality of Water in the Everglades Agricultural Area." In Proceedings of the Sixth International Peat Congress, Duluth, Minnesota, 700-704.

Topp, G.C., J.L. David, and A.P. Annan. 1980. "Electromagnetic Determination of Soil Water Content: Measurement in Coaxial Transmission Line." Water Resources Bulletin 16: 574-582.

Trevett, J.W. 1986. Imaging Radar for Resources Surveys. New York: Chapman and Hall.

Truman, C.C., H.F. Perkins, L.E. Asmussen, and H.D. Allison. 1988a. "Some Applications of Ground-Penetrating Radar in the Southern Coastal Plains Region of Georgia." Research Bulletin 362, The Geogia Agricultural Experiment stations, College of Agriculture, The University of Georgia.

Truman,C.C., H.F. Perkins, L.E. Asmussen, and H.D. Allison. 1988b. "Using Ground-Penetrating Radar to Investigate Variability in Selected Soil Properties." Journal of Soil and Water Conservation 43(4): 341-345.

Tsung Leung, J.A. Kong, and R.T. Shin. 1985. Theory of Microwave Remote Sensing. London: Wiley-Inter Science.

Ulaby, F.T., R.K. Moore, A.K. Fung. 1981-1982. Microwave Remote Sensing. Volume 2. London: Addison-Wesly.

Ulriksen, C.P.F. 1980. Investigation of Peat Thickness with Radar. Professional Paper, Lund Institute of Technology Department of Engineering Geology, Lund, Sweden. LUTVDG/(TVGL-3008)/(1-18).

Ulriksen, C. Peter F. 1983. Application of Impulse Radar to Civil Engineering. Geophysical Survey Systems, New Hampshire.

Ulriksen, C.P.F. 1987. Radar Lake Morphometry: Part I, Feasibility Study. LUTVDG/1-91, Department of Engineering Geology, Institute of Science & Technology, Lund University.

Walsh, J., and R. Donnelly. 1987. "A General Theory of the Interaction of Electromagnetic Waves with Isotropic, Horizontally Layered Media." Radio Science 22(4): 545-547.

Wang, J.R. 1980. "The Dielectric Properties of Soil-Water Mixtures at Microwave Frequencies." Radio Science 15(5): 977-985.

Wang, J.R., and T.J. Schmugge. 1980. "An Evaporical Model for the Complex Permittivity of Soils as a Function of Water Content." IEEE Transaction Geoscience and Remote Sensing. GE-18: 288-295.

Watts, R.D., and D.L. Wright. 1981. "Systems for Measuring Thickness of Temperate and Polar Ice from the Ground or from the Air." Journal of Glaciology 27: 459-469.

Young, J.D., and R. Caldecott. 1976. Underground Pipe Detector. U.S. Patent No. 3,967,282.

Young, J.D., and R. Caldecott. 1977. Underground Pipe Detector. U.S. Patent No. 4,062,010.

Zhody, A.A.A.R., G.P. Eaton, and D.R. Mabey. 1984. Application of Surface Geophysics to Ground-Water Investigations: Ch. D. 1, Techniques of Water Resources Inventory, U.S. Geological Survey. Washington, D.C.

Zobeck, T.M., J.G. Lyon, D.R. Mapes, and A. Ritchie, Jr. 1985. "Calibrating Ground-Penetrating Radar for Soil Applications." Soil Science Society American Journal 49: 1587-1590.

BIOGRAPHICAL SKETCH

Sheng Liang, also known as Sheng Lewis Liang, was born in Chia Yi, Taiwan, Republic of China, on August 30, 1944. Upon graduating from Chia Yi High School, he was admitted to National Chung Hsing University in September 1965. He received a B.S. in soil and water conservation in June 1969. In August 1969, he was employed as a teaching assistant and in August 1973, was promoted to an instructor in the Department of Soil and Water Conservation, National Chung Hsing University. In August 1974, he was awarded a two-year fellowship (13th annual) from the National Science Council, Republic of China, to attend the University of Hawaii at Manoa, Honolulu, Hawaii and received a M.S. in agronomy and soil science in August 1976. He became an associate professor in August 1977. Another one-year fellowship (18th annual) from the National Science Council, Republic of China, and a four-month graduate assistantship from the National Soil Erosion Lab, U.S.D.A., afforded him a 16-month stay at Purdue University, West Lafayette, Indiana. He became a professor in August 1986. He was also awarded a two-year fellowship from the Ministry of Education, Republic of China, and went to the Department of Environment and Civil Engineering, Utah State

University, Logan, Utah, in September 1986. He transferred to the Remote Sensing Application Lab, Department of Agricultural Engineering, University of Florida, to complete his Ph.D. degree in January 1987. He is a permanent member of the Chinese Soil and Water Conservation Society and the American Geophysical Union.

I certify that I have read this study and that in my opinion it conforms to acceptable standards of scholarly presentation and is fully adequate, in scope and quality, as a dissertation for the degree of Doctor of Philosophy.

Sun Fu Shih, Chairman
Professor of
Agricultural Engineering

I certify that I have read this study and that in my opinion it conforms to acceptable standards of scholarly presentation and is fully adequate, in scope and quality, as a dissertation for the degree of Doctor of Philosophy.

Donald L. Myhre
Professor of
Soil Science

I certify that I have read this study and that in my opinion it conforms to acceptable standards of scholarly presentation and is fully adequate, in scope and quality, as a dissertation for the degree of Doctor of Philosophy.

Byron E. Ruth
Professor of
Civil Engineering

I certify that I have read this study and that in my opinion it conforms to acceptable standards of scholarly presentation and is fully adequate, in scope and quality, as a dissertation for the degree of Doctor of Philosophy.

Jerome J. Gaffney
Associate Professor of
Agricultural Engineering

I certify that I have read this study and that in my opinion it conforms to acceptable standards of scholarly presentation and is fully adequate, in scope and quality, as a dissertation for the degree of Doctor of Philosophy.

Fedro S. Zazueta
Associate Professor of
Agricultural Engineering

This dissertation was submitted to the Graduate Faculty of the College of Engineering and to the Graduate School and was accepted as partial fulfillment of the requirements for the degree of Doctor of Philosophy.

August 1990

for Winfred M. Phillips
Dean, College of Engineering

Madelyn M. Lockhart
Dean, Graduate School